Canadian Technical Report of
Fisheries and Aquatic Sciences 2441

December 2002

Time Series Analysis of Temperature, Salinity, Chlorophyll and Oxygen Data from Tracadie Bay, PEI

M. Dowd, F. Page and R. Losier

Fisheries and Oceans Canada
Science Branch, Ocean Sciences Division
Biological Station
531 Brandy Cove Road, St. Andrews, NB, Canada E3B 2L9

This is the two hundred and forty-eighth Technical Report of
the Biological Station, St. Andrews, NB

Cat. No. Fs 97-6/2441E ISSN 0706-6457

Correct citation for this publication:

Dowd, M., Page, F., and Losier, R. 2002. Time series analysis of temperature, salinity, chlorophyll and oxygen data from Tracadia Bay, PEI. Can. Tech. Rep. Fish. Aquat. Sci. 2441: iii + 86 p.

ABSTRACT

Dowd, M., Page, F., and Losier, R. 2002. Time series analysis of temperature, salinity, chlorophyll and oxygen data from Tracadia Bay, PEI. Can. Tech. Rep. Fish. Aquat. Sci. 2441: iii + 86 p.

This report examines oceanographic data collected in Tracadie Bay, PEI, Canada as part of the Fisheries and Oceans Canada (DFO) Strategic Science Fund initiative entitled "Coastal Oceanography for Sustainable Aquaculture Development", or COSAD (Page et al. 1999). The purpose of this report is to present and analyze a portion of these data comprising time series measurements of water properties in Tracadie Bay. This includes observations on temperature, salinity, chlorophyll (fluorescence) and oxygen from moored instruments deployed at various locations throughout the bay during 1998 and 1999. This report presents these data and carries out time series and spectral analysis for the purpose of ascertaining some basic information on the oceanographic properties of the bay. It includes analysis of a spatial array of VEMCO temperature recorders deployed during summer 1999. Temperature changes up to 8°C within a tidal cycle near the entrance channel to the Gulf of St. Lawrence were observed. The low frequency (<1/100 hr^{-1}) portion of these time series are highly coherent and show a mean temperature increase of a few °C as one moves from the mouth to the head of the bay. The high frequency temperature signal is dominated by power in the semi-diurnal and diurnal bands, likely due to tidal circulation and solar heating. The semi-diurnal signal is attenuated as one moves landward. Time series observations of temperature, salinity, oxygen and chlorophyll from a SeaBird SEACAT were also examined. Only minor depth differences in these variables were found based on data from concurrent surface and bottom deployments. Salinity had proportionally greater semi-diurnal energy than the other water property variables, which were predominately diurnal. Relationships among the water property variables were examined using coherency and phase spectra.

RÉSUMÉ

Dowd, M., Page, F., and Losier, R. 2002. Time series analysis of temperature, salinity, chlorophyll and oxygen data from Tracadia Bay, PEI. Can. Tech. Rep. Fish. Aquat. Sci. 2441: iii + 86 p.

Le présent rapport examine des données océanographiques qui ont été prélevées dans la baie Tracadie, à l'Î.-P.-É., au Canada, dans le cadre d'un projet du Fonds stratégique des sciences, de Pêches et Océans Canada (MPO), intitulé « Océanographie côtière à l'appui du développement de l'aquaculture » (OCADA) (Page et coll., 1999). L'objet du rapport est de présenter et d'analyser une partie des données du projet, soit les mesures prises pour obtenir des séries chronologiques des caractéristiques de l'eau de la baie Tracadie. Les données comprennent des observations de température, de salinité, de concentrations de chlorophylle (fluorescence) et de teneur en oxygène obtenues par le mouillage d'instruments amarrés à divers endroits de la baie, en 1998 et en 1999. Le rapport présente ces données et fait une analyse spectrale et une analyse de la série chronologique afin de vérifier certains renseignements de base sur les caractéristiques océanographiques de la baie. Nous avons notamment procédé à l'analyse d'un réseau spatial de thermographes Vemco mouillés pendant l'été de 1999. Un seul cycle de marées peut provoquer des écarts de température allant jusqu'à 8 °C, près du chenal de l'entrée du golfe du Saint-Laurent. Les signaux de température à basse fréquence (<1/100 hr^{-1}) de ces séries chronologiques sont extrêmement cohérentes et indiquent une hausse de température moyenne de quelques degrés Celsius seulement, à partir de l'embouchure jusque vers le fond de la baie. Les signaux de température à haute fréquence sont dominés par l'énergie des bandes semi-diurnes et diurnes, ce qui est sans doute attribuable à la circulation des marées et au réchauffement solaire. Le signal semi-diurne est atténué à mesure que l'on s'approche de la terre ferme. Nous avons également examiné une série chronologique d'observations de la température, de la salinité, de l'oxygène et de la chlorophylle provenant de données prélevées par une sonde CTP (SeaBird SEACAT). Les données provenant d'instruments mouillés en parallèle, à la surface et au fond de l'eau, n'indiquent que de faibles différences en profondeur dans ces variables. Proportionnellement, la salinité a une plus grande énergie semi-diurne que les autres variables des caractéristiques de l'eau, qui étaient à prédominance diurne. Nous avons examiné les rapports entre les variables des caractéristiques de l'eau en nous basant sur la cohérence et sur le spectre de phase.

physical oceanography
Physiographic data
water temp
salinity

chlorophyll
time series analysis

INTRODUCTION

Tracadie Bay is a shallow, nearly enclosed tidal lagoon located on the north shore of Prince Edward Island, Canada (Fig. 1). It was one of the main study sites for a DFO Strategic Science Fund initiative entitled "Coastal Oceanography for Sustainable Aquaculture Development", or COSAD, which took place from 1997 through 1999 (Page et al. 1999). The COSAD project helped to provide a physical oceanographic foundation to address the issues of carrying capacity of both finfish and shellfish. It adopted the perspective that progress towards these objectives could be made by describing, understanding, and modelling inshore physical oceanography. The general objectives were: 1) develop an understanding of the physical oceanography of typical coastal environments in Atlantic Canada by gathering empirical data on the hydrography, current patterns and meteorology within these environments and to develop high-resolution, three-dimensional finite element circulation models for these environments; 2) use the empirical observations and circulation models to estimate the transport pathways, flux and exchange rates of water and suspended materials between and within aquaculture sites; and 3) use these estimates in conjunction with information on shellfish and finfish needs to help understand the carrying capacities of the study areas.

Tracadie Bay is notable for its extensive shellfish aquaculture development focused on the blue mussel (*Mytilus* spp.). Maps of Tracadie Bay are shown in Fig. 1 and 2. The Tracadie Bay system is made up of Tracadie Bay proper, as well as adjoining Winter Bay. These together cover an area of about 15 km^2. Tracadie Bay is connected to the Gulf of St. Lawrence through a narrow opening. The adjacent shoreline region of the Gulf is a dynamic beach environment characterized by an extensive surf zone. The entrance channel connecting the bay to the ocean branches into two channels separated by intertidal flats. The bay is shallow (<7 m), with some drying intertidal areas. Tracadie Bay is connected to Winter Bay through a relatively narrow constriction. Some branching channels are found at the head of Winter Bay. Gregory et al. (1993) report a freshwater input ranging from 0.7 $m^3 s^{-1}$ in August/September to 7 $m^3 s^{-1}$ in April. They also report an average tidal to freshwater volume ratio of 177. Tracadie Bay and Winter Bay are ice covered in the winter months.

An earlier report focused on aspects of the circulation and tides in Tracadie Bay as determined from observations of sea level, current, winds, and drifters (Dowd et al. 2001). That study determined that the tidal regime of the bay is comprised of mixed diurnal (O_1, K_1) and semidiurnal (M_2) tides. The tidal range is less than 1 m. The tides vary from having daily to twice-daily peaks over the spring-neap cycle. Tidal changes in sea level are both attenuated and lagged relative to tides in the adjacent Gulf of St. Lawrence. Strong tidal currents are found in the channel areas, but interior areas have weak (<10 cm s^{-1}) currents. During summer months, there was little evidence for wind-driven circulation, except at the head of the bay.

The purpose of this report is twofold: (1) to present time series data on temperature, salinity, chlorophyll and oxygen collected during the Tracadie Bay phase of the COSAD project during 1998-99, and (2) to carry out a preliminary statistical analysis of this water property data in order to obtain a basic characterization of its properties. This latter activity takes the form of time series and spectral analysis of the data. Standard analysis procedures are used and therefore details of the methods are not included in this report. The interested reader is referred to the literature on statistical time series analysis, of which Priestley (1981) is an excellent example. The report is structured as follows. First, data from a spatially distributed array of temperature recorders is examined. Next, time series data from moored instruments measuring various water properties, including temperature, salinity, chlorophyll and oxygen, are presented and analyzed. Finally, a summary and discussion of the results is undertaken.

TEMPERATURE TIME SERIES FROM AN ARRAY OF TEMPERATURE RECORDERS

Time series measurements of temperature were collected concurrently at a variety of sites in Tracadie Bay during the summer of 1999. These temperature records were obtained from Vemco MiniLog temperature recorders. These instruments measured temperature at 5-min intervals during the deployment period. (Pressure, or sea level, was also measured by some of these instruments and is analyzed in Dowd et al. 2001.) The full set of time series records of temperature obtained from these instruments during the summer of 1999 is given in Appendix A.

TIME SERIES OF TEMPERATURE

Figure A.1 shows the location of the temperature recorders at 10 stations in Tracadie Bay. Note that sites T4 and T7 had instruments deployed at both the surface and the bottom. The temperature time series obtained from these concurrent

deployments are presented in Fig. A.2. The low frequency component of these time series was isolated using a low-pass, zero-phase Butterworth filter with a cutoff frequency 1/100 hr^{-1}. The main features of the temperature records are the following. Observations from outside Tracadie Bay (site T1) are suggestive that waters in the adjacent Gulf of St. Lawrence are stratified from surface to bottom. (Unfortunately, the surface record only covers a short period and definitive conclusions cannot be made regarding the vertical structure of temperature.) The offshore bottom water is substantially colder than the waters of the bay and exhibits some irregular, high frequency signals. Within Tracadie Bay, the low frequency changes in temperature follow a reasonably consistent pattern. An initial warming is seen from days 170-175. This is followed by a period of stable, but oscillating, temperatures. After day 190 the temperature again begins to climb and then stabilizes. In channel areas near the mouth (sites T3 and T4), there are large tidal oscillations in temperature. Interior regions exhibit smaller and less regular changes in temperature. These have a magnitude of a few degrees or less and appear to be mainly diurnal in nature. At site T4, in the middle of Tracadie Bay, the surface and bottom temperatures show some small differences. The low frequency portion of this spatially distributed array also suggests the existence of an along-inlet temperature gradient, with increasing temperature as one moves landward.

Time series analysis of the temperature observations was carried out on a subset of the records that covered the full study period and are concurrent in time. This data set included sites T3, T4 (surface), T6, T8, and T10. The low frequency portion of these series was isolated by low-pass filtering the original series, and the results are given in Fig. 3. The low frequency oscillations in temperature show a similar pattern for all locations. The major feature is the along-inlet temperature gradient. That is, the temperature in the main entrance channel near the mouth (T3) tends to be lower than other locations. The heads of Tracadie Bay (T10) and Winter Bay (T8) tend to have the warmest temperatures. For the entire analysis period, the mean temperature difference between the mouth (T3) and the head (T8, T10) is about 2°C. However, differences of up to 4.5°C occur during some periods, such as around day 185.

Temperature anomaly time series were constructed by subtracting the low-pass filtered series from the original temperature time series. These high frequency oscillations in temperature, or temperature anomalies, are shown in Fig. 4. The temperature anomalies in the entrance channel (T3) shows large oscillations in temperature, with a range of up to 8°C. These oscillations can be compared against the sea level and boundary transport time series record for the corresponding period, given in Fig. 5. (Note that the boundary transport was diagnosed from the sea level record based on the bathymetry of Tracadie Bay; see Dowd (2002) for more details). The variations in the diurnal and semi-diurnal oscillations in temperature correspond to the spring-neap cycle in sea level (and transport). The tidal maximum in temperature occurs at the end of the ebb tide. The remaining temperature records from the interior of the bay have a smaller temperature range and a periodic, less regular, but more peaked signal. These peaks appear mainly diurnal. The source of these variations likely includes both tidal advection as well as diurnal solar heating. This is discussed further in the final section of this report.

The covariance and correlation matrices for the selected temperature series are given in Table 1a-f. These were computed for the original series, as well as its decomposition into low frequency (subtidal) and high frequency (anomaly) components. The variance of the original series at T3 (entrance channel) is about twice that of the other interior series (Table 1a). The original records for the interior sites (T4, T6, T8, T10) are highly correlated with one another, but less so with site T3 (Table 1b). For the low frequency component of these series, the variances are roughly equal and they are all quite highly correlated (Table 1c,d). The high frequency, or temperature anomaly series indicates that this part of the variance at site T3 is much higher than for the other series (Table 1e). The interior sites are more highly correlated with one another than with the entrance channel T3 (Table 1f)

The phasing properties among the temperature anomaly time series were first examined using cross-correlation functions. We identify the lag associated with the peak in the cross-correlation function as the characteristic time lag of the series. These time lags were computed for temporal subsets of the input series. That is, a moving time window was used to compute the time evolution of the characteristic time lag for each pair-wise combination of the series. Figure 6 shows the characteristic time lags for the temperature anomaly series. The most notable feature of the cross-correlation analysis is that the characteristic time lag varies significantly over the records; the series appears to move in and out of phase, and also change from leading to lagging and back again. This might be related to the spring-neap

Table 1a. Covariance matrix amongst sites for the original temperature time series.

	T3	T4	T6	T8	T10
T3	3.8360	1.8551	1.8455	1.9157	1.7648
T4	1.8551	1.8243	1.7665	1.7407	1.6593
T6	1.8455	1.7665	2.0796	1.7222	1.8313
T8	1.9157	1.7407	1.7222	1.8598	1.7301
T10	1.7648	1.6593	1.8313	1.7301	1.9529

Table 1b. Correlation matrix amongst sites for the original temperature time series.

	T3	T4	T6	T8	T10
T3	1.0000	0.7013	0.6534	0.7172	0.6448
T4	0.7013	1.0000	0.9069	0.9450	0.8791
T6	0.6534	0.9069	1.0000	0.8757	0.9087
T8	0.7172	0.9450	0.8757	1.0000	0.9078
T10	0.6448	0.8791	0.9087	0.9078	1.0000

Table 1c. Covariance matrix amongst sites for the low frequency temperature time series.

	T3	T4	T6	T8	T10
T3	1.9946	1.6089	1.4498	1.4597	1.2449
T4	1.6089	1.6843	1.5936	1.5618	1.4321
T6	1.4498	1.5936	1.7036	1.4862	1.4836
T8	1.4597	1.5618	1.4862	1.5150	1.3899
T10	1.2449	1.4321	1.4836	1.3899	1.4237

Table 1d. Correlation matrix amongst sites for the low frequency temperature time series.

	T3	T4	T6	T8	T10
T3	1.0000	0.8778	0.7865	0.8397	0.7388
T4	0.8778	1.0000	0.9408	0.9777	0.9248
T6	0.7865	0.9408	1.0000	0.9251	0.9526
T8	0.8397	0.9777	0.9251	1.0000	0.9464
T10	0.7388	0.9248	0.9526	0.9464	1.0000

Table 1e. Covariance matrix amongst sites for the temperature anomaly time series.

	T3	T4	T6	T8	T10
T3	2.0253	0.3468	0.4311	0.5363	0.5454
T4	0.3468	0.1761	0.1724	0.2007	0.2226
T6	0.4311	0.1724	0.3323	0.2278	0.3101
T8	0.5363	0.2007	0.2278	0.3457	0.3212
T10	0.5454	0.2226	0.3101	0.3212	0.4770

Table 1f. Correlation matrix amongst sites for the temperature anomaly time series.

	T3	T4	T6	T8	T10
T3	1.0000	0.5806	0.5255	0.6410	0.5549
T4	0.5806	1.0000	0.7125	0.8132	0.7681
T6	0.5255	0.7125	1.0000	0.6721	0.7789
T8	0.6410	0.8132	0.6721	1.0000	0.7911
T10	0.5549	0.7681	0.7789	0.7911	1.0000

cycle. We turn next to spectral analysis to further examine these time series data as a function of frequency.

SPECTRAL ANALYSIS

The temperature anomaly records were examined in the frequency domain using spectral analysis. Figure 7 shows the auto-spectra for the five temperature time series. (Note that the frequency axis shows a maximum value of 0.15 hr^{-1}, corresponding to a period of 6.67 h. Little power was found at higher frequencies and, consequently, we consider only the frequency range 0-0.15 hr^{-1} hereafter). Site T3, in the entrance channel, has a great deal more power than the other records (note the change in scale in Fig. 7). Both diurnal and semi-diurnal peaks are evident. There are some smaller peaks in the low frequency subtidal bands, as well as in frequency bands associated with shallow water tides (e.g. ~8.3-h period). The auto-spectra from the interior stations have less total variance. They are dominated by peaks in the diurnal band, and have very little power the semi-diurnal bands. Some low frequency power is also evident. Diurnal peaks in the most landward stations (T8, T10) are larger than at the other interior stations.

The coherency spectra for the pair-wise combinations of the five temperature anomaly series are shown in Fig. 8. This quantity measures the correlation between series as a function of frequency. The main feature of the coherency spectra is the high coherency (K>0.8) at the diurnal frequency for all record pairs. The low (subtidal) frequencies also exhibit high coherency, but there is relatively little power here. In some cases, the coherency in the semi-diurnal M_2 band is reasonably large (e.g. T3/T6 and T8/T10); however, again, there is little power in these bands. Figure 9 shows the corresponding phase spectra. The phase relations in the diurnal frequency band are summarized in Table 2 in terms of time lags amongst the series. It is seen that site T3, in the entrance channel, leads all the other series. This lead, however, decreases as we move landward, with stations T8 and T10 being nearly in phase with T3, and with one another. These most landward sites also tend to lead the remaining stations in the interior. Finally, Fig. 10 shows the gain spectra. These illustrate the properties of the transfer function of a linear, time-invariant system, treating one series as input and the other as output. The gain spectra illustrate the strong attenuation of the semi-diurnal M_2 temperature signal in the entrance channel (T3)

Table 2. Time lags (in hours) for the diurnal band as determined from the phase spectra of the temperature anomaly time series. The rows and columns are indexed by station number. Negative time lags indicate that the row station leads to column station.

Site	T4	T6	T8	T10
T3	-1.41	-0.76	-0.46	-0.19
T4		0.51	1.07	1.12
T6			0.45	0.66
T8				0.10

with respect to all other records. The centrally located interior stations (T4, T6) also have attenuation in the diurnal signals relative to the more landward stations (T8, T10).

TEMPERATURE, SALINITY, CHLOROPHYLL AND OXYGEN FROM SEACAT MOORINGS

Moored instruments were used to obtain time series observations of water properties including temperature, salinity, dissolved oxygen and fluorescence (chlorophyll). The two instruments used were SeaBird Electronics SEACAT 16plusDO temperature-conductivity recorders. One of these was outfitted with oxygen and fluoresence sensors. (Note that fluorescence is related to chlorophyll and that we use the latter term hereafter.) These instruments were configured to record measurements at 15-min intervals.

Observational efforts were concentrated at the mouth of Winter Bay (site SC1), with a more limited set of measurements also obtained at an alternate site in the main entrance channel into Tracadie Bay (site SC2). The locations of these sites are given in Fig. B.1 of Appendix B. Further information on the deployments are given in Table 3. Both surface and bottom deployments of the instruments were carried out. Note also that the sensors for chlorophyll and oxygen were not calibrated to actual values, and showed a tendency to drift over time (the original data is not shown). In order to make use of these data the following procedure was carried out. The time series data from these sensors were first zero-phase, low-pass filtered (Butterworth) with cut-off frequency of 1/100 hr^{-1}. Anomalies in these variables about the low-pass filtered series were then determined. These anomalies were then standardized by normalizing the series by its standard deviation. Only these standardized oxygen and chlorophyll anomaly time series are considered hereafter. In other words, we focus on the properties of the high frequency variability in these variables. Figures B.2-B.13 in Appendix B present the time series data for the measured water property variables for all 12 SEACAT deployments.

Figures 11 and 12 show the low frequency variations in temperature and salinity at site SC1 (mouth of Winter Bay) during 1998 and 1999. These were obtained by low-pass filtering the original series and piecing together each of the records for successive deployments in the proper time sequence. Both surface and bottom data are included in these figures. In Fig. 11, the temperature is seen to reach its peak values around Julian day 200-220 during both years. Oscillations about the seasonal cycle are evident. There are only slight differences between the concurrent surface and bottom records. In Fig. 12, the salinity series show a slight (1 psu) decrease during each year. The bay waters appear more saline (1 psu) during 1999 compared to 1998. Some differences between concurrent surface and bottom salinities are evident, with surface waters being less saline and more variable than bottom waters.

SPECTRAL ANALYSIS

Spectral analysis was carried out on the time series for each of the water property variables for each of the 12 deployments. These analyses are based on the anomalies in the temperature and salinity time series about their respective low-pass filtered records. As discussed above, the standardized anomaly time series for chlorophyll and oxygen were used. Non-stationarity in some of the anomaly series appears to be present and should be kept in mind when interpreting the results from the spectral analysis.

Figures 13-16 show the auto-spectra for each of the water property variables for site SC2, at the main entrance channel into Tracadie Bay. The data available for this case is from a single period during late summer 1998, with instruments located at both the surface and the bottom. Deviations in the water properties through depth are small at this channel site, which is characterized by strong currents. The variance in the series is concentrated in both the diurnal and semi-diurnal frequency bands. Power also appears in the low frequency, or subtidal, bands. The temperature, chlorophyll and oxygen series all have

Table 3. Deployment information for the SEACAT moorings. The identifiers are used in tables and figures. The sites SC1 and SC2 are given in Appendix B. The time interval is in Julian days (JD) with the year indicated. Variables measured are temperature (T), salinity (S), chlorophyll (C) and oxygen (O). The depth column refers to the deployment location in the vertical.

Identifiers	Location	Time Interval	Variables	Depth
sc1-189-98-m (or #1,1m)	SC1	JD 189-230, 1998	T,S,C	mid
sc1-232-98-s (or #1,2s)	SC1	JD 232-272, 1998	T,S,C,O	surface
sc1-231-98-b (or #1,2b)	SC1	JD 231-272, 1998	T,S,C	bottom
sc1-166-99-s (or #1,3s)	SC1	JD 166-180, 1999	T,S,C,O	surface
sc1-166-99-b (or #1,3b)	SC1	JD 166-180, 1999	T,S,C	bottom
sc1-179-99-s (or #1,4s)	SC1	JD 179-193, 1999	T,S,C,O	surface
sc1-179-99-b (or #1,4b)	SC1	JD 179-193, 1999	T,S,C	bottom
sc1-193-99-s (or #1,5s)	SC1	JD 193-209, 1999	T,S,C,O	surface
sc1-193-99-b (or #1,5b)	SC1	JD 193-209, 1999	T,S,C	bottom
sc1-208-99-b (or #1,6b)	SC1	JD 208-228, 1999	T,S,C	bottom
sc2-272-98-s (or #2,1s)	SC2	JD 272-300, 1998	T,S,C,O	surface
sc2-272-98-b (or #2,1b)	SC2	JD 272-300, 1998	T,S,C	bottom

proportionally more power in the diurnal band relative to the semi-diurnal band, while the salinity series has relatively more power in the semi-diurnal band.

Figures 17-20 show the auto-spectra for the water property variables at site SC1, located at the mouth of Winter Bay. Each of the figures covers a single variable (temperature, salinity, chlorophyll, and oxygen) and includes all deployments carried out at the site. The auto-spectra are arranged chronologically, for both the surface and bottom deployments. Figure 17 indicates that the temperature time series is diurnally dominated, with some semi-diurnal power present. There appears to be little difference in the spectra for concurrent surface and bottom deployments. The total variance in the 1998 deployments is much lower than for the 1999 cases. (This may be due to smaller spatial gradients in temperature in the bay, or it may simply have its origin in the fact that deployment locations changed slightly so that the instrument may be beside, rather than directly in, the primary channel into Winter Bay.) The salinity auto-spectra of Fig. 18 is largely dominated by semi-diurnal signals, and shows some differences in the spectral character between surface and bottom records. The chlorophyll auto-spectra (Fig. 19) are dominated by a diurnal peak and low frequency power is evident. The total power, or variance, is consistent in all these standardized series, but the partitioning of this variance between the semi-diurnal and diurnal frequency bands varies over time and depth. The oxygen auto-spectra (Fig. 20) is mainly dominated by power in the diurnal band; however, in the deployment on Julian day 179 in 1999 we see that some low frequency power is evident.

SURFACE VERSUS BOTTOM DEPLOYMENTS

The relationship among the water property variables for surface and bottom records was further examined using cross-spectral analysis. Five deployments were available that had concurrent surface and bottom records of temperature, salinity and chlorophyll. Cross-spectra were computed for each of these cases. The results are given in Fig. 21-35 in terms of the phase, coherency and gain spectra. Tables 4 and 5 summarize the coherency and phase properties at the diurnal and semi-diurnal, M_2, frequencies, respectively.

Results from the cross-spectral analysis for site SC2 (the entrance channel) are given in Fig. 21-23. For this site, only one case was available with concurrent surface and bottom records. Both surface and bottom records of temperature and salinity are highly coherent and nearly in phase over all frequencies. The gain hovers near one for periods of less than 10 h, indicating that the two series tend to closely track one another in all but the high frequency bands. Chlorophyll is highly coherent and in phase for the diurnal and semi-diurnal frequencies.

Results from the cross-spectral analysis for site SC1 (the mouth of Winter Bay) are given in Fig. 24-35. Here, four cases were available with concurrent surface and bottom records. Surface and bottom temperatures show a similar spectral distribution of power in three of four cases, the exception being the 1998 deployment (Fig. 24). The coherency and gain tend to decline with increasing frequency, suggesting a frequency-dependent decorrelation effect. The

Table 4. Comparison of surface and bottom SEACAT deployments at the diurnal frequency. The coherency K and phase ϕ (°) are given for comparisons of surface and bottom temperature, salinity and chlorophyll records at the diurnal frequency (1/24 h^{-1}).

	Temperature		Salinity		Chlorophyll	
Site pairs	K	ϕ	K	ϕ	K	ϕ
sc2-272-98-s/b	0.98	-3	0.99	-4	0.88	-7
sc1-232-98-s/b	0.92	-10	0.74	60	0.81	-21
sc1-166-99-s/b	0.81	11	0.66	-3	0.72	24
sc1-179-99-s/b	0.90	-2	0.70	6	0.94	8
sc1-193-99-s/b	0.97	14	0.94	8	0.95	6

Table 5. Comparison of surface and bottom SEACAT deployments at the semi-diurnal M_2 frequency. The coherency K and phase ϕ (°) are given for comparisons of surface and bottom temperature, salinity and chlorophyll records at the M_2 tidal frequency (1/12.42 h^{-1}).

	Temperature		Salinity		Chlorophyll	
Site pairs	K	ϕ	K	ϕ	K	ϕ
sc2-272-98-s/b	0.99	-16	0.99	-18	0.81	-4
sc1-232-98-s/b	0.85	-14	0.92	-12	0.25	-9
sc1-166-99-s/b	0.62	-7	0.71	-31	0.56	64
sc1-179-99-s/b	0.67	19	0.86	-12	0.32	-51
sc1-193-99-s/b	0.96	-1	0.99	-5	0.65	-46

diurnal band is generally more coherent than the semi-diurnal band (Tables 4 and 5). The phase is within 20° of zero for both these bands and shows no systematic sign. Salinity has a relatively greater semi-diurnal power as compared to temperature. The bottom salinity appears to have slightly less total power relative to the surface and the spectral partitioning of the power differs, but not in a systematic manner. The semi-diurnal coherency for salinity is higher than in diurnal bands and the phasing for this band indicates that surface salinity leads the bottom salinity with a mean phase of 15°, or about half an hour. Chlorophyll records are dominated by diurnal power and also exhibit significant low frequency (subtidal) power in some cases. The coherency between the surface and the bottom is relatively high in the diurnal band (Table 4). Outside of the diurnal frequency, these chlorophyll records seem to be rather unrelated. Overall, the surface and bottom water properties are more tightly coupled at site SC2 (the entrance channel) than at site SC1 (the mouth of Winter Bay).

RELATIONSHIP AMONG WATER PROPERTY VARIABLES

Figures 36-47 show the results from cross-spectral analyses among the different water property variables collected by the moored SEACATs. These analyses are carried out for each deployment, since the variables are recorded simultaneously. For each of the 12 deployments, coherency and phase spectra are computed for each of the pair-wise combinations of the variables temperature, salinity, chlorophyll and oxygen (where available). The coherency spectra of Fig. 36-47 show that coherency is generally quite high for many frequency bands. However, these should be interpreted in light of the auto-spectra, which indicate that power is concentrated mainly in the diurnal and semi-diurnal bands. Rather than comment on the phase and coherency spectra on a case by case basis, the information was synthesized by focusing on the diurnal and semi-diurnal frequency bands. The coherency and phase associated with these bands was extracted directly and the results of this procedure are shown in Fig. 48-53. These figures are now organized in terms of pair-wise comparisons of the water property variables. Only those cases with coherency greater than 0.6 were considered as significant. Phase relationships among the water property variables in the diurnal and semi-diurnal frequency bands suggest the following conclusions:

- Temperature and salinity are highly coherent in both the diurnal and semi-diurnal frequency bands for nearly all records. In the semi-diurnal band these variables are out of phase by 180°; in

the diurnal band the phase difference is 100°, with temperature leading salinity.

- Temperature and chlorophyll are coherent in about half the cases for both frequency bands. In the diurnal band, the temperature series leads the chlorophyll series by about 60° on average. For the semi-diurnal band, there is no clear pattern to the phase relations for the coherent analysis pairs.

- Temperature and oxygen are highly coherent in the diurnal band, with the two series being nearly in phase. There is little coherence in the semi-diurnal band, reflecting the relative lack of oxygen signals in that band.

- Salinity and chlorophyll are highly coherent in about half the cases for both frequency bands. In the diurnal band, chlorophyll leads salinity in all these cases with a mean phase of 66°. The phase patterns in the semi-diurnal band are less clear.

- Salinity and oxygen are coherent in the diurnal band for all four records from site SC1 (Winter Bay), with oxygen leading salinity with a mean phase of 115°. No clear patterns are evident in the semi-diurnal band.

- Chlorophyll and oxygen are coherent in the diurnal band for all cases at site SC1 (Winter Bay), but not at SC2 (entrance channel). The oxygen leads the chlorophyll series by about 60°. No clear patterns are evident in the semi-diurnal band.

SUMMARY AND CONCLUSIONS

The analysis of time series records of temperature at various locations in Tracadie Bay during summer 1999 suggest the following characterization. A temperature gradient in the bay is clearly evident, with the mean temperature at the head of the bay exceeding the temperature at the mouth by a few degrees Celsius. These slowly evolving, low frequency (subtidal) changes in temperature show nearly the same pattern at all sites in the bay. They are likely due to changes in the water temperatures in the adjacent Gulf of St. Lawrence resulting from larger scale oceanographic processes, such as coastal upwelling. Superimposed on these low frequency changes in temperature are higher frequency oscillations, mainly at periods of 1 d (diurnal) and 1/2 d (semi-diurnal). These changes are largest near the mouth of the bay (up to 8°C in 1 d) and comprised of both diurnal and semi-diurnal oscillations. At the interior sites in Tracadie Bay, these oscillations in temperature are much smaller, only a few degrees, and are mainly diurnal in nature.

The higher frequency oscillations in temperature result mainly from tidal advection of temperature in the presence of an along-inlet temperature gradient. The increased temperature in Tracadie Bay is caused by solar heating of bay waters, which tends to raise water temperatures. The dilution of bay waters with the colder offshore waters by tidal flushing tends to decrease temperatures. This tidal flushing effect is more pronounced in the seaward parts of the inlet, relative to the landward parts. The net result of these competing processes is a horizontal temperature gradient in the bay. Note that the observed oscillations in temperature are of the same magnitude as the mean gradient. The semi-diurnal changes in temperature are most likely due to the M_2 tide, as no other forcing mechanisms operates in this frequency band. Oscillations at daily periods may, however, have sources in both tidal circulation as well as solar heating. In Tracadie Bay, the daily tidal components K_1 and O_1, due to combined effects of the moon and the sun's gravitational pull, are dominant (Dowd et al. 2001). These have periods of 23.9 and 25.8 h, respectively. Solar heating will, of course, have a 24-h period. The relative contribution of these two sources of temporal variations in temperature is discussed below.

Suppose we assume an average daily solar heating rate of 200 watts m^{-2} (this was the mean value of incoming solar radiation measured by a meteorological station deployed at Tracadie Bay in 1998). The density of seawater is approximately 1025 kg m^{-3}, with a specific heat of 4000 J kg^{-1} $°C^{-1}$. Using a mean depth for Tracadie Bay of 3 m and, assuming that this water column absorbs all the available thermal energy from the sun, implies a change of 1.4 °C per day. This value is somewhat less than the daily changes observed in the interior temperatures. It suggests that tidal advection of waters in the presence of spatial gradients in temperature contributes to the observed daily cycle of temperature measured at a fixed measurement point. For Tracadie Bay it is difficult to separate the solar heating and advection effects on temperature variations since both occur within the same period (in a system with only semi-diurnal tides this would not be the case). Note also that the end of the ebb tide tends to be around the time of maximal solar heating (see Fig. 5). A complete accounting for the temperature distribution of the bay would require a full heat budget for the bay.

Time series observations of other water property variables in addition to temperature were recorded using the moored SEACAT instruments. These also recorded temperature, salinity, chlorophyll and oxygen levels over time. Recall that only the detrended and standardized oxygen series were used due to uncertainties in sensor calibration and drift, i.e. we have focused on the high frequency variations in these variables. For concurrent surface and bottom deployments, little systematic difference in temperature, salinity and chlorophyll was found (oxygen was only available for surface deployments). This lack of vertical structure was likely due to the well mixed nature of the water column in the shallow, high current channel areas where the deployments were carried out.

The variance in the temperature anomaly record is concentrated mainly in the diurnal frequency band, as discussed earlier. The salinity record, on the other hand, has its variance more concentrated in the semi-diurnal band. Variations in salinity originate only from tidal advection in the presence of spatial gradients in salinity. These gradients arise because the bay waters are slightly fresher than the adjacent offshore waters. Temperature and salinity are 180° out of phase in the semi-diurnal band. This results from temperature being high within the bay relative to outside waters, while salinity is low in the bay compared to outside waters. These opposing spatial gradients in the presence of oscillatory tidal advection give rise to the observed phasing relationship. In the diurnal band, temperature leads salinity by only 100° and the coherency is lower. This difference is due to the fact that temperature variability has its source in both tidal advection and daily solar heating, whereas salinity is only affected by the former.

The oxygen and chlorophyll series both exhibit signals mainly in the diurnal frequency band, with very little power in the semi-diurnal bands. A harmonic regression at a daily period for the 12 deployments indicated that the peak daily value for chlorophyll occurs at 00:42 GMT (21:42 local), on average, with a standard deviation of about 1.92 h. For oxygen, the five deployments yield a daily peak at 20:52 GMT (17:52 local) on average, with a standard deviation of 1.31 h. The diurnal variability in chlorophyll has its origin in both physical (advection) and biological (primary production) processes. Oxygen originates from these processes but, since it is a dissolved gas, it is also exchanged between the ocean and the atmosphere. It is unclear whether any spatial gradients in chlorophyll and oxygen are present in the bay and whether or not oscillations arise from tidal advection. The lack of oscillations in the semi-diurnal band seems to support the contention of small or non-existent spatial gradients, otherwise a semi-diurnal peak would be observed. It suggests a biological origin to the daily oscillations in chlorophyll due to cycles of primary production. Oxygen may be generated as a by-product of this primary production, and is also influenced by air-sea exchange.

In the diurnal band, cross-spectral analysis indicated that temperature and oxygen are in phase and lead chlorophyll by about 4 h. A number of explanations for this result are possible. First, the capacity of seawater to hold dissolved gases is temperature dependent. The fact that temperature and oxygen are in phase might be due to this phenomenon, but would require the oxygen to very rapidly equilibrate between the bay and the atmosphere. An alternative explanation supposes that the oxygen source is due to primary production. Note that the cycle of primary production is related to the time derivative of the biomass of primary producers, which we may assume scales with the chlorophyll level. A sinusoidal oscillation in chlorophyll at the daily period would give rise to a primary production cycle that is 90° out of phase and leading oxygen. For this idealized example, the peak in oxygen production would occur 8 h before the peak in chlorophyll. The addition of respiration might reduce this lag time making this explanation not inconsistent with the observed results. Finally, a physical oceanographic explanation might be plausible if the spatial distribution of chlorophyll and oxygen in the bay are different. When these are advected by the same tidal flow field a phasing difference would be recorded at a fixed point. Clearly, the relation between the oxygen and chlorophyll variability would have to be confirmed with further observations, and any hypotheses about its origin tested systematically.

ACKNOWLEDGEMENTS

This work was funded by the Department of Fisheries and Oceans through the Strategic Science Fund project "Coastal Oceanography for Sustainable Aquaculture Development". The authors wish to thank their partners in this initiative, including the PEI Department of Fisheries, Aquaculture and Environment and the PEI Mussel Growers Association, particularly the members from Tracadie Bay. We are also grateful to Gary Bugden and Edward Horne of the Bedford Institute of Oceanography for reviewing this report.

REFERENCES

Dowd, M., Page, F.H., Losier, R., McCurdy, P. and Bugden, G. 2001. Physical Oceanography of Tracadie Bay, PEI: Analysis of Sea Level, Current, Wind and Drifter Data. Can. Tech. Rep. Fish. Aquat. Sci. 2347: 77 p.

Dowd, M. 2002. Seston dynamics in a tidal embayment with shellfish aquaculture: a model study using equations. Estuar. Coast. Shelf Sci. (in press).

Gregory, D., Petrie, B., Jordan, F. and Langille, P. 1993. Oceanographic, geographic and hydrological parameters of Scotia-Fundy and southern Gulf of St. Lawrence inlets. Can. Tech. Rep. Hydrog. Ocean Sci. 143: 248 p.

Page, F., Greenberg, D., Bugden, G., Losier, R., Shore, J., Horne, E., Robinson, S., Chang, B. and Sephton, T. 1999. Oceanographic component of the Canadian Department of Fisheries and Oceans Science Strategic Research Program on Coastal Oceanography for Sustainable Aquaculture Development (COSAD). Bull. Aquacult. Assoc. Can. 99-2: 14-16.

Priestley, M.B. 1981. Spectral Analysis and Time Series. Academic Press, London. 890 p.

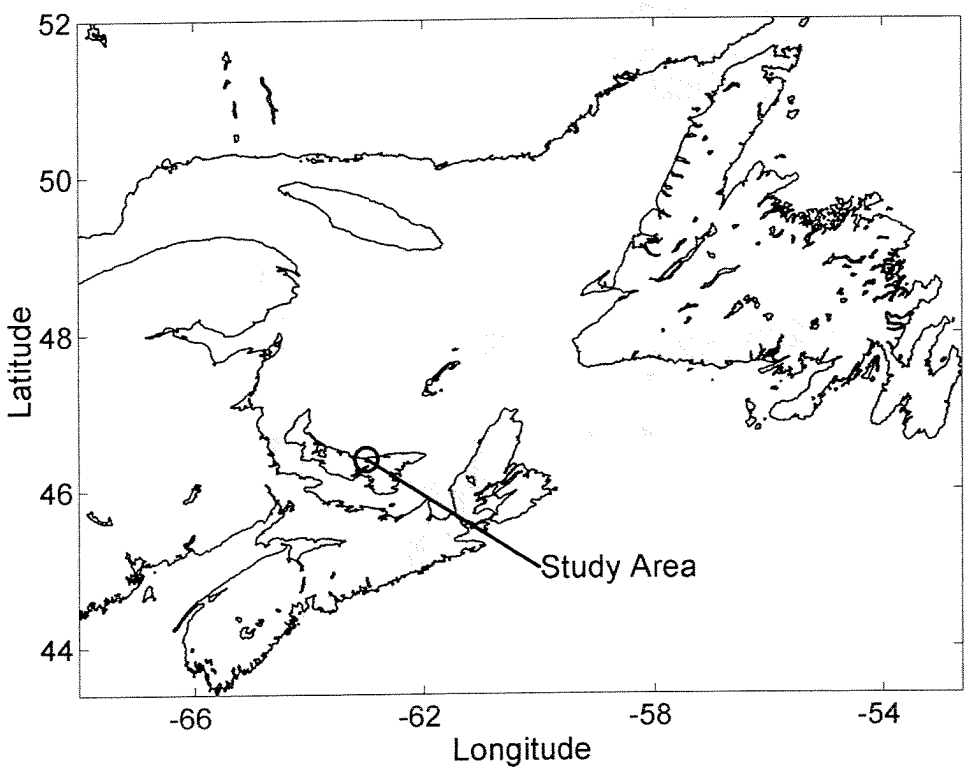

Fig. 1. Location of the study area of Tracadie Bay, PEI, Canada.

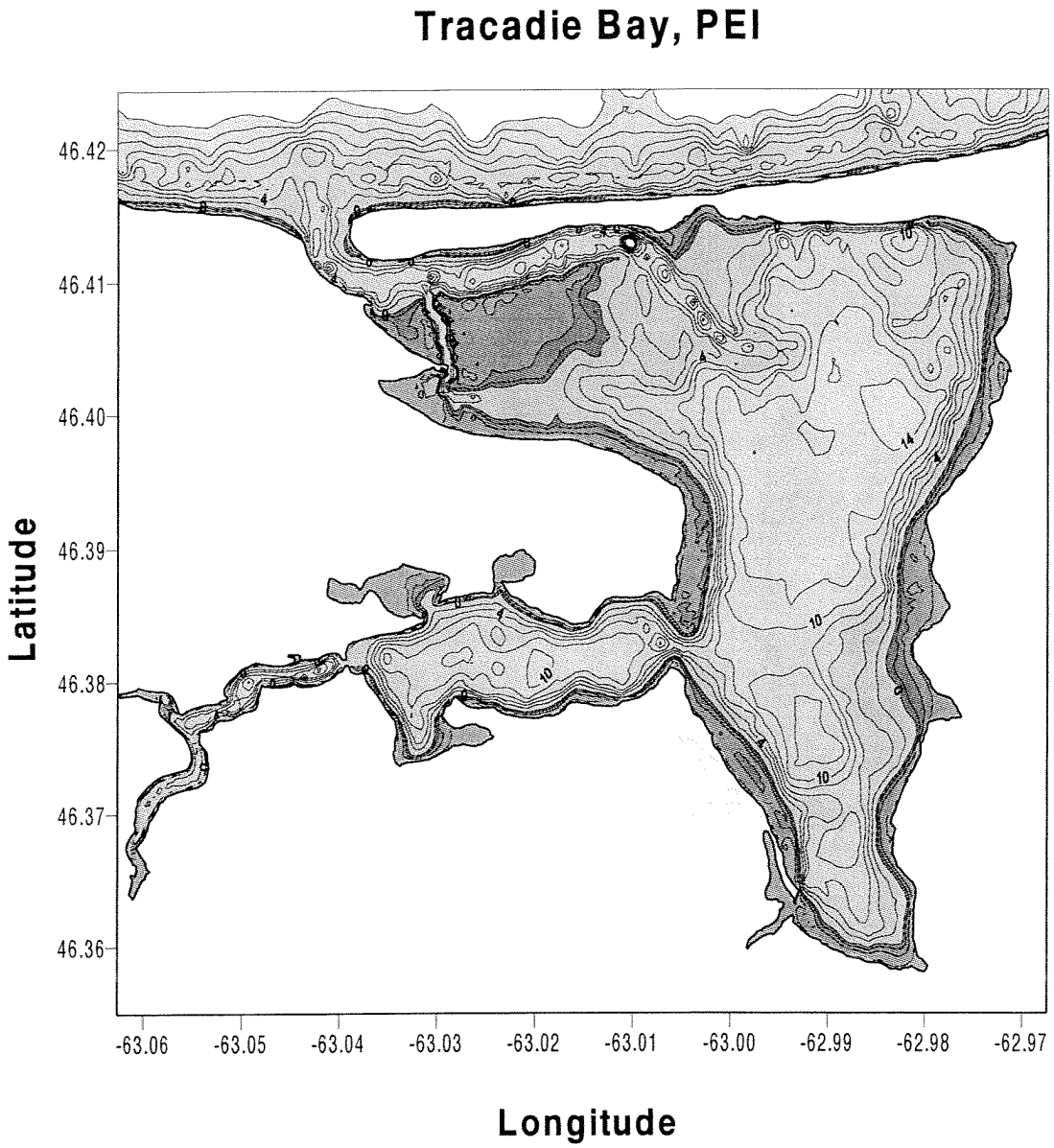

Fig. 2. Map of Tracadie Bay. This contour map of the bathymetry shows the depth in feet relative to mean low water. The lighter gray areas are subtidal (positive depths). The dark gray areas are the intertidal zone, which is delineated by the zero contour.

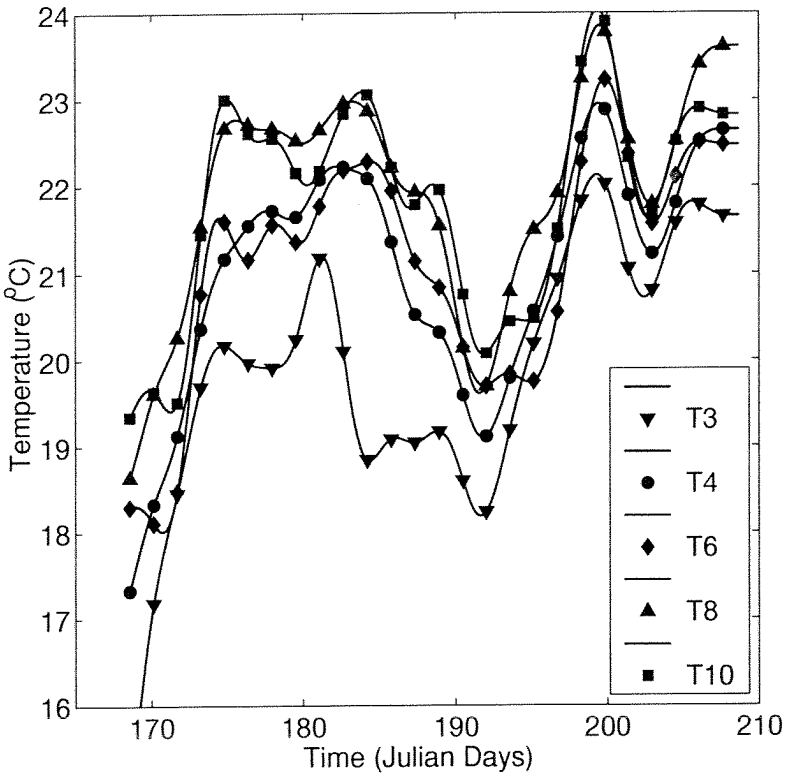

Fig. 3. Low frequency signal in the temperature time series for the selected sites. Time is in Julian days for 1999.

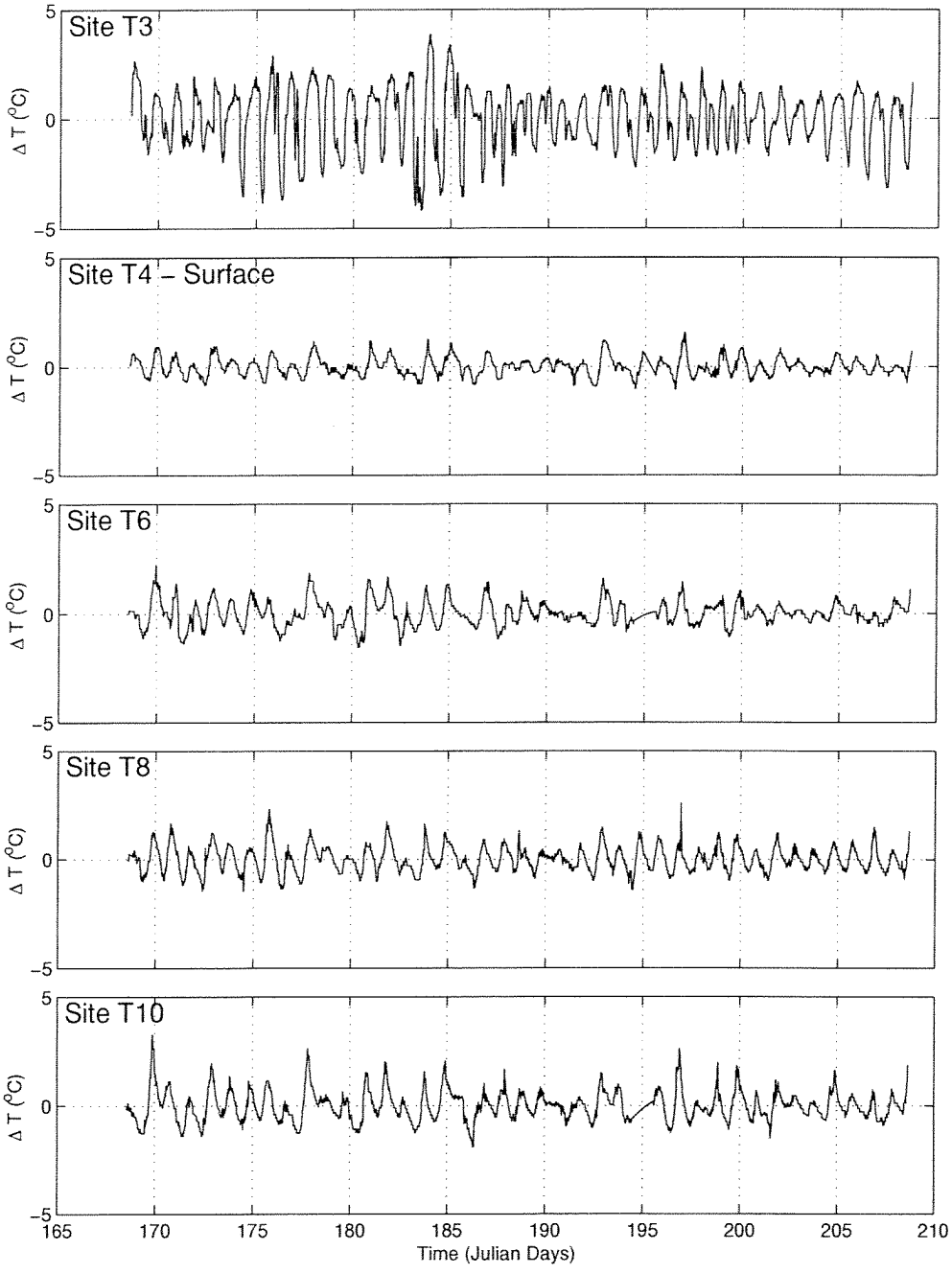

Fig. 4. High frequency signal in the temperature time series for the selected sites. The temperature anomaly is about the low-pass filtered original series. Time is in Julian days for 1999.

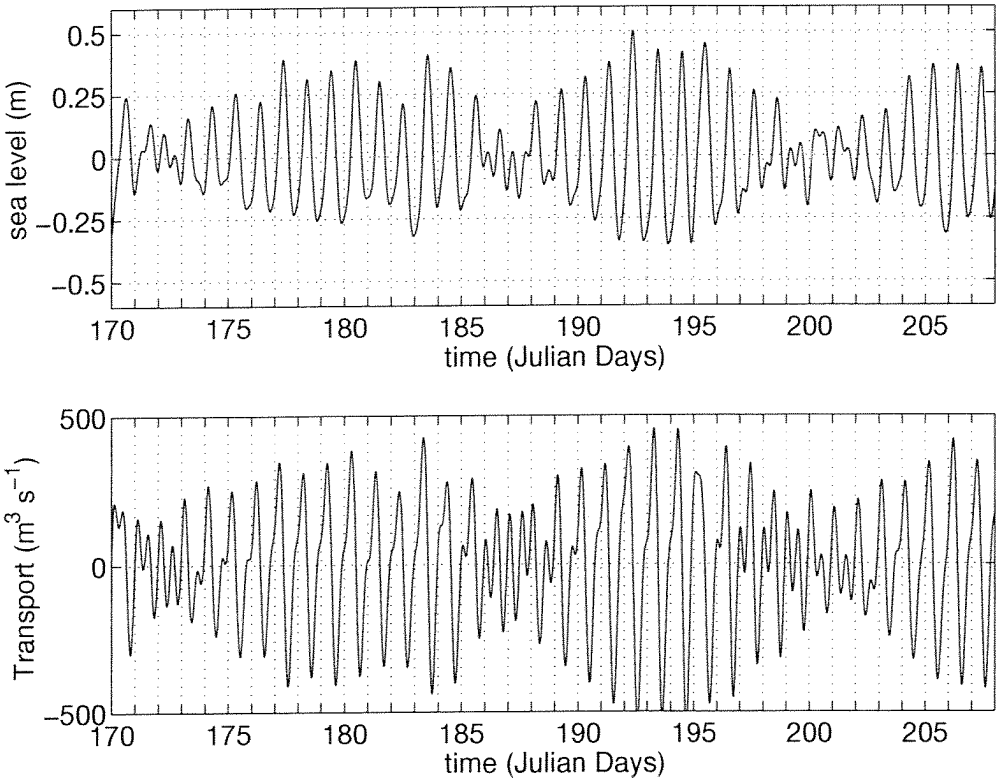

Fig. 5. Sea level anomaly and the volume transport into Tracadie Bay. This covers the period in 1999 corresponding to the deployment of the array of temperature recorders. Sea level is derived from a pressure sensor at site T4. Volume transport into the bay is computed from this measured sea level (see text).

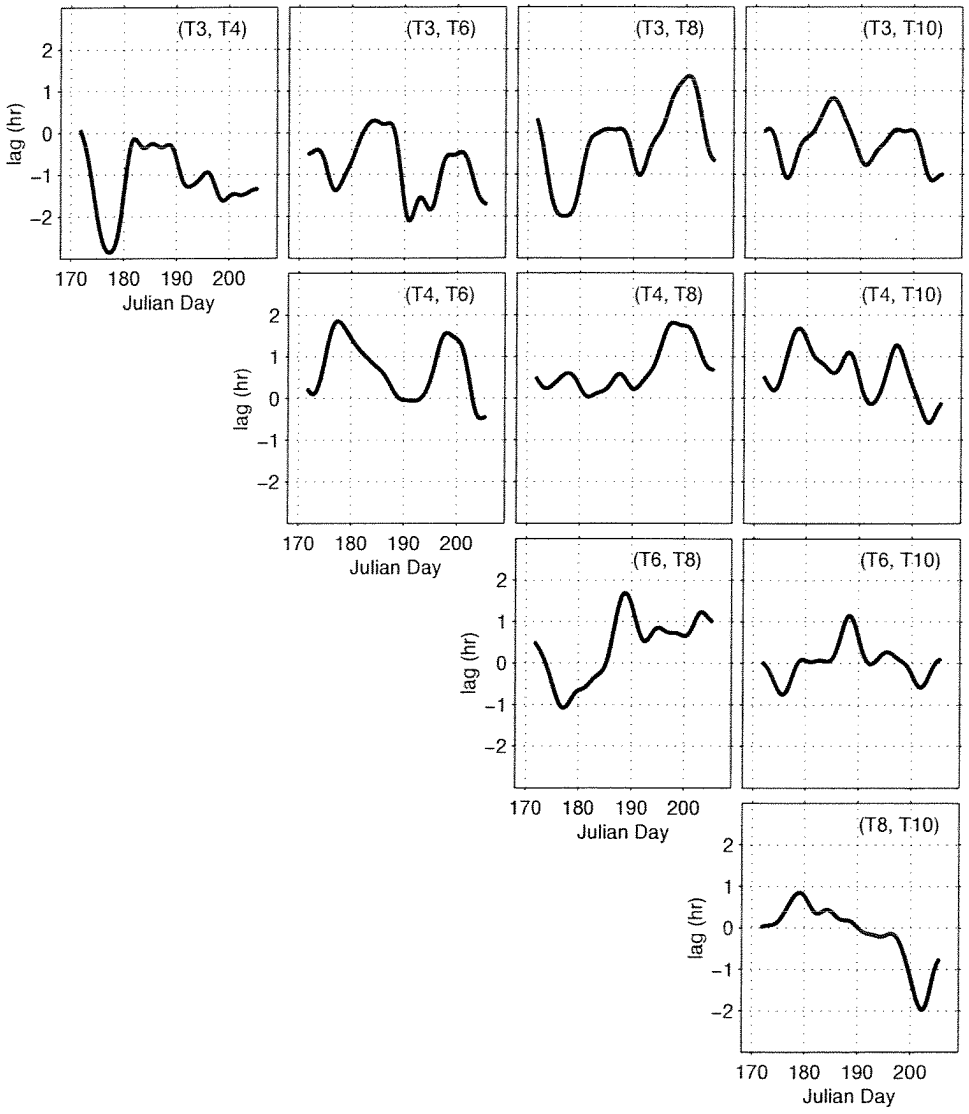

Fig. 6. Time evolution of the characteristic time lag of the cross-correlation amongst the temperature anomaly time series (site pairs are given in upper right of each panel). A moving window comprising a 600-h time interval was used to compute these quantities (see text).

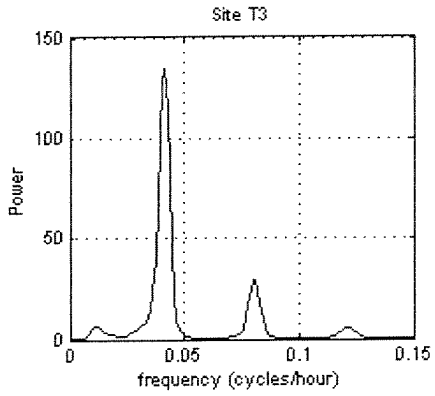
Site T3
Power
frequency (cycles/hour)
0
50
100
150
0.05
0.1
0.15

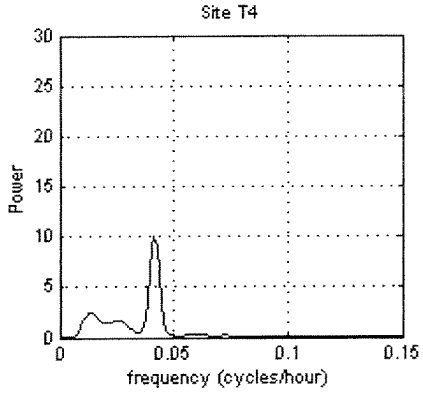
Site T4
Power
frequency (cycles/hour)
0
5
10
15
20
25
30
0.05
0.1
0.15

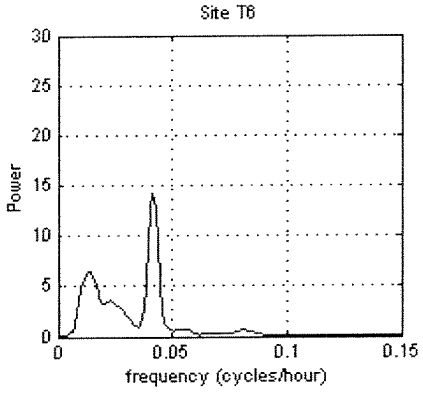
Site T6
Power
frequency (cycles/hour)
0
5
10
15
20
25
30
0.05
0.1
0.15

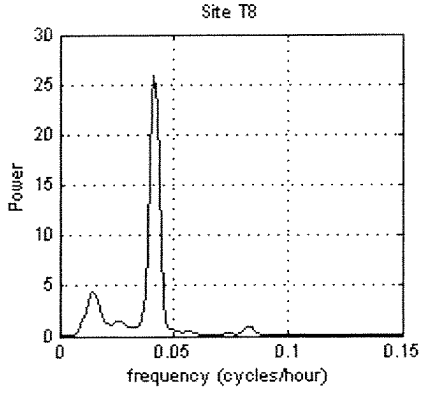
Site T8
Power
frequency (cycles/hour)
0
5
10
15
20
25
30
0.05
0.1
0.15

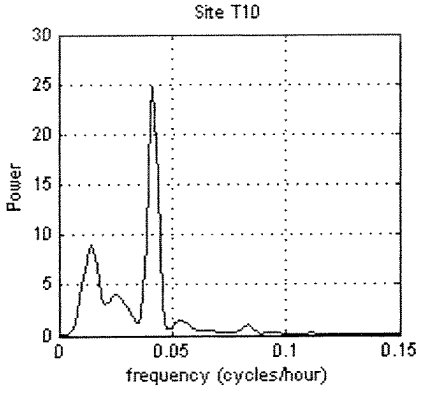
Site T10
Power
frequency (cycles/hour)
0
5
10
15
20
25
30
0.05
0.1
0.15

Fig. 7. Power spectral density of the temperature anomaly time series for the selected stations in Fig 4. Frequency is in units of cycles per hour (cph) and power has units $°C^2\,cph^{-1}$.

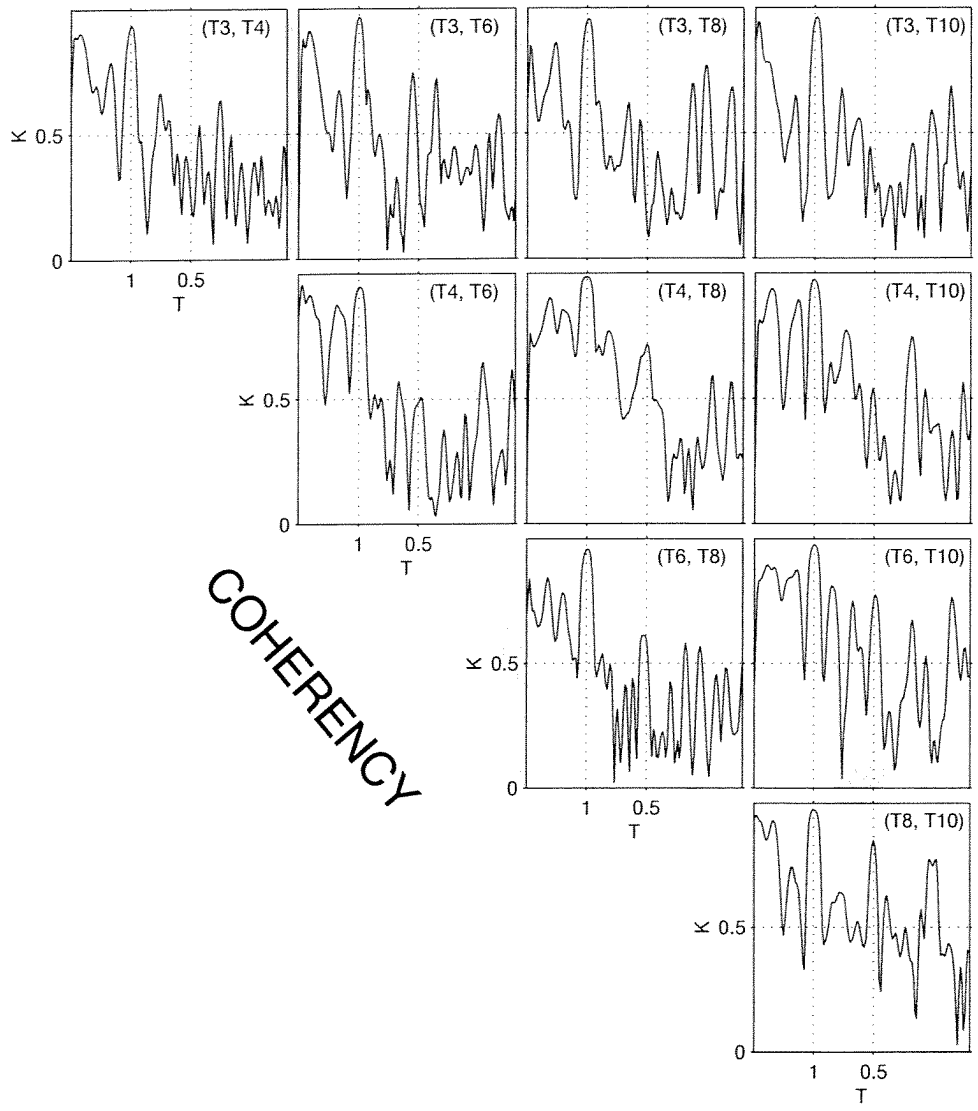

Fig. 8. Coherency spectra for the temperature anomaly time series. The coherency is given by K, and T represents the period in days.

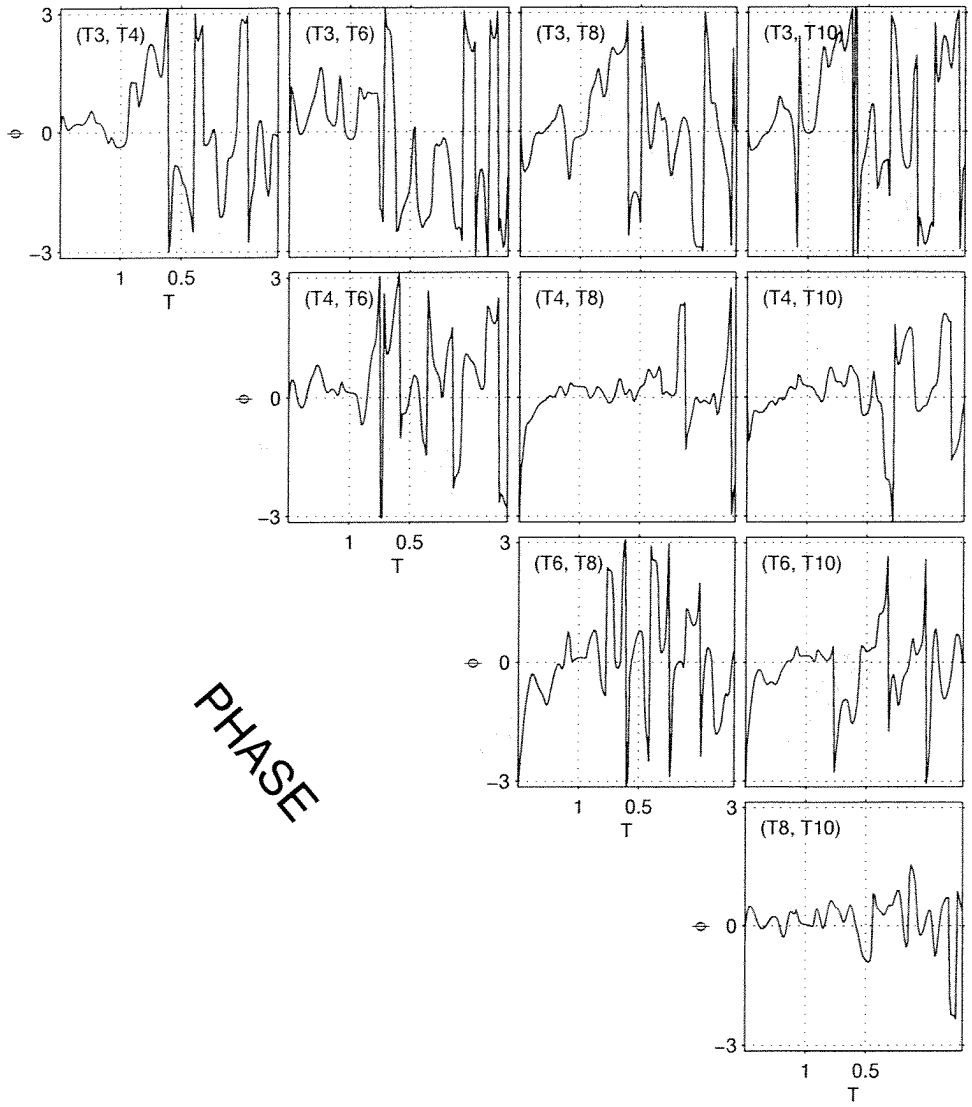

Fig. 9. Phase spectra for the temperature anomaly time series. The phase is given by ϕ and is in radians. The period T is in days.

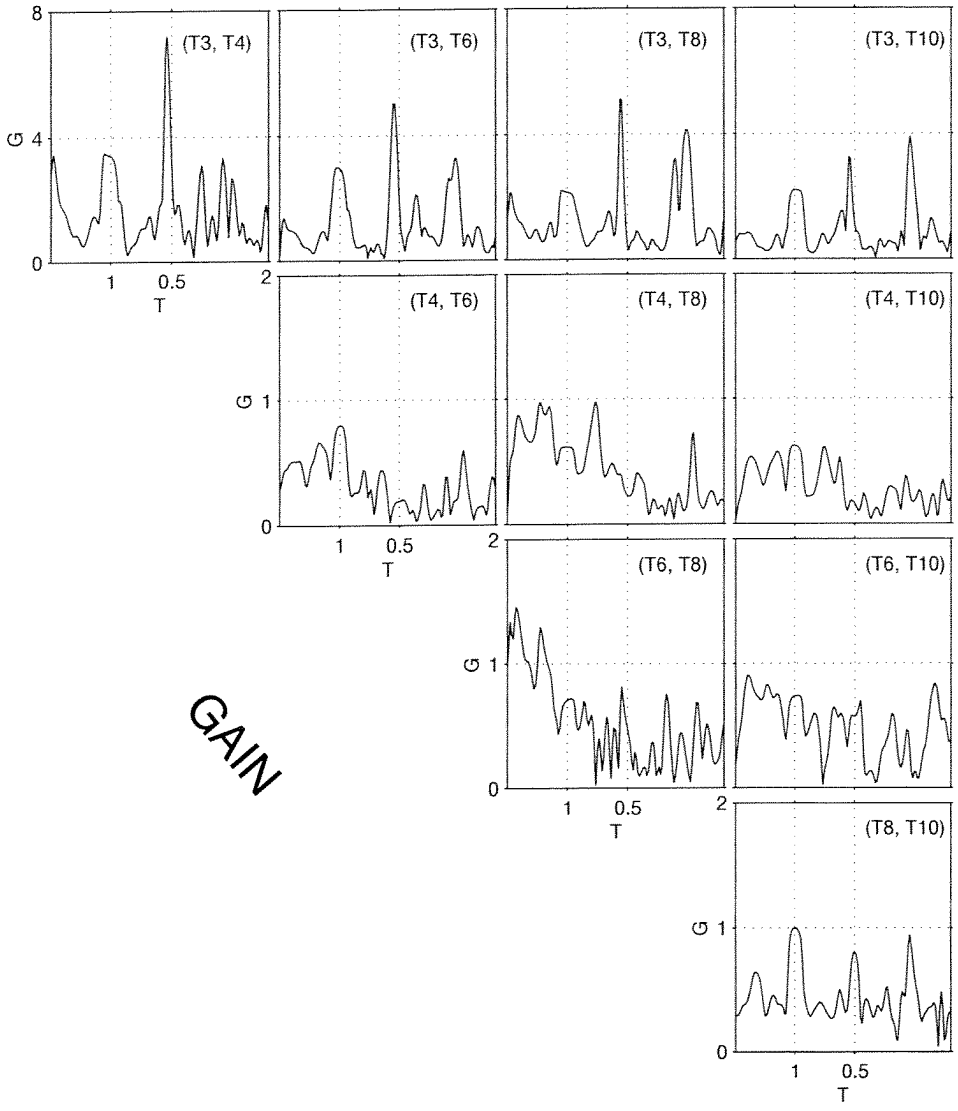

Fig. 10. Gain spectra for the temperature anomaly time series. The gain is given by G, and T is the period in days.

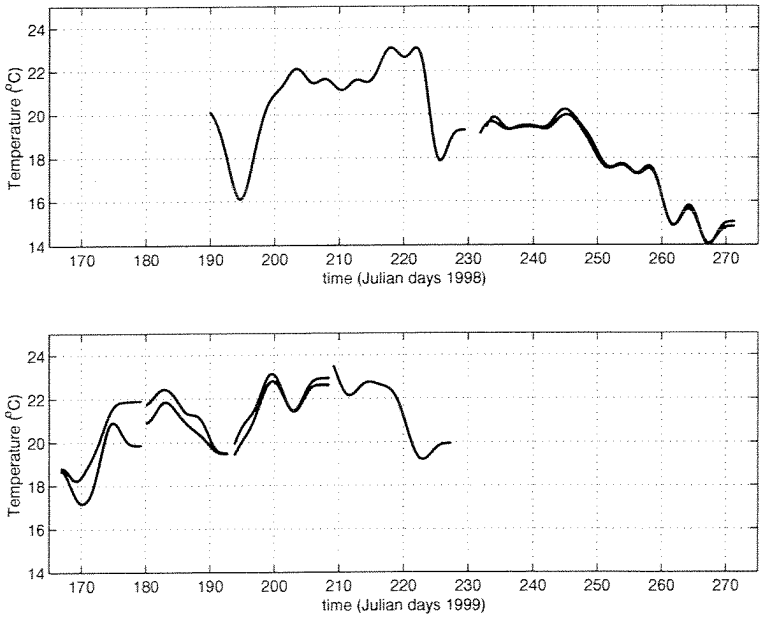

Fig. 11. Low frequency component of the SEACAT temperature series (surface and bottom) at site SC1 at the mouth of Winter Bay for 1998 and 1999.

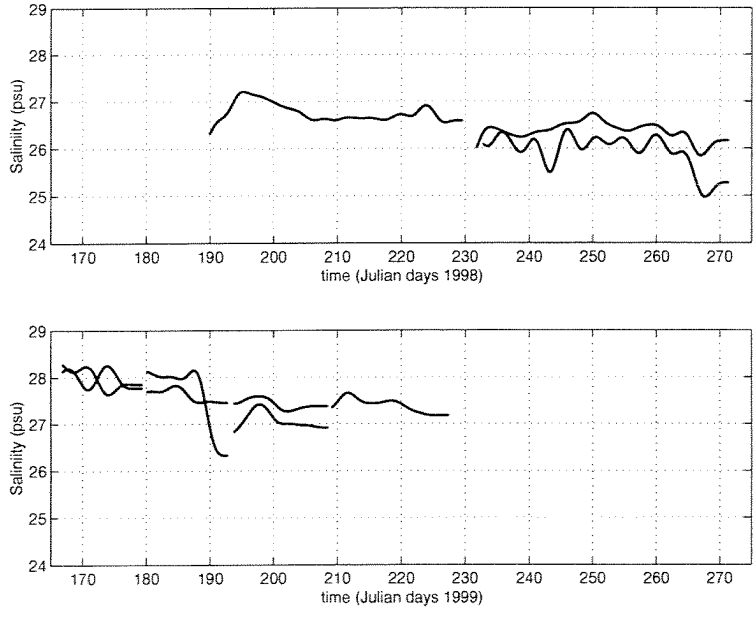

Fig. 12. Low frequency component of the SEACAT salinity time series (surface and bottom) at site SC1 at the mouth of Winter Bay for 1998 and 1999.

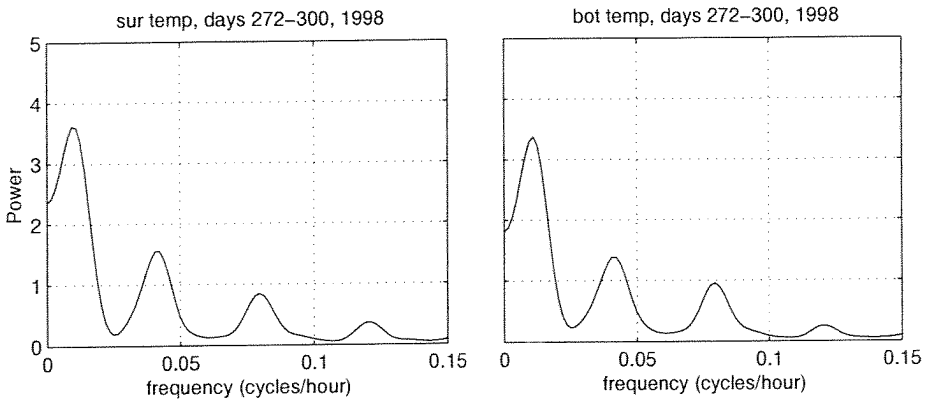

Fig. 13. Power spectral density of the surface and bottom temperature anomaly time series at site SC2 (entrance channel). Frequency is in units of cycles per hour (cph) and power has units $°C^2\ cph^{-1}$. The time period is given.

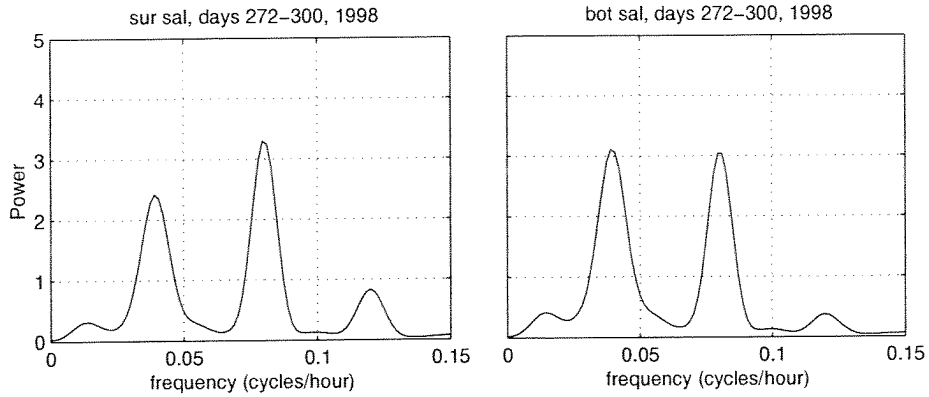

Fig. 14. Power spectral density of the surface and bottom salinity anomaly time series at site SC2 (entrance channel). Frequency is in units of cycles per hour (cph) and power has units $psu^2\ cph^{-1}$. The time period is given.

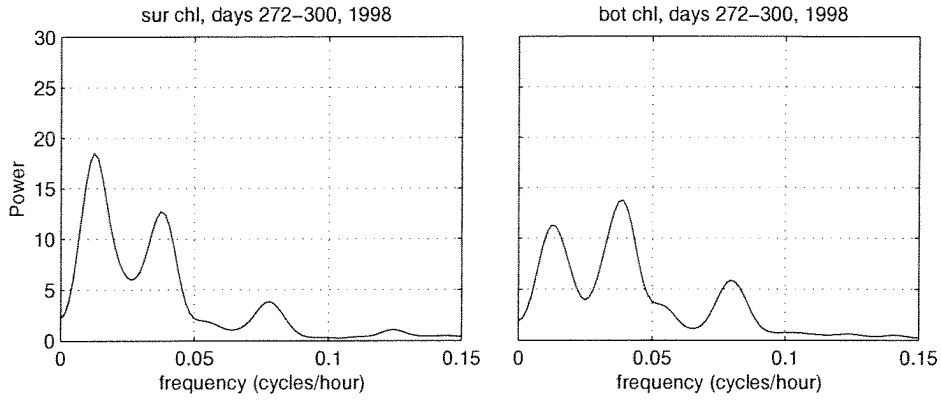

Fig. 15. Power spectral density of the surface and bottom chlorophyll anomaly time series at site SC2 (entrance channel). Frequency is in units of cycles per hour (cph) and power has units cph^{-1}. The time period is given.

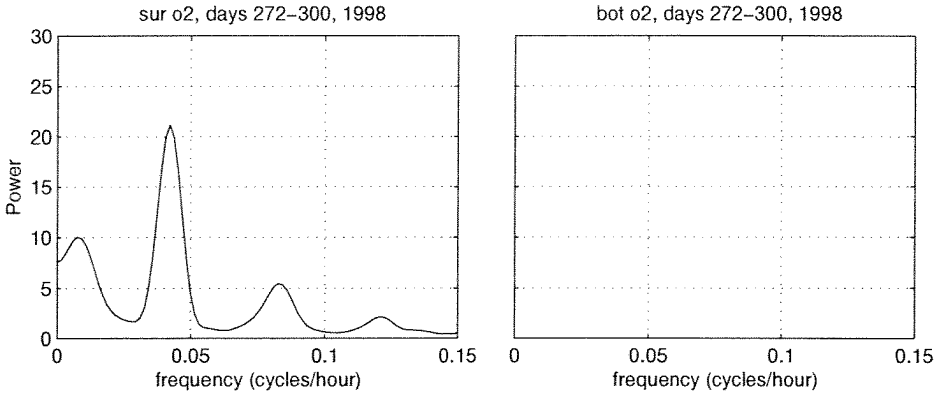

Fig. 16. Power spectral density of the surface and bottom oxygen anomaly time series at site SC2 (entrance channel). Frequency is in units of cycles per hour (cph) and power has units of cph^{-1}. The time period is given. Note that no oxygen data was available for the bottom deployment.

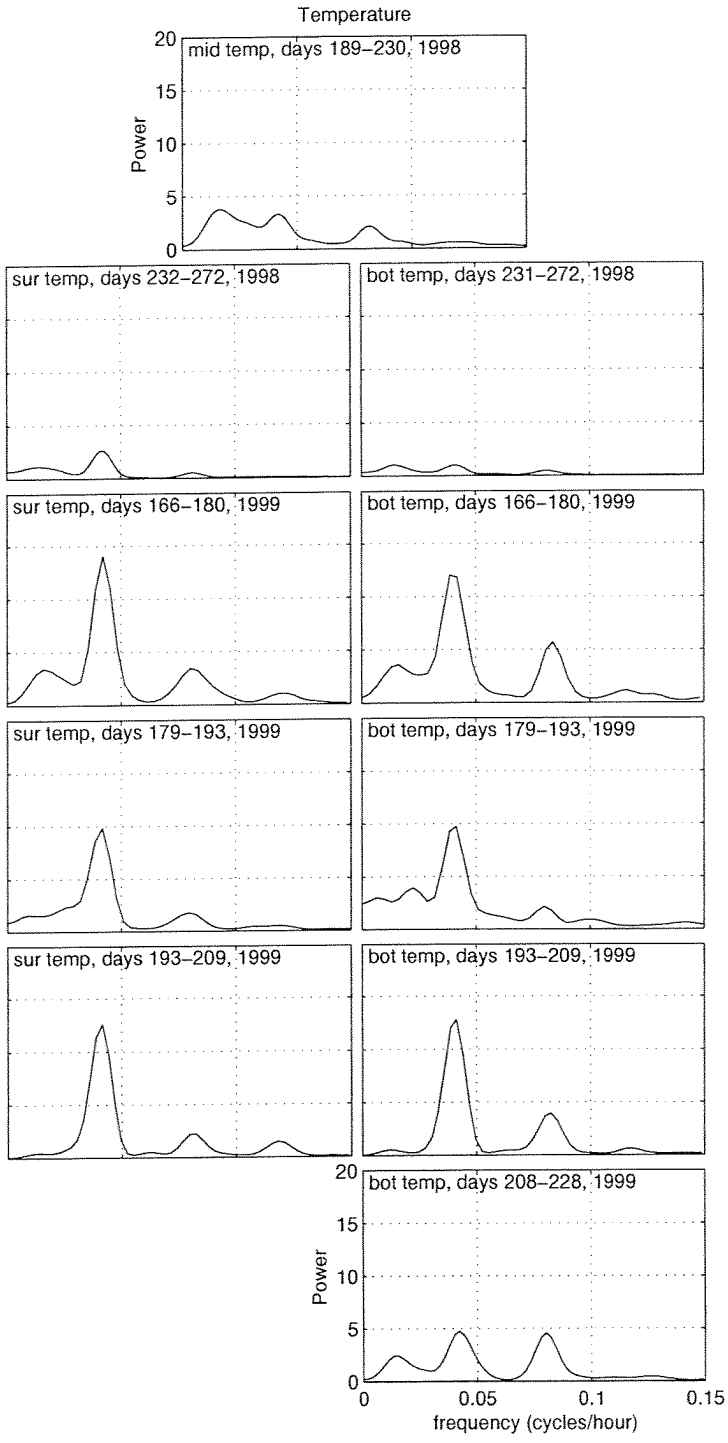

Fig. 17. Power spectral density of the temperature anomaly time series from site SC1 (the mouth of Winter Bay). The deployments are arranged chronologically from top to bottom with the time period given. Surface (left panels) and bottom (right panels) deployments are also indicated. Frequency is in units of cycles per hour (cph) and power has units of $°C^2\ cph^{-1}$.

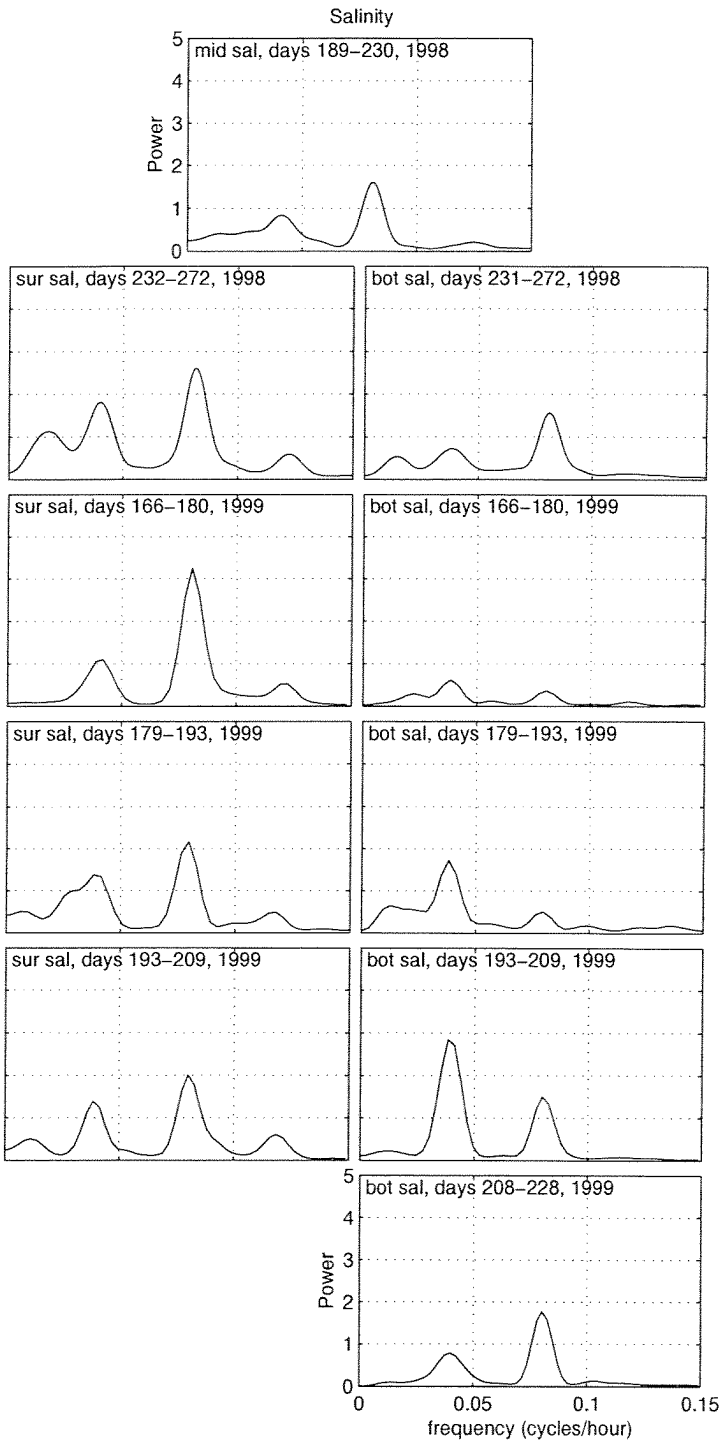

Fig. 18. Power spectral density of the salinity anomaly time series from site SC1 (the mouth of Winter Bay). The deployments are arranged chronologically from top to bottom with the time period given. Surface (left panels) and bottom (right panels) deployments are also indicated. Frequency is in units of cycles per hour (cph) and power has units of $psu^2\ cph^{-1}$.

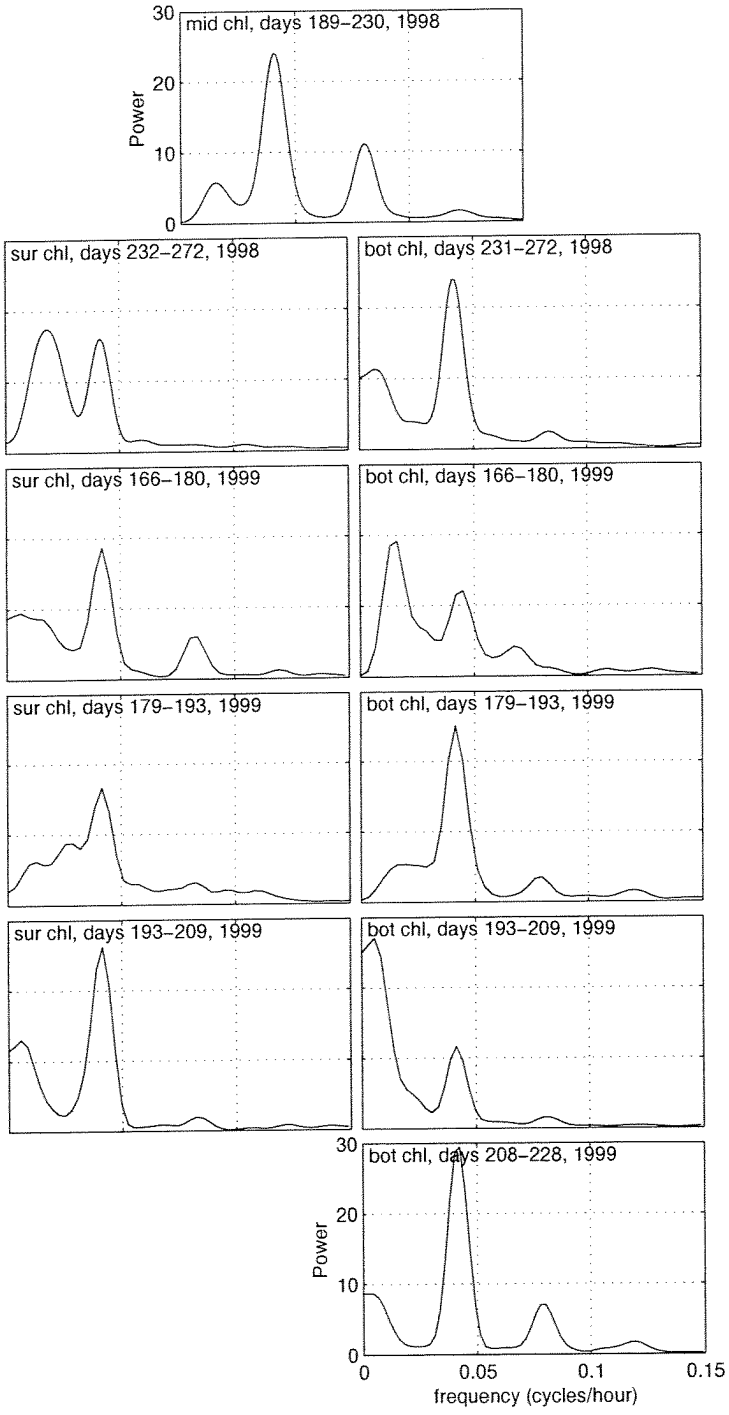

Fig. 19. Power spectral density of the chlorophyll anomaly time series from site SC1 (the mouth of Winter Bay). The deployments are arranged chronologically from top to bottom with the time period given. Surface (left panels) and bottom (right panels) deployments are also indicated. Frequency is in units of cycles per hour (cph) and power has units of cph^{-1}.

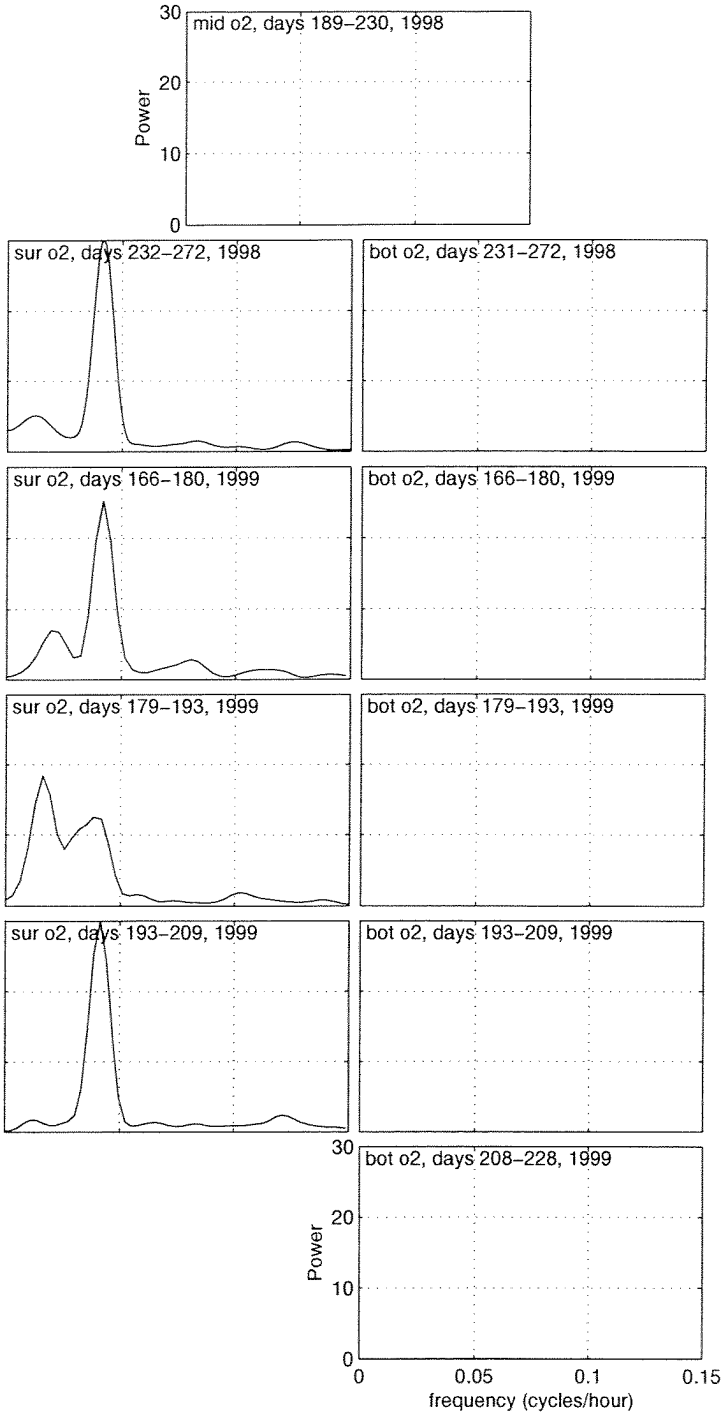

Fig. 20. Power spectral density of the oxygen anomaly time series from site SC1 (the mouth of Winter Bay). The deployments are arranged chronologically from top to bottom with the time period given. Surface (left panels) and bottom (right panels) deployments are also indicated. Frequency is in units of cycles per hour (cph) and power has units of cph^{-1}.

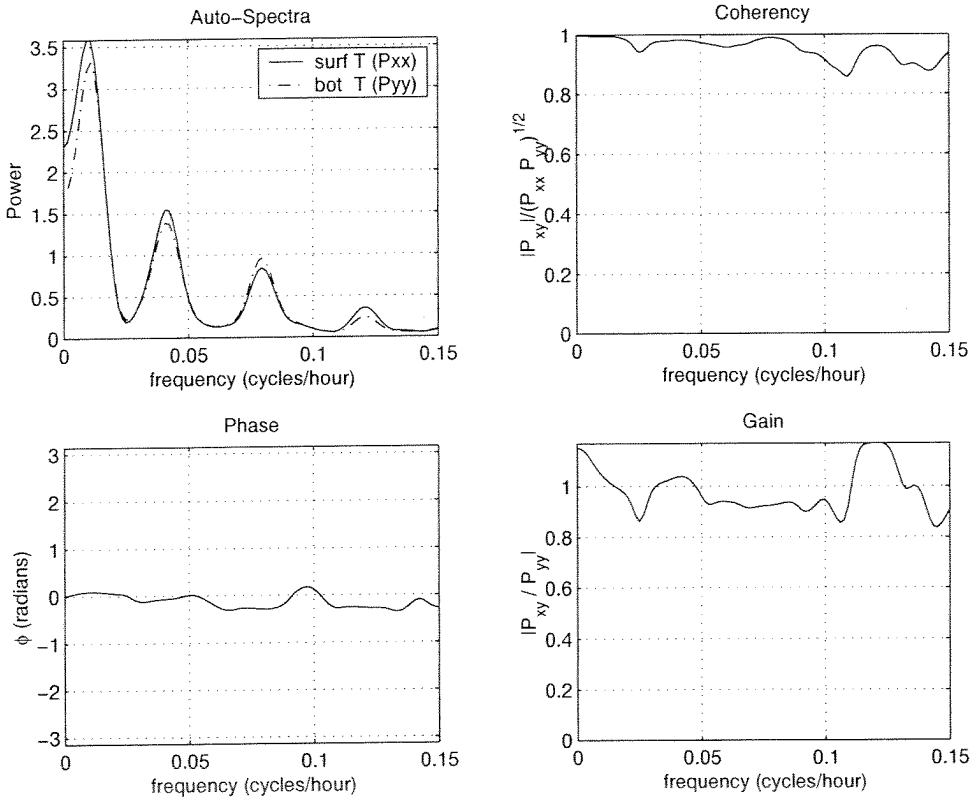

Fig. 21. Cross-spectral analysis of surface and bottom temperature time series from site SC2 for the period Julian days 272-300, 1998. Frequency is in units of cycles per hour (cph). The power spectral density for the two series is given by P_{xx} and P_{yy}, respectively. The cross-spectral density is given by P_{xy}. These have units $°C^2$ cph^{-1}. The phase ϕ is in radians.

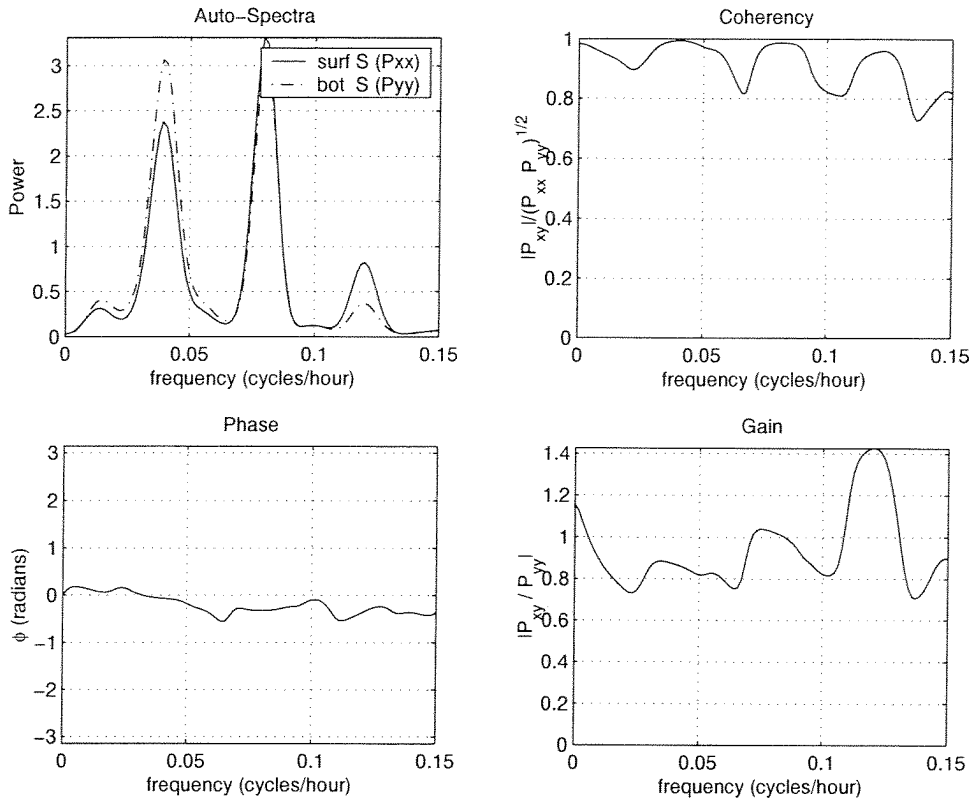

Fig. 22. Cross-spectral analysis of surface and bottom salinity time series from site SC2 for the period Julian days 272-300, 1998. Frequency is in units of cycles per hour (cph). The power spectral density for the two series is given by P_{xx} and P_{yy}, respectively. The cross-spectral density is given by P_{xy}. These have units psu^2 cph^{-1}. The phase ϕ is in radians.

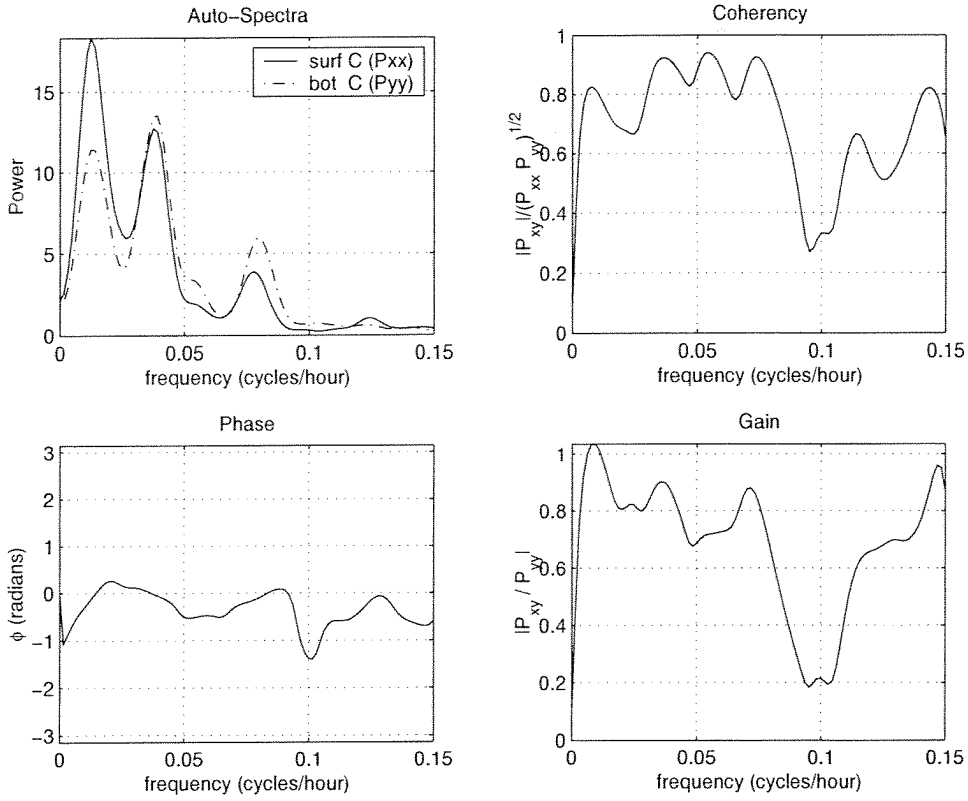

Fig. 23. Cross-spectral analysis of surface and bottom chlorophyll time series from site SC2 for the period Julian days 272-300, 1998. Frequency is in units of cycles per hour (cph). The power spectral density for the two series is given by P_{xx} and P_{yy}, respectively. The cross-spectral density is given by P_{xy}. These have units cph^{-1}. The phase ϕ is in radians.

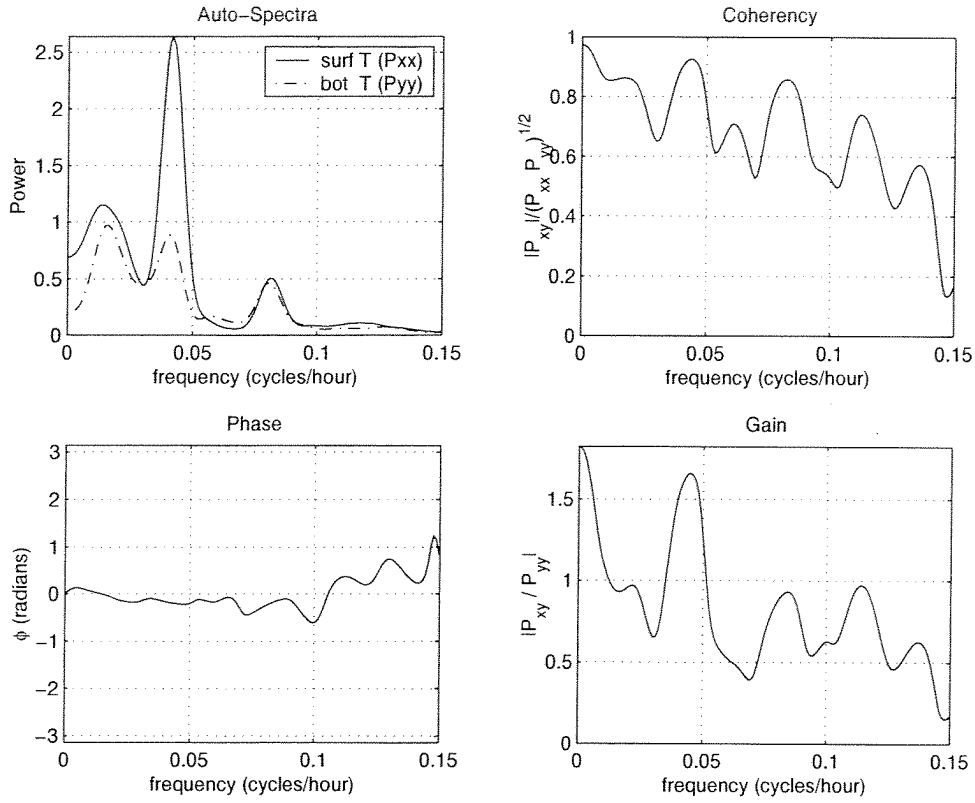

Fig. 24. Cross-spectral analysis of surface and bottom temperature time series from site SC1 for the period Julian days 232-272, 1998. Frequency is in units of cycles per hour (cph). The power spectral density for the two series is given by P_{xx} and P_{yy}, respectively. The cross-spectral density is given by P_{xy}. These have units $°C^2\ cph^{-1}$. The phase ϕ is in radians.

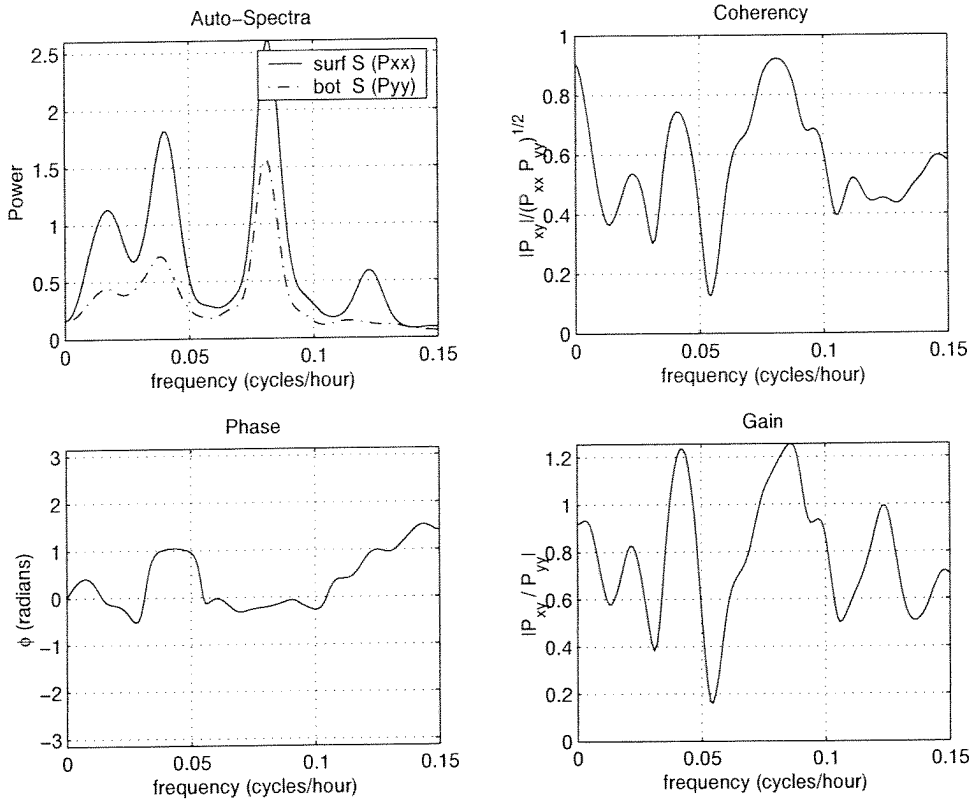

Fig. 25. Cross-spectral analysis of surface and bottom salinity time series from site SC1 for the period Julian days 232-272, 1998. Frequency is in units of cycles per hour (cph). The power spectral density for the two series is given by P_{xx} and P_{yy}, respectively. The cross-spectral density is given by P_{xy}. These have units psu^2 cph^{-1}. The phase ϕ is in radians.

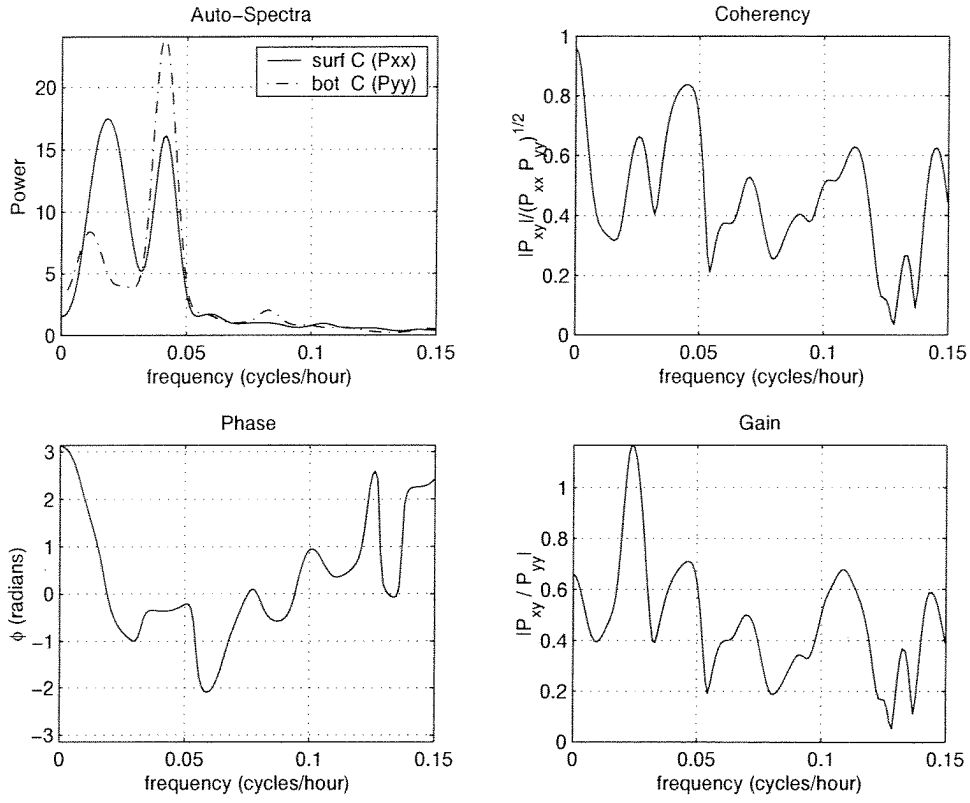

Fig. 26. Cross-spectral analysis of surface and bottom chlorophyll time series from site SC1 for the period Julian days 232-272, 1998. Frequency is in units of cycles per hour (cph). The power spectral density for the two series is given by P_{xx} and P_{yy}, respectively. The cross-spectral density is given by P_{xy}. These have units cph^{-1}. The phase ϕ is in radians.

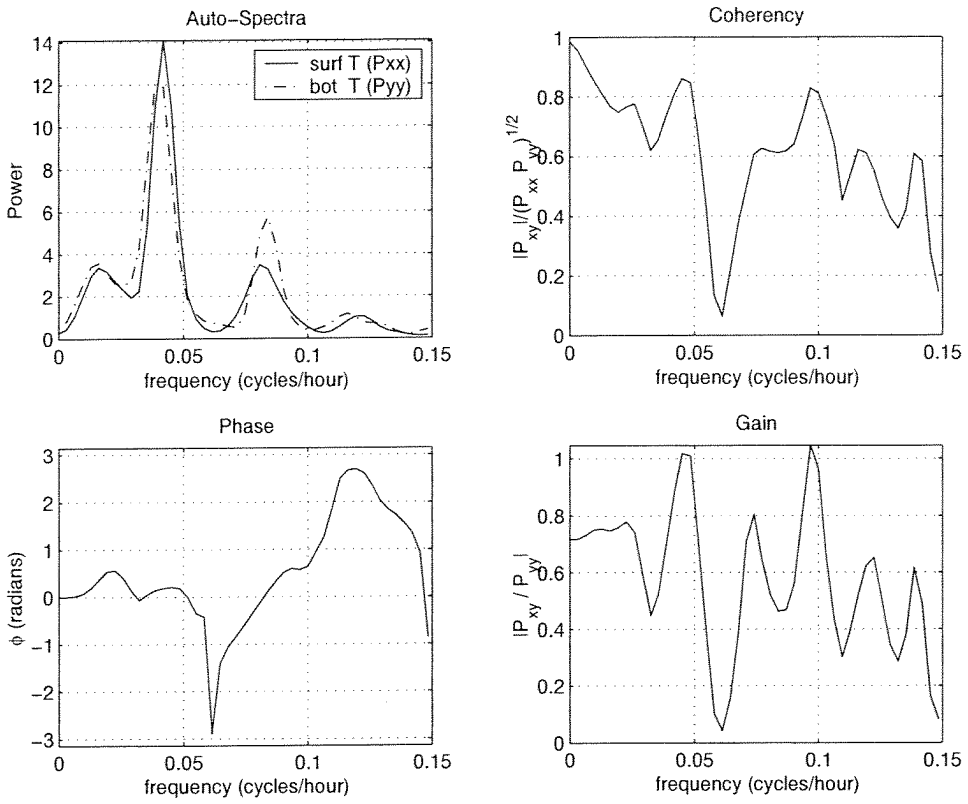

Fig. 27. Cross-spectral analysis of surface and bottom temperature time series from site SC1 for the period Julian days 166-180, 1999. Frequency is in units of cycles per hour (cph). The power spectral density for the two series is given by P_{xx} and P_{yy}, respectively. The cross-spectral density is given by P_{xy}. These have units $°C^2\ cph^{-1}$. The phase ϕ is in radians.

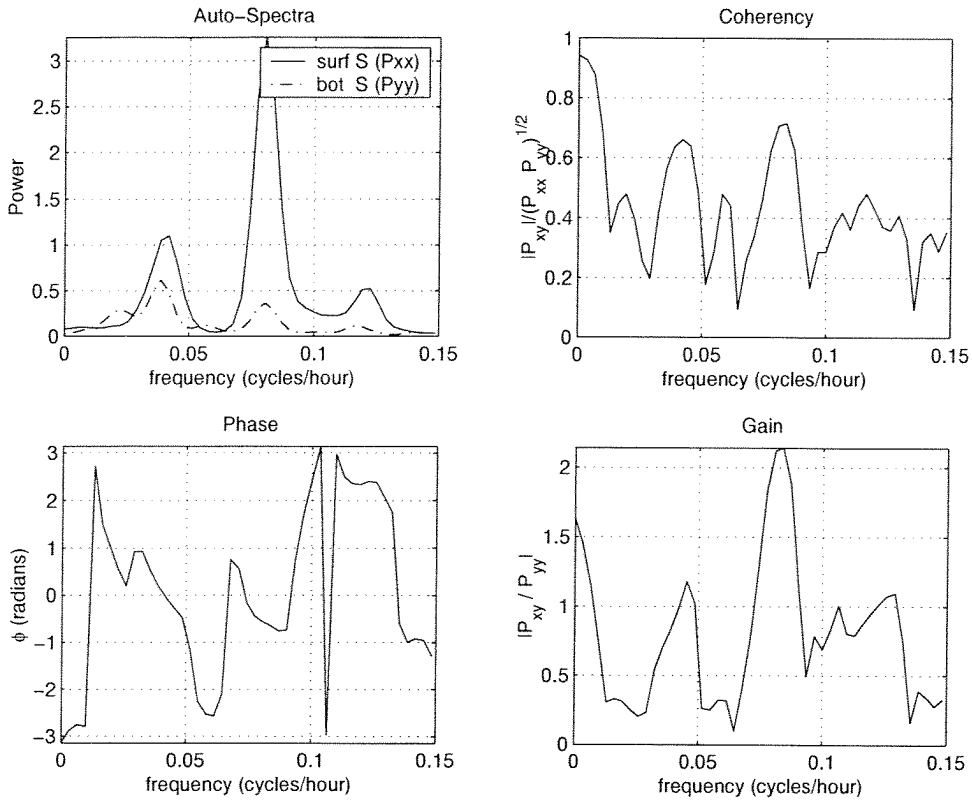

Fig. 28. Cross-spectral analysis of surface and bottom salinity time series from site SC1 for the period Julian days 166-180, 1999. Frequency is in units of cycles per hour (cph). The power spectral density for the two series is given by P_{xx} and P_{yy}, respectively. The cross-spectral density is given by P_{xy}. These have units psu^2 cph^{-1}. The phase ϕ is in radians.

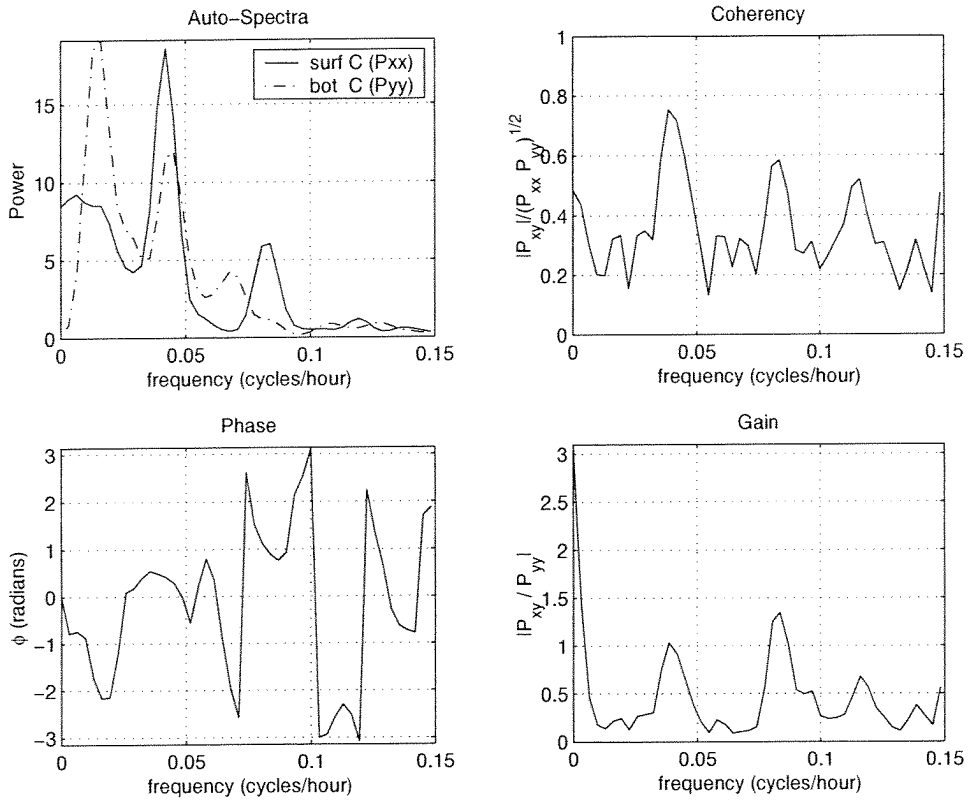

Fig. 29. Cross-spectral analysis of surface and bottom chlorophyll time series from site SC1 for the period Julian days 166-180, 1999. Frequency is in units of cycles per hour (cph). The power spectral density for the two series is given by P_{xx} and P_{yy}, respectively. The cross-spectral density is given by P_{xy}. These have units cph^{-1}. The phase ϕ is in radians.

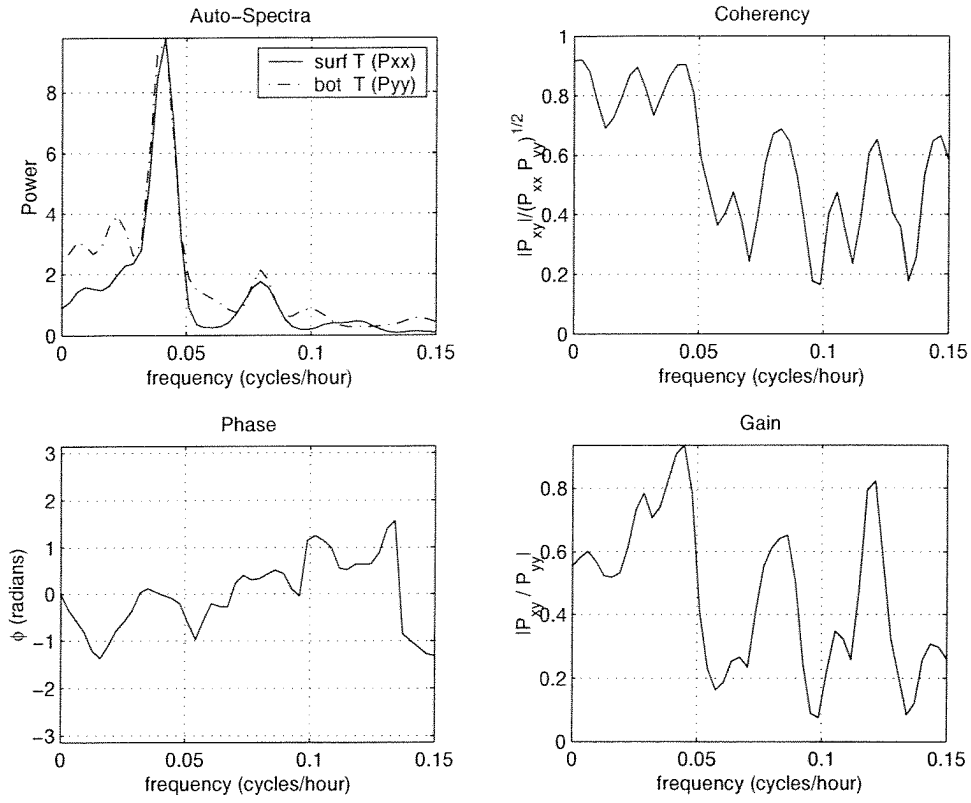

Fig. 30. Cross-spectral analysis of surface and bottom temperature time series from site SC1 for the period Julian days 173-193, 1999. Frequency is in units of cycles per hour (cph). The power spectral density for the two series is given by P_{xx} and P_{yy}, respectively. The cross-spectral density is given by P_{xy}. These have units $°C^2$ cph^{-1}. The phase ϕ is in radians.

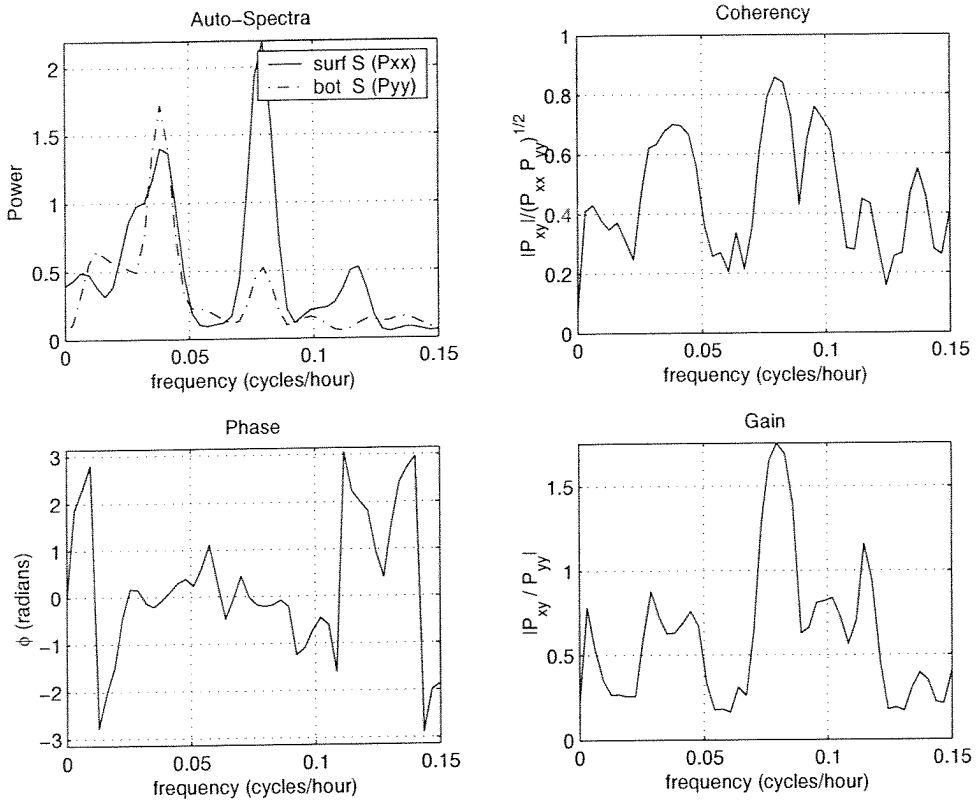

Fig. 31. Cross-spectral analysis of surface and bottom salinity time series from site SC1 for the period Julian days 179-193, 1999. Frequency is in units of cycles per hour (cph). The power spectral density for the two series is given by P_{xx} and P_{yy}, respectively. The cross-spectral density is given by P_{xy}. These have units $psu^2\ cph^{-1}$. The phase ϕ is in radians.

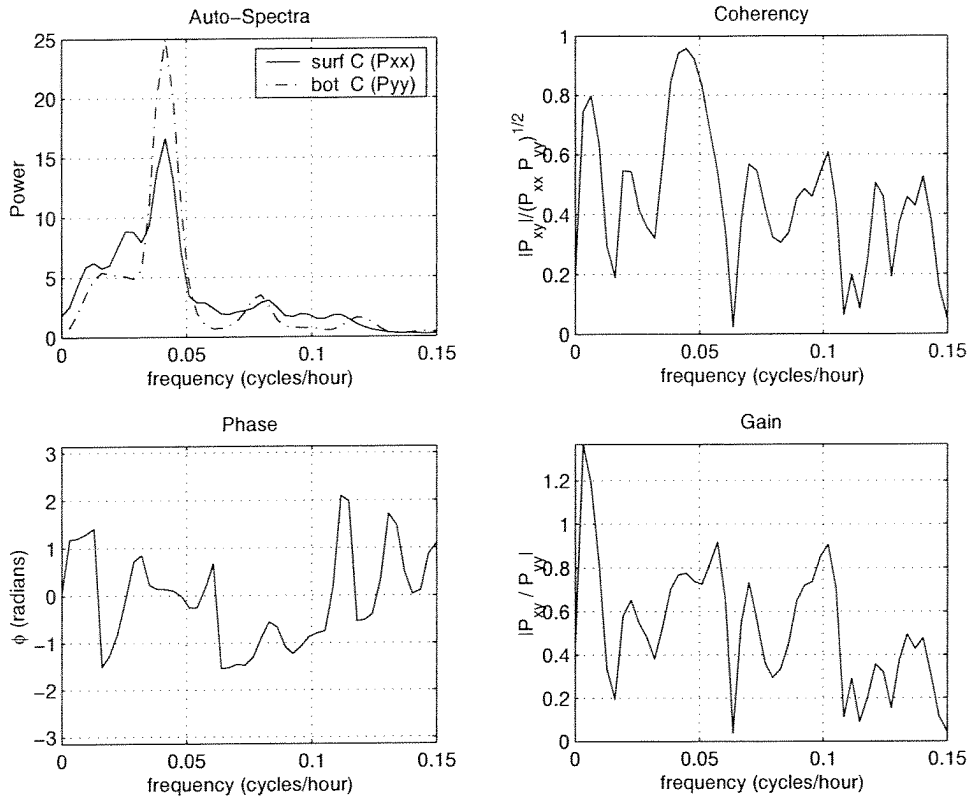

Fig. 32. Cross-spectral analysis of surface and bottom chlorophyll time series from site SC1 for the period Julian days 179-193, 1999. Frequency is in units of cycles per hour (cph). The power spectral density for the two series is given by P_{xx} and P_{yy}, respectively. The cross-spectral density is given by P_{xy}. These have units cph^{-1}. The phase ϕ is in radians.

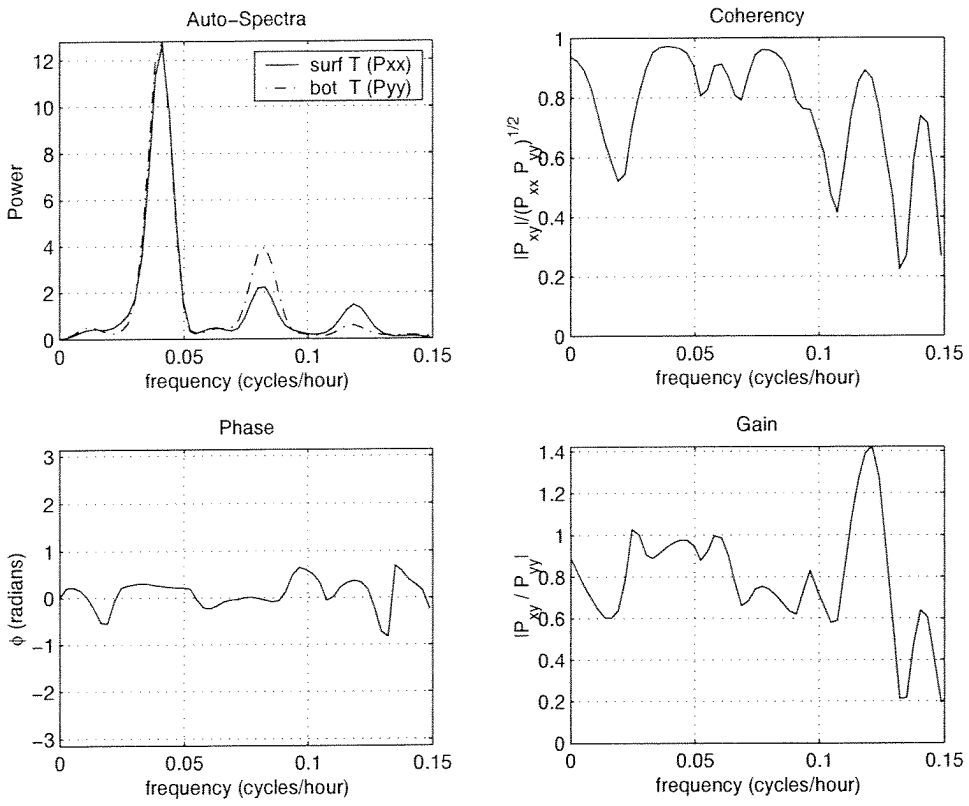

Fig. 33. Cross-spectral analysis of surface and bottom temperature time series from site SC1 for the period Julian days 193-209, 1999. Frequency is in units of cycles per hour (cph). The power spectral density for the two series is given by P_{xx} and P_{yy}, respectively. The cross-spectral density is given by P_{xy}. These have units $°C^2$ cph^{-1}. The phase ϕ is in radians

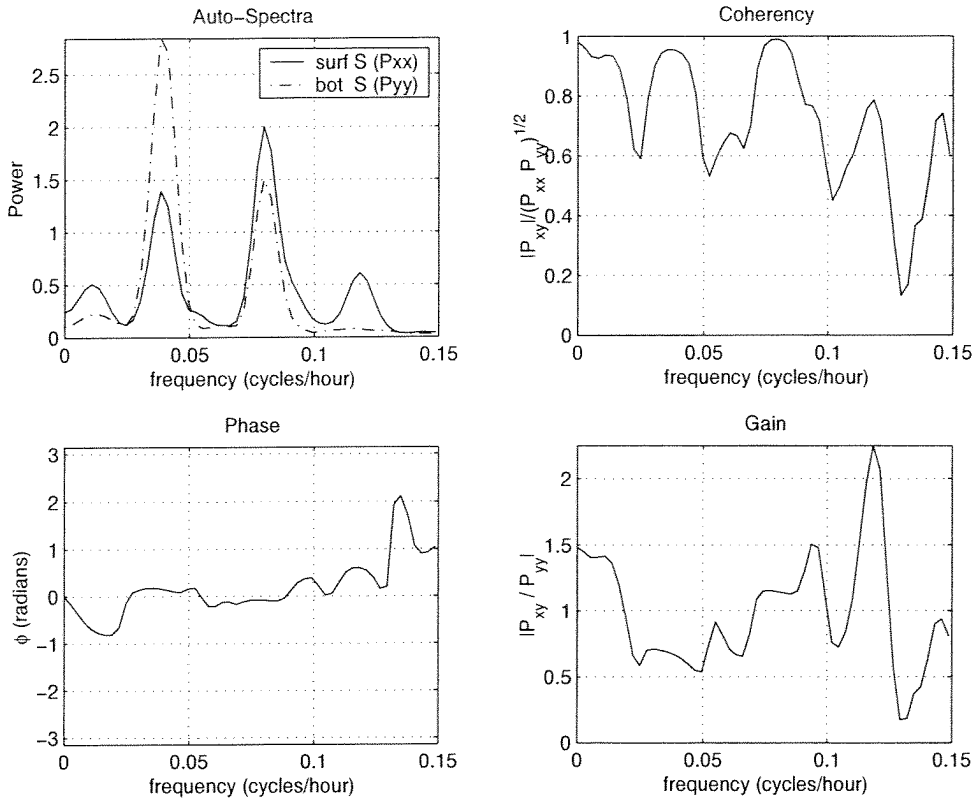

Fig. 34. Cross-spectral analysis of surface and bottom salinity time series from site SC1 for the period Julian days 193-209, 1999. Frequency is in units of cycles per hour (cph). The power spectral density for the two series is given by P_{xx} and P_{yy}, respectively. The cross-spectral density is given by P_{xy}. These have units psu^2 cph^{-1}. The phase ϕ is in radians.

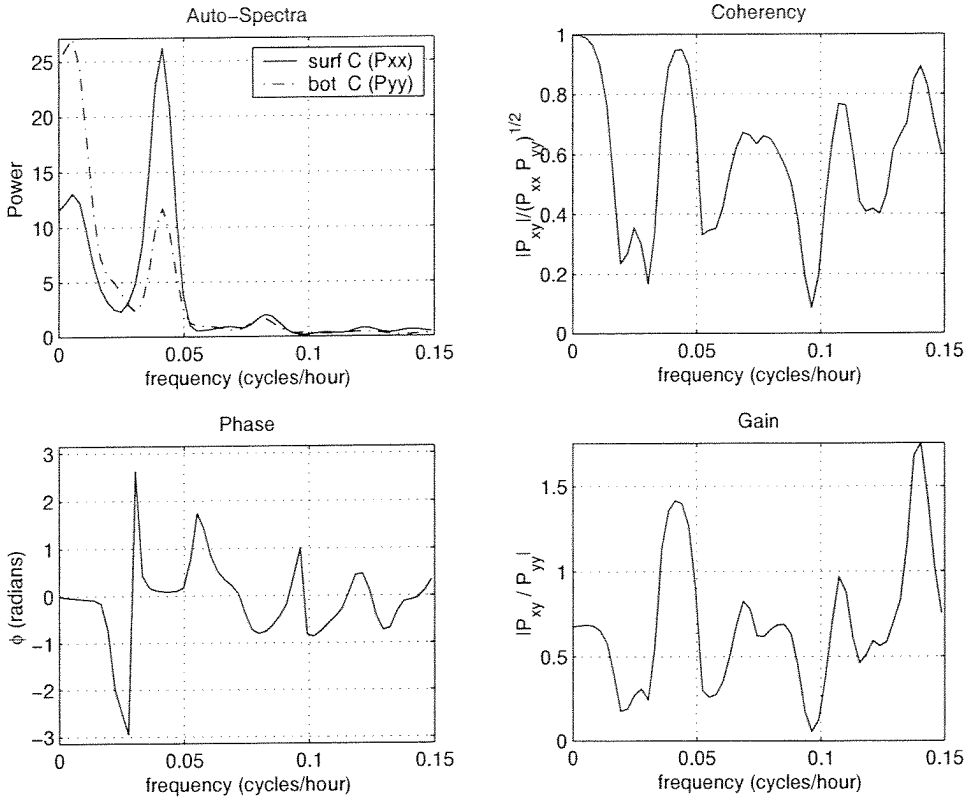

Fig. 35. Cross-spectral analysis of surface and bottom chlorophyll time series from site SC1 for the period Julian days 193-209, 1999. Frequency is in units of cycles per hour (cph). The power spectral density for the two series is given by P_{xx} and P_{yy}, respectively. The cross-spectral density is given by P_{xy}. These have units cph^{-1}. The phase ϕ is in radians.

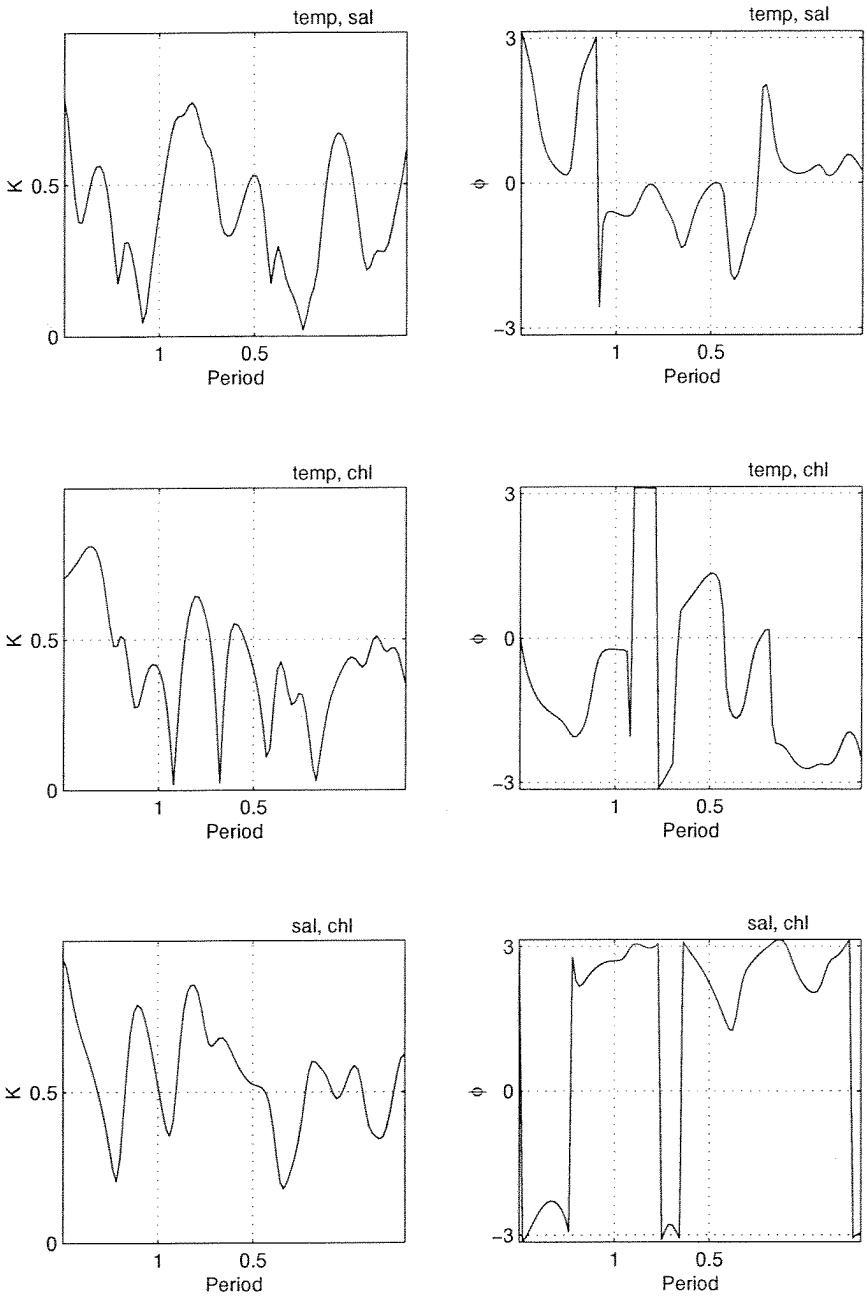

Fig. 36. Cross-spectral analysis for a surface deployment at site SC2 on Julian days 272-300, 1998. Coherency, K, and phase, ϕ, spectra are given with the analysis variables indicated above each panel. The period is reported in days and phase is in radians.

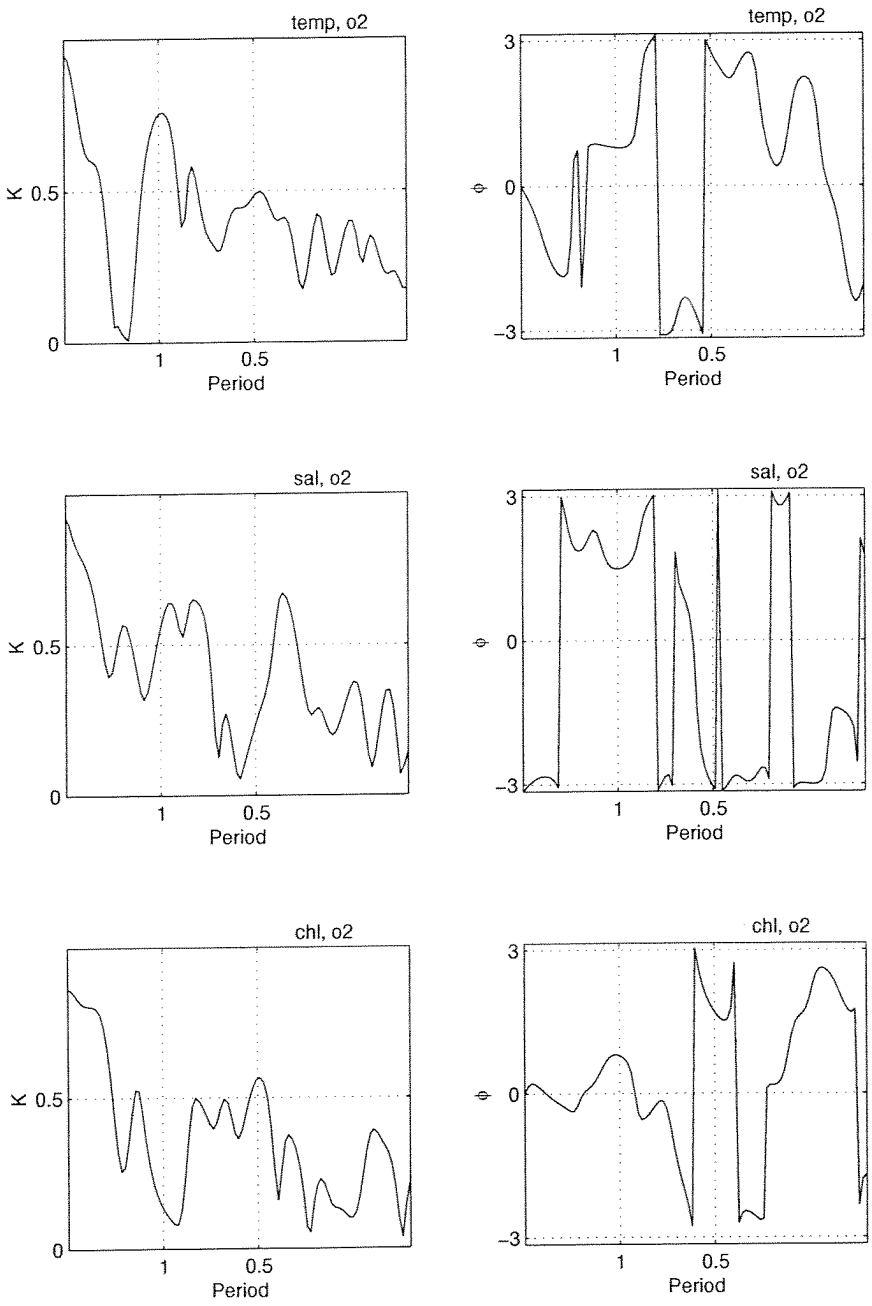

Fig. 36. (continued).

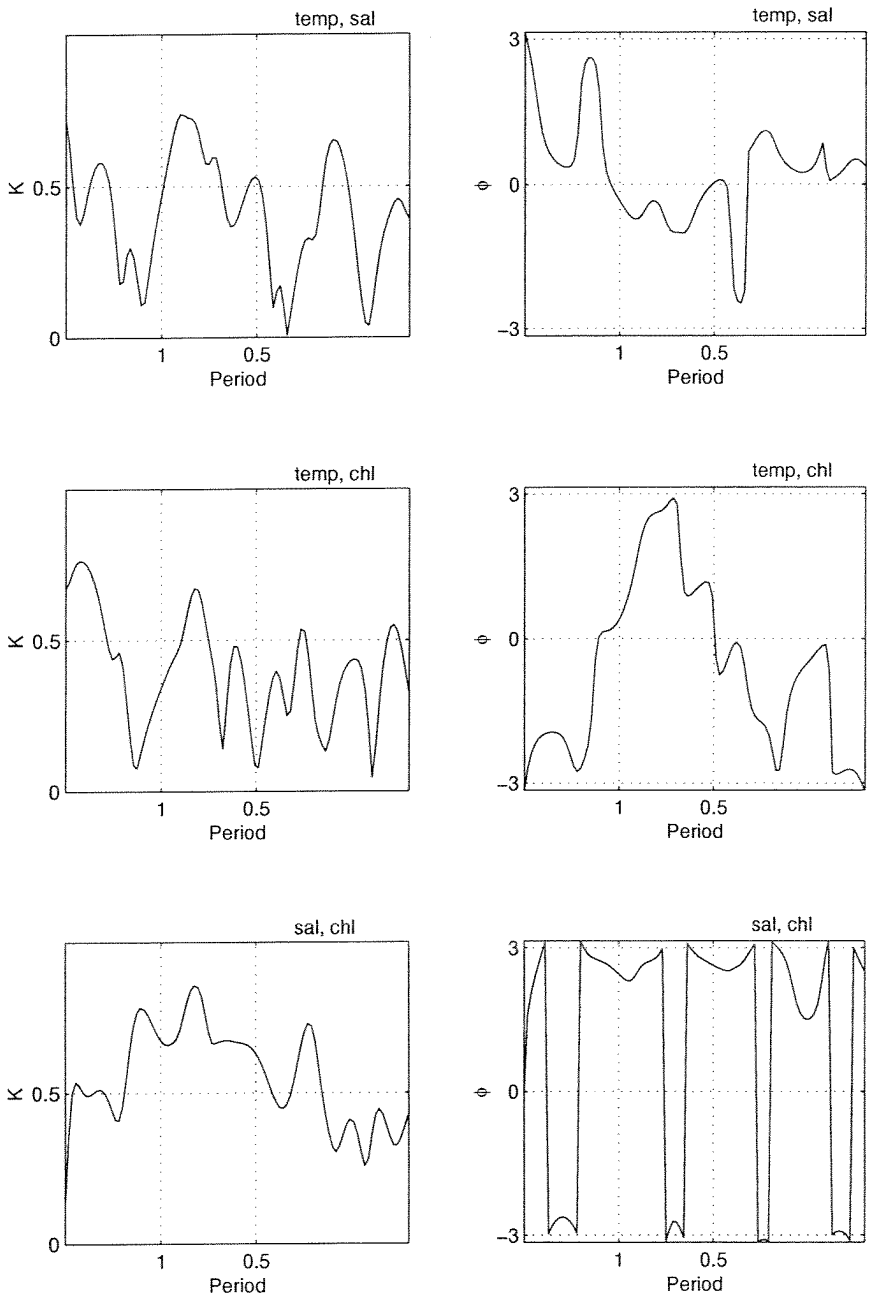

Fig. 37. Cross-spectral analysis for the bottom deployment at site SC2 on Julian days 272-300, 1998. Coherency, K, and phase, ϕ, spectra are given, with the analysis variables indicated above each panel. The period is reported in days and phase is in radians.

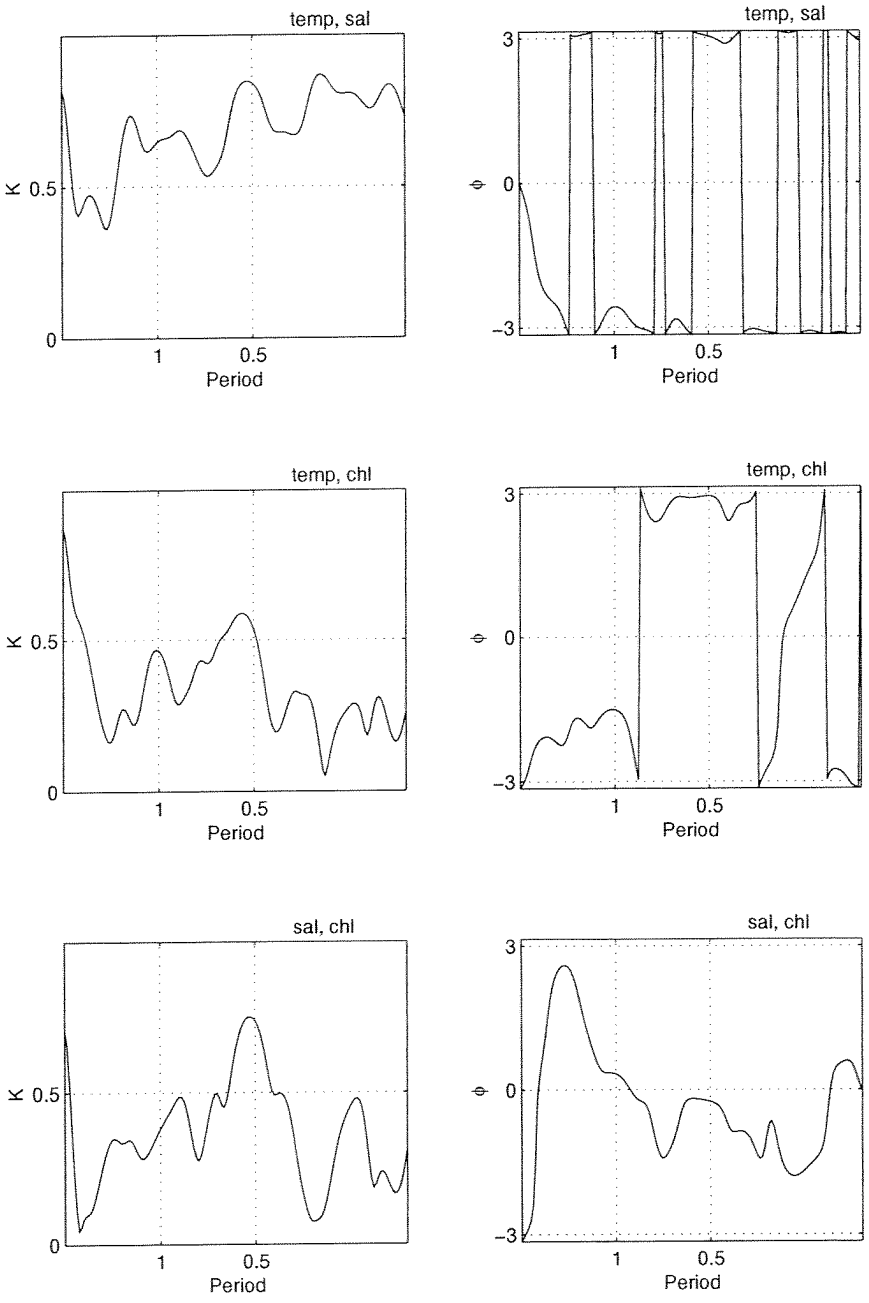

Fig. 38. Cross-spectral analysis for mid-depth deployment at site SC1 on Julian days 189-230, 1998. Coherency, K, and phase, ϕ, spectra are given, with the analysis variables indicated above each panel. The period is reported in days and phase is in radians.

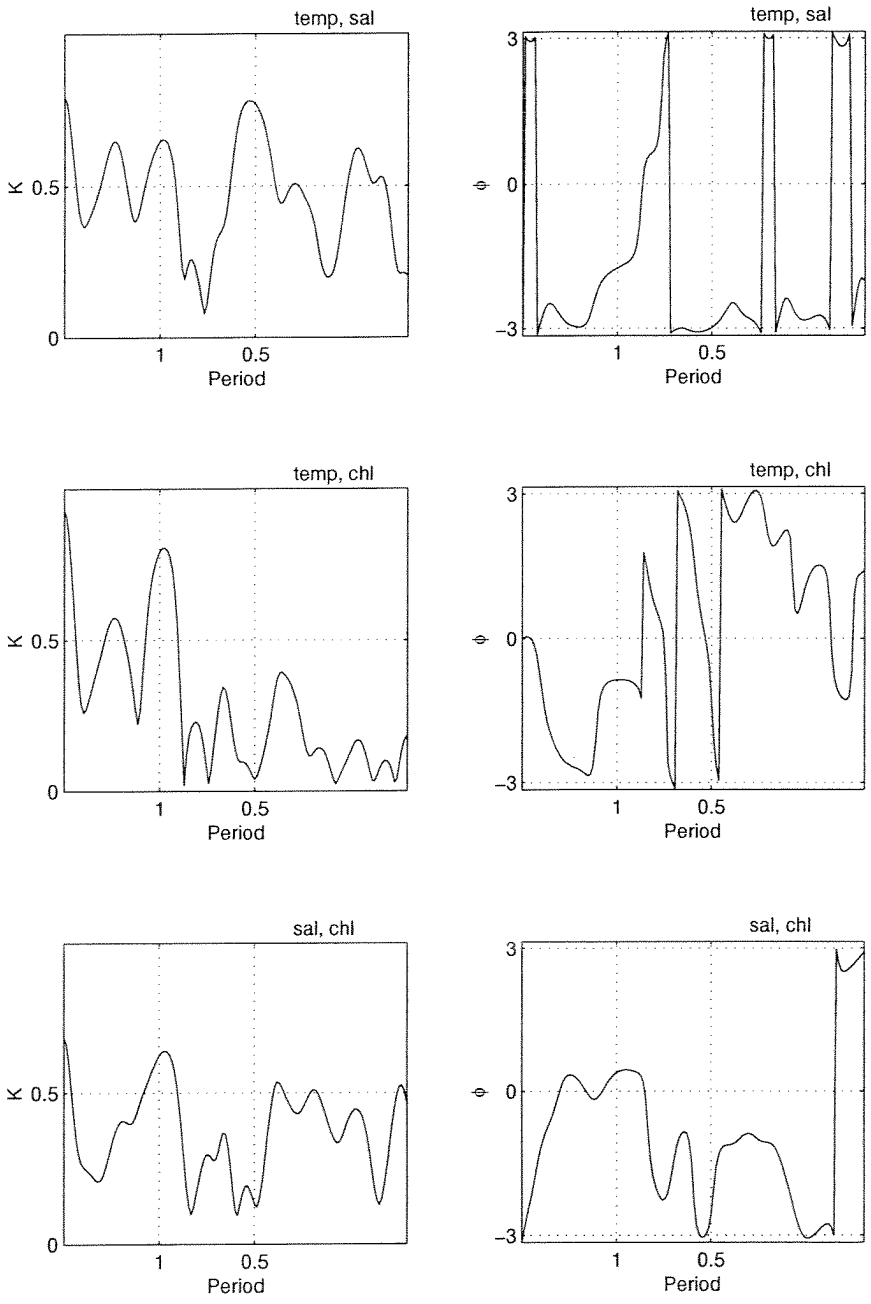

Fig. 39. Cross-spectral analysis for the surface deployment at site SC1 (Winter Bay) on Julian days 232-272, 1998. Coherency, K, and phase, ϕ, spectra are given, with the analysis variables indicated above each panel. The period is reported in days and phase is in radians.

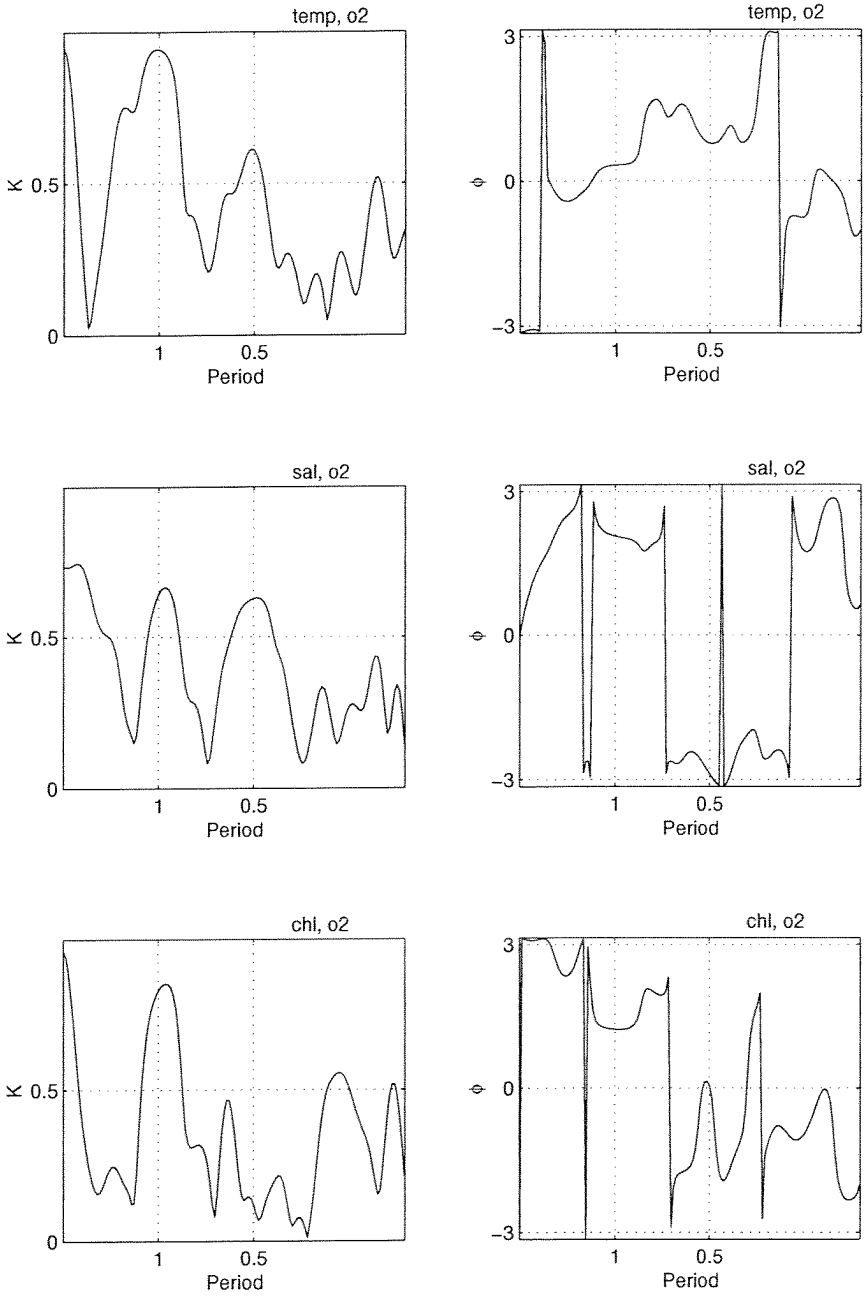

Fig. 39. (continued).

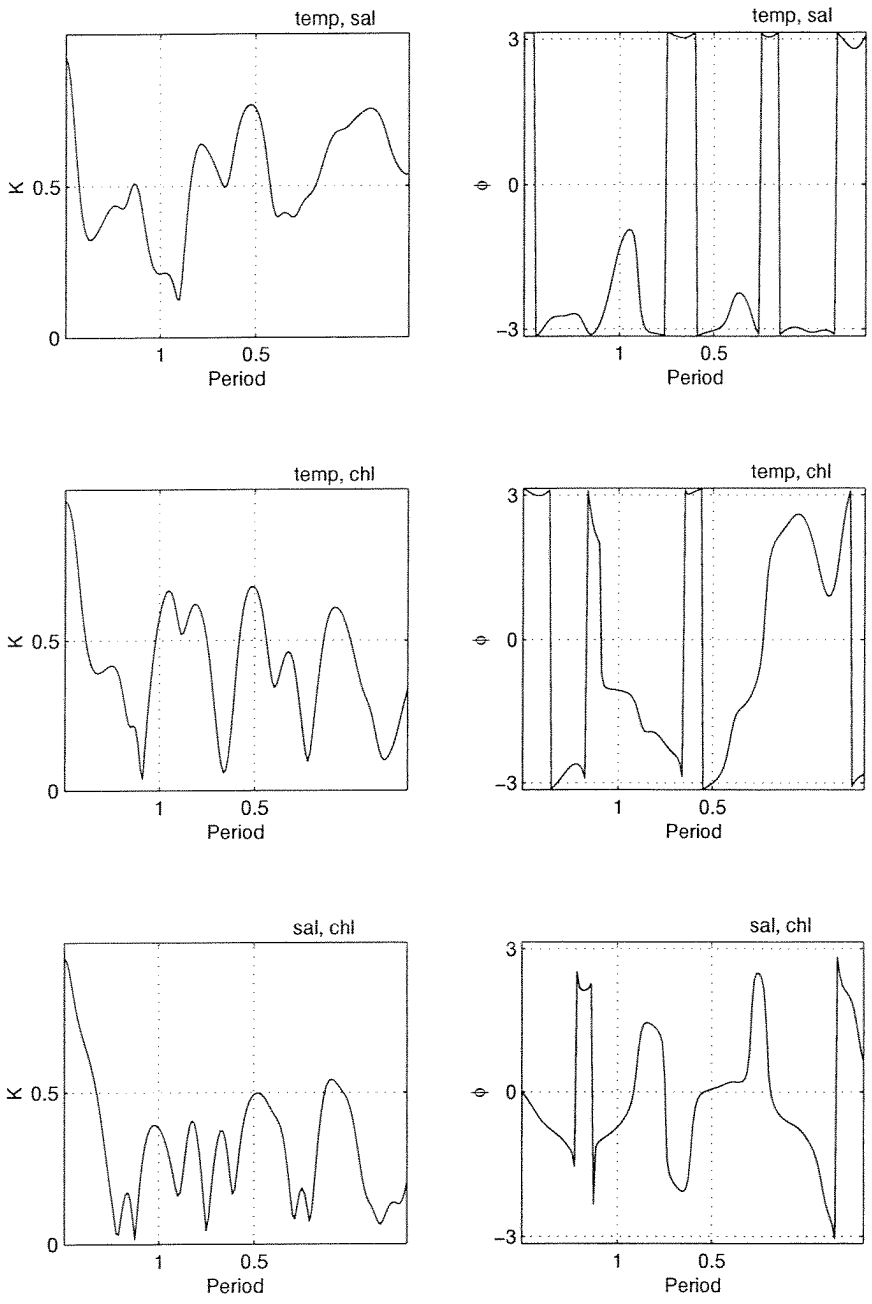

Fig. 40. Cross-spectral analysis for the bottom deployment at site SC1 (Winter Bay) on Julian days 231-272, 1998. Coherency, K, and phase, ϕ, spectra are given, with the analysis variables indicated above each panel. The period is reported in days and phase is in radians.

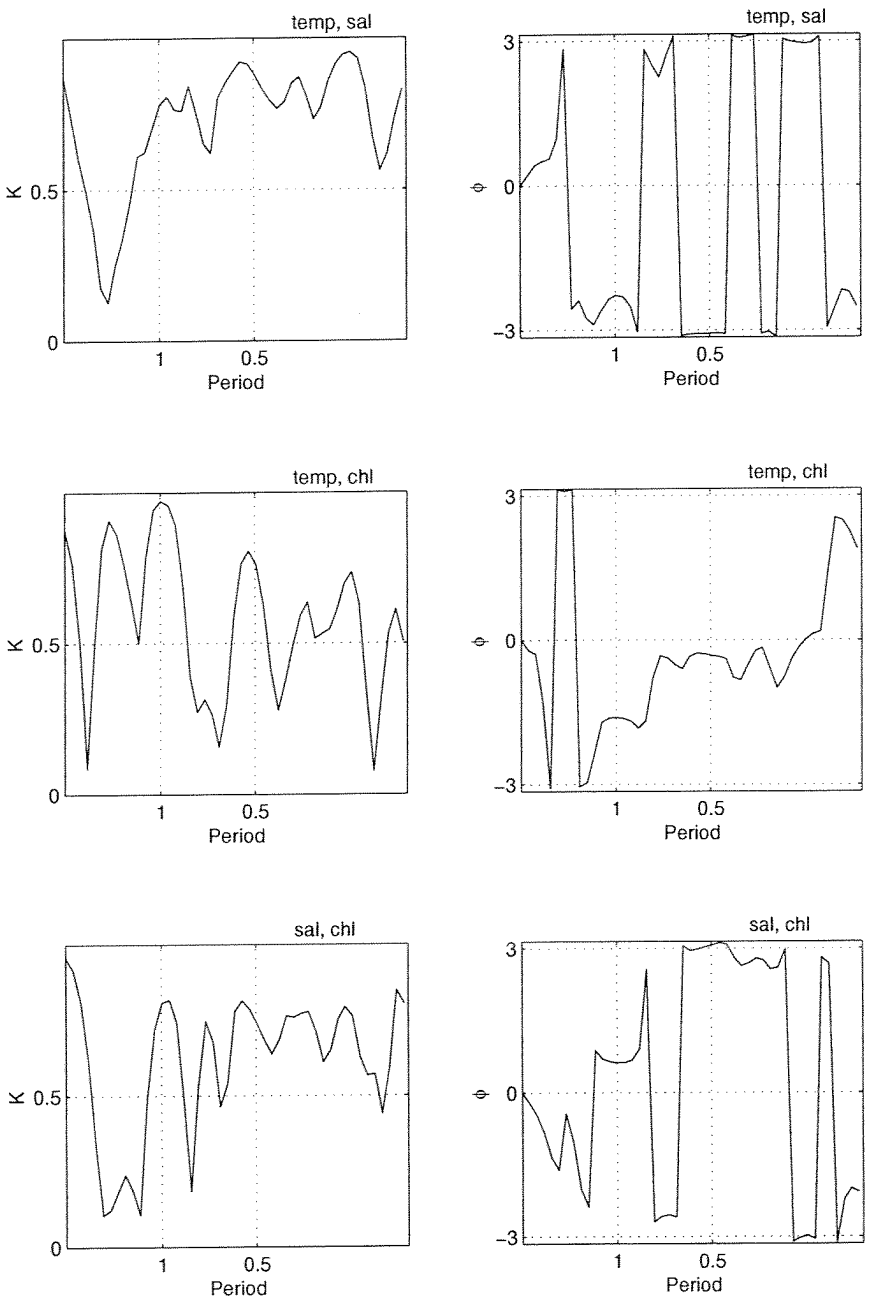

Fig. 41. Cross-spectral analysis for the surface deployment at site SC1 (Winter Bay) on Julian days 166-180, 1999. Coherency, K, and phase, ϕ, spectra are given, with the analysis variables indicated above each panel. The period is reported in days and phase is in radians.

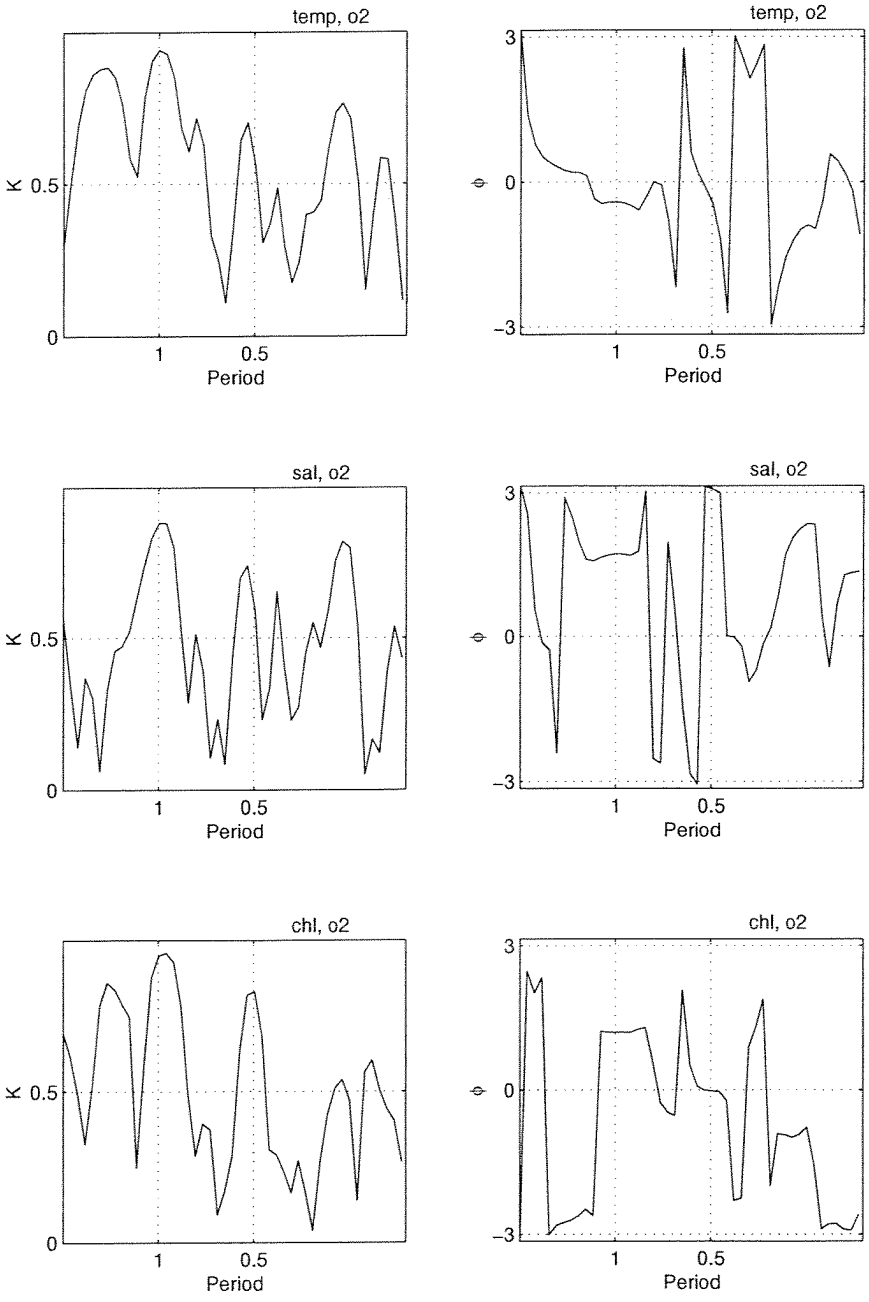

Fig. 41. (continued).

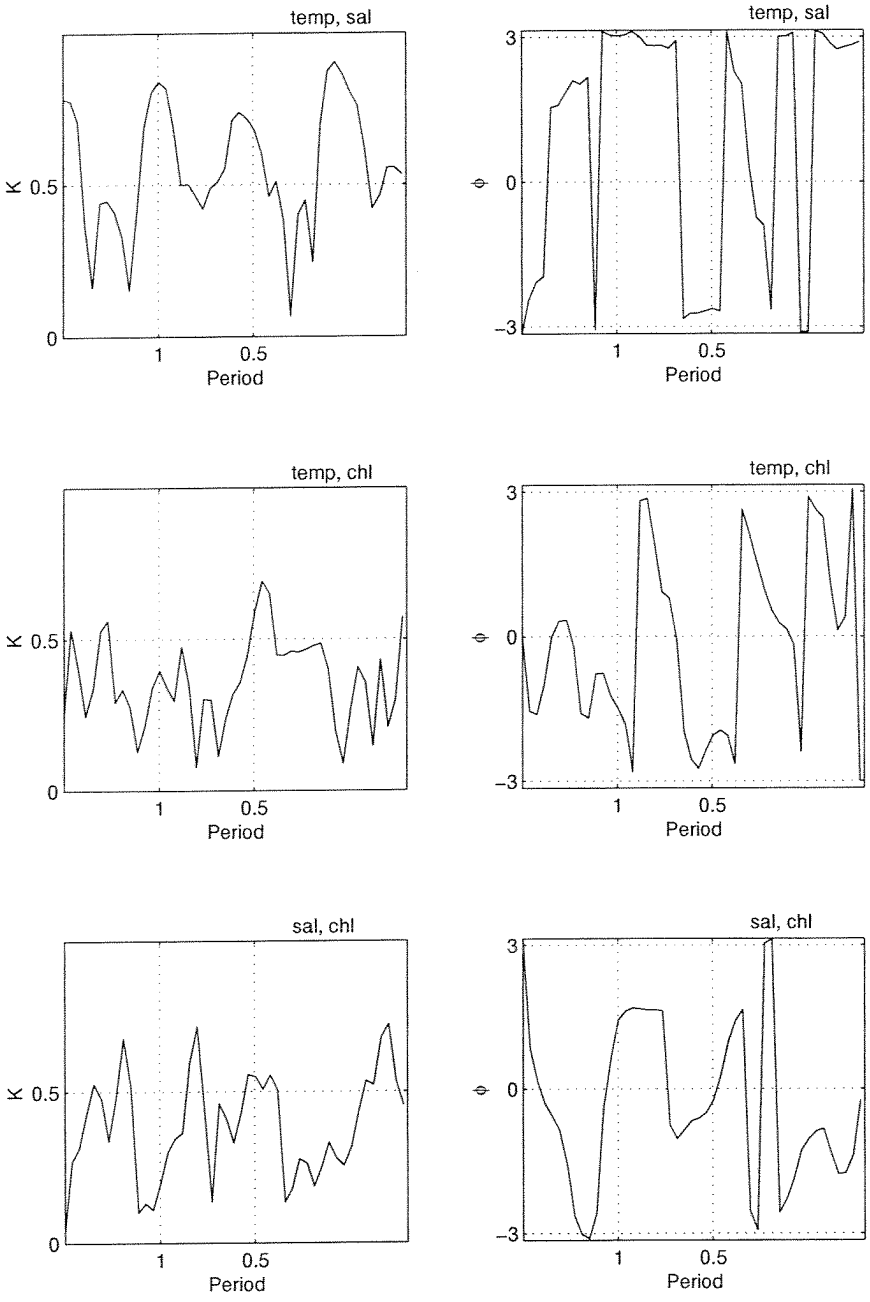

Fig. 42. Cross-spectral analysis the bottom deployment at site SC1 (Winter Bay) on Julian days 166-180, 1999. Coherency, K, and phase, ϕ, spectra are given, with the analysis variables indicated above each panel. The period is reported in days and phase is in radians.

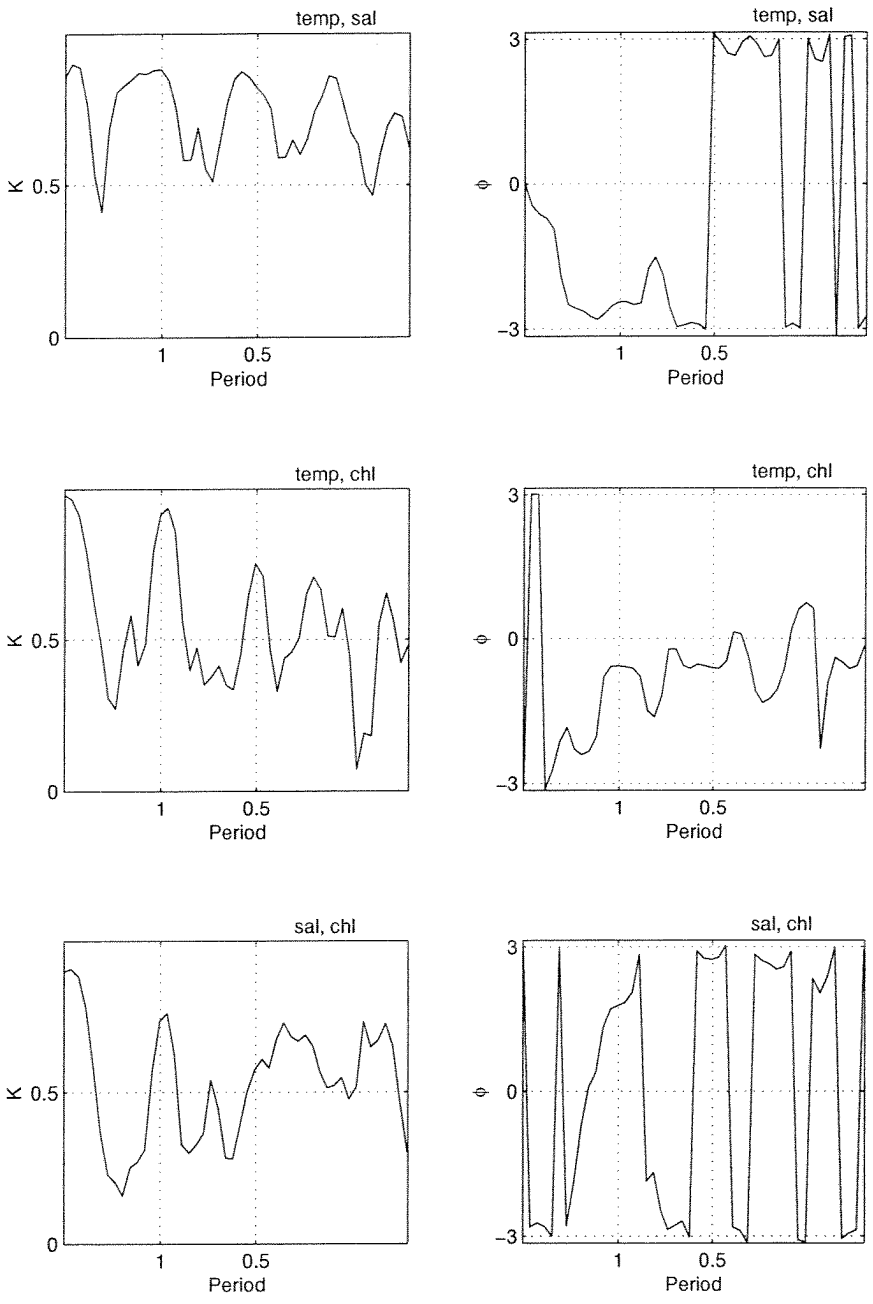

Fig. 43. Cross-spectral analysis for the surface deployment at site SC1 (Winter Bay) on Julian days 179-193, 1999. Coherency, K, and phase, ϕ, spectra are given, with the analysis variables indicated above each panel. The period is reported in days and phase is in radians.

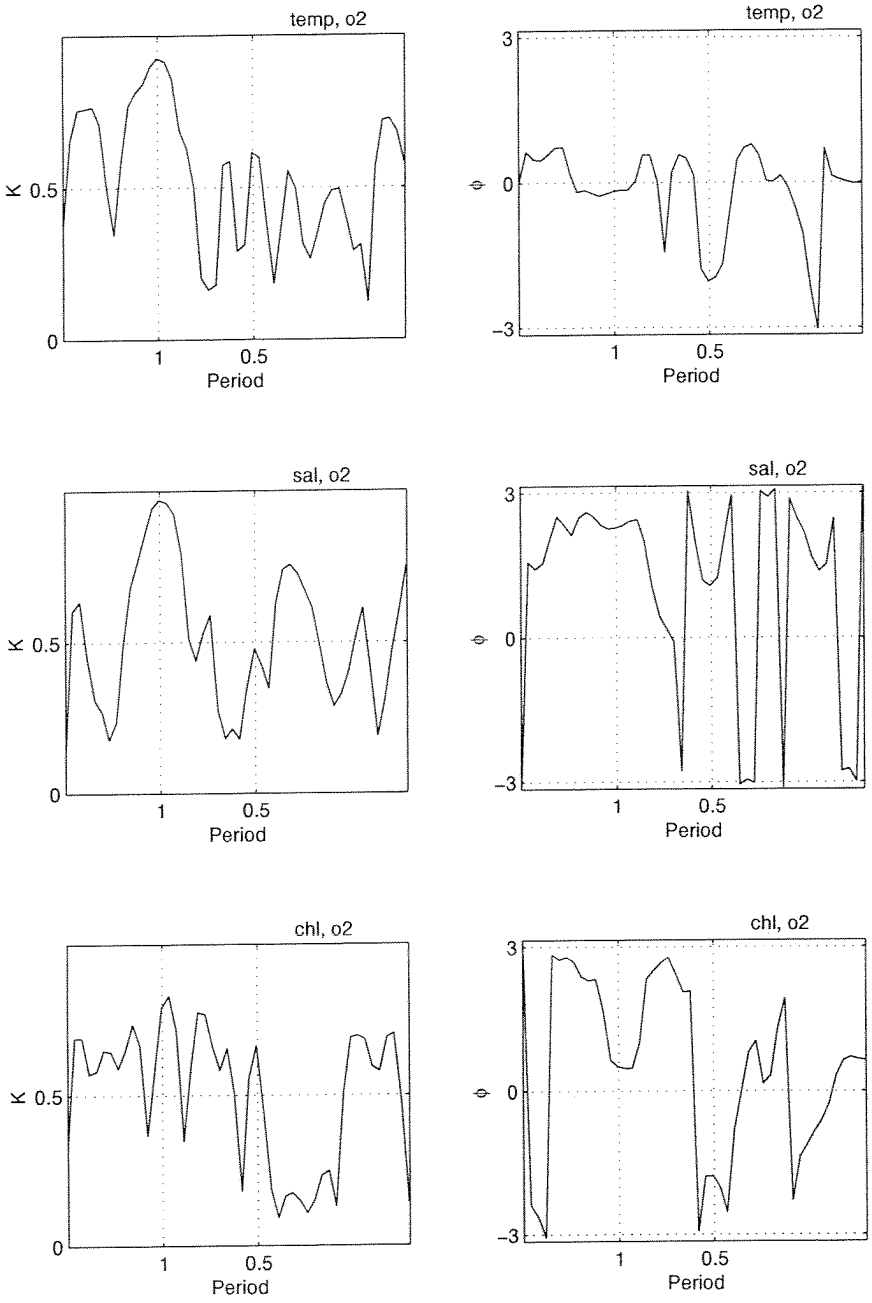

Fig. 43. (continued).

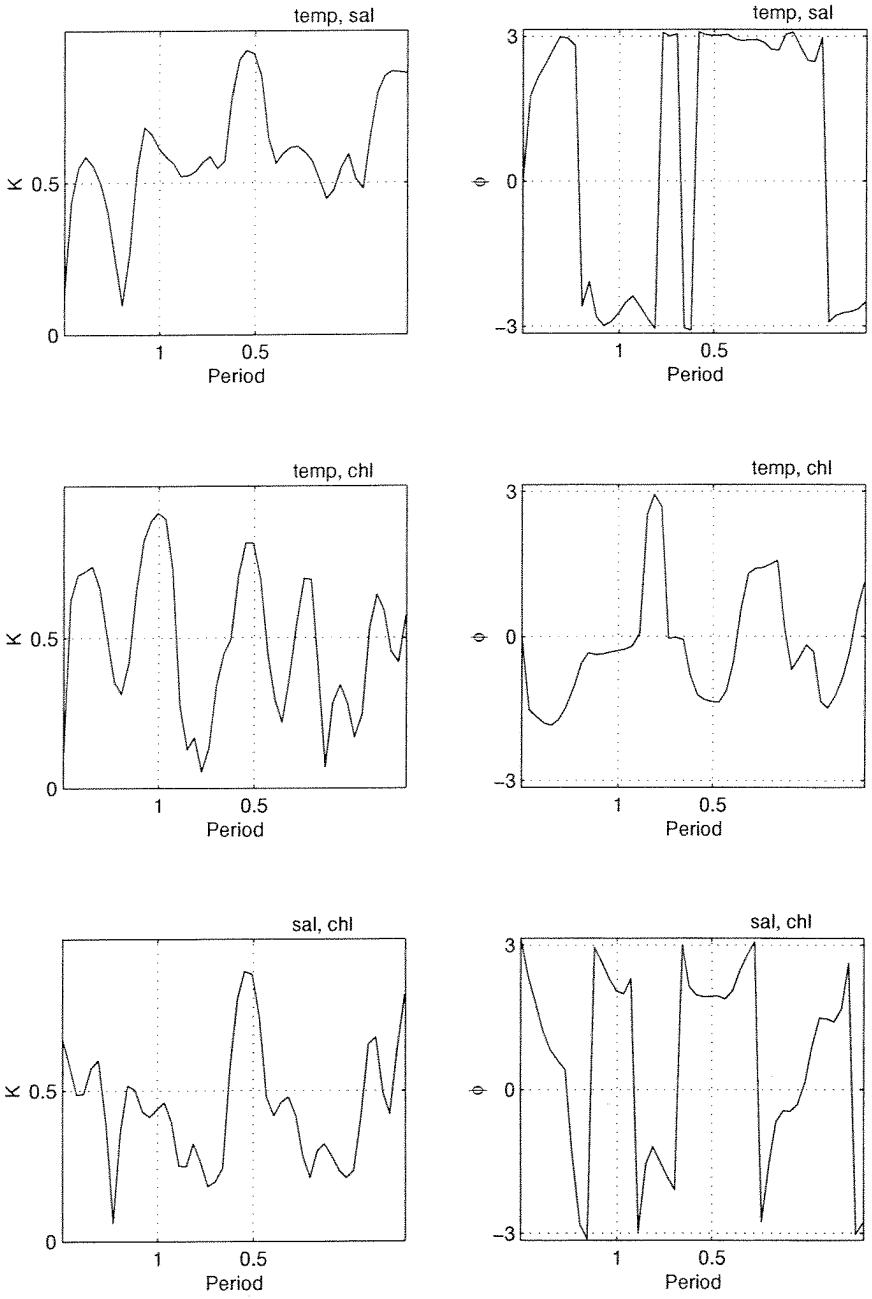

Fig. 44. Cross-spectral analysis for the bottom deployment at site SC1 (Winter Bay) on Julian days 179-193, 1999. Coherency, K, and phase, ϕ, spectra are given, with the analysis variables indicated above each panel. The period is reported in days and phase is in radians.

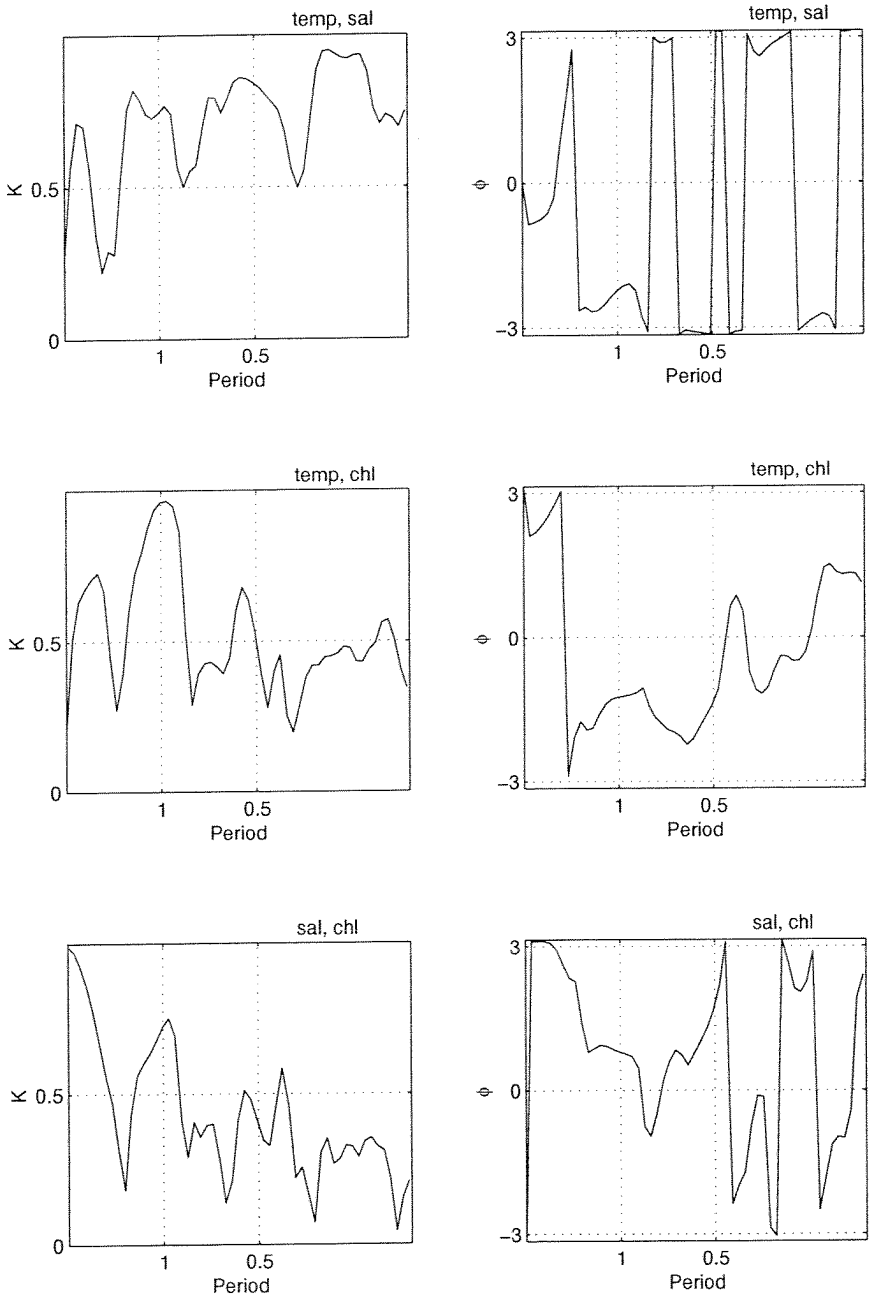

Fig. 45. Cross-spectral analysis for the surface deployment at site SC1 (Winter Bay) on Julian days 193-209, 1999. Coherency, K, and phase, ϕ, spectra are given, with the analysis variables indicated above each panel. The period is reported in days and phase is in radians.

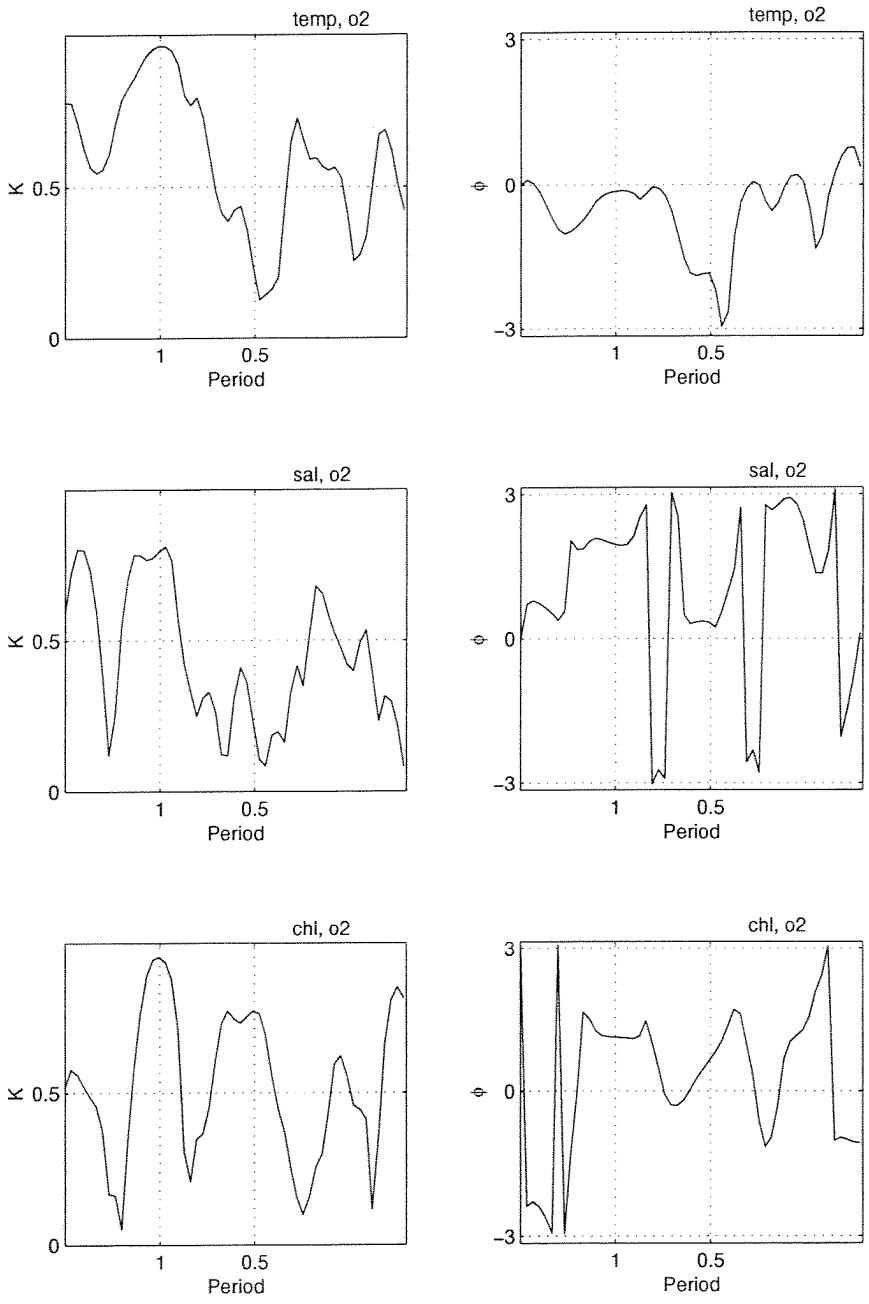

Fig. 45. (continued).

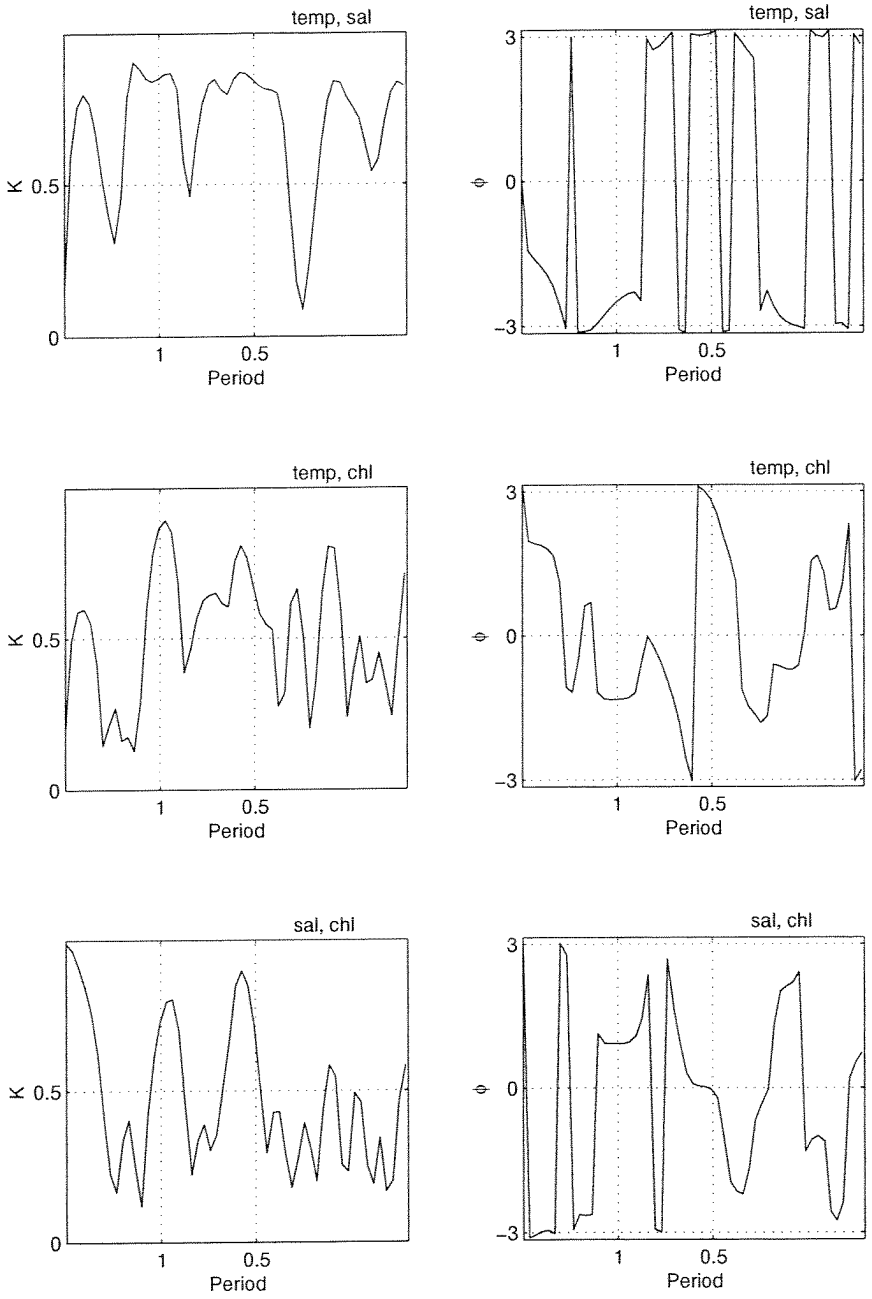

Fig. 46. Cross-spectral analysis for the bottom deployment at site SC1 (Winter Bay) on Julian days 193-209, 1999. Coherency, K, and phase, ϕ, spectra are given, with the analysis variables indicated above each panel. The period is reported in days and phase is in radians.

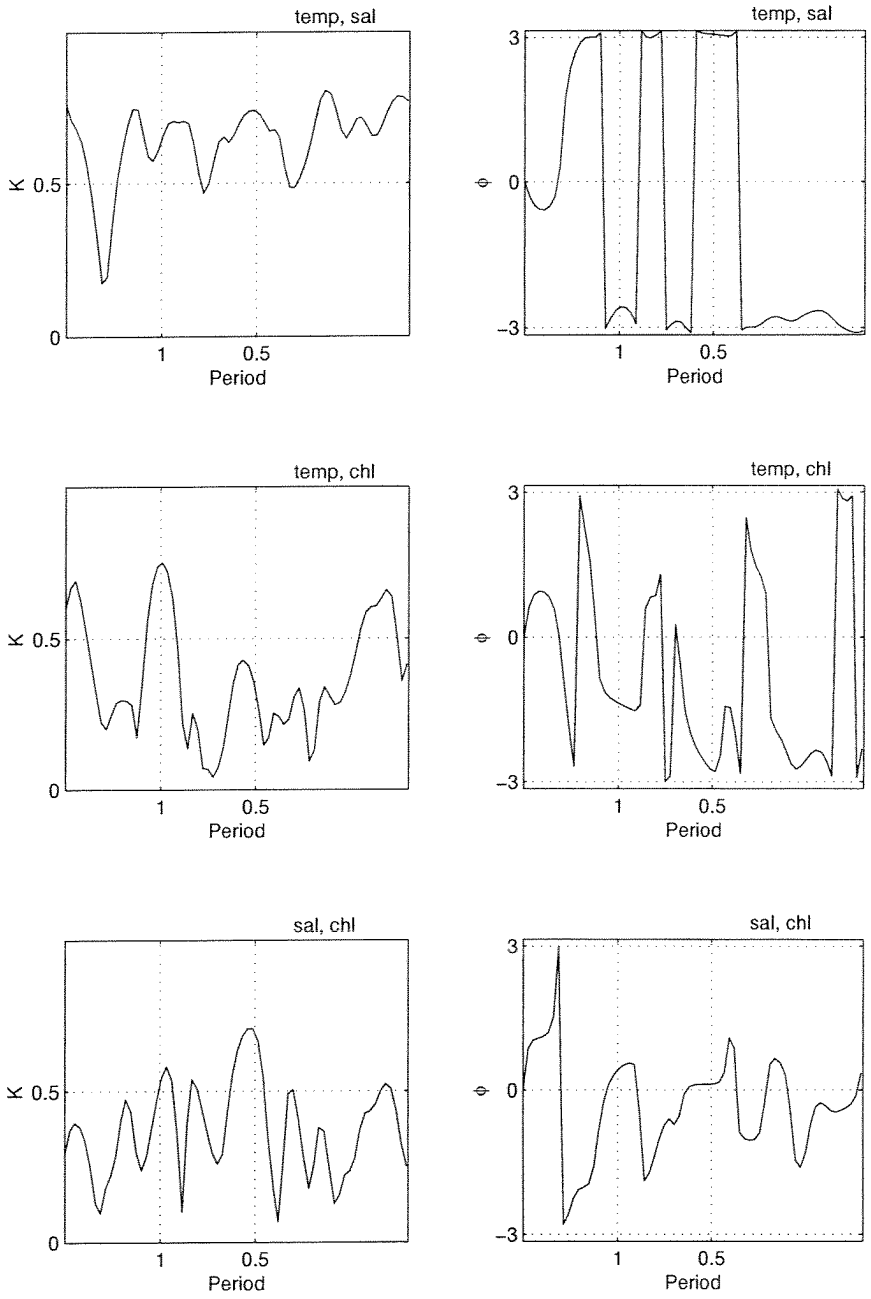

Fig. 47. Cross-spectral analysis for the bottom deployment at SC1 (Winter Bay) on Julian days 208-228, 1999. Coherency, K, and phase, ϕ, spectra are given, with the analysis variables indicated above each panel. The period is reported in days and phase is in radians.

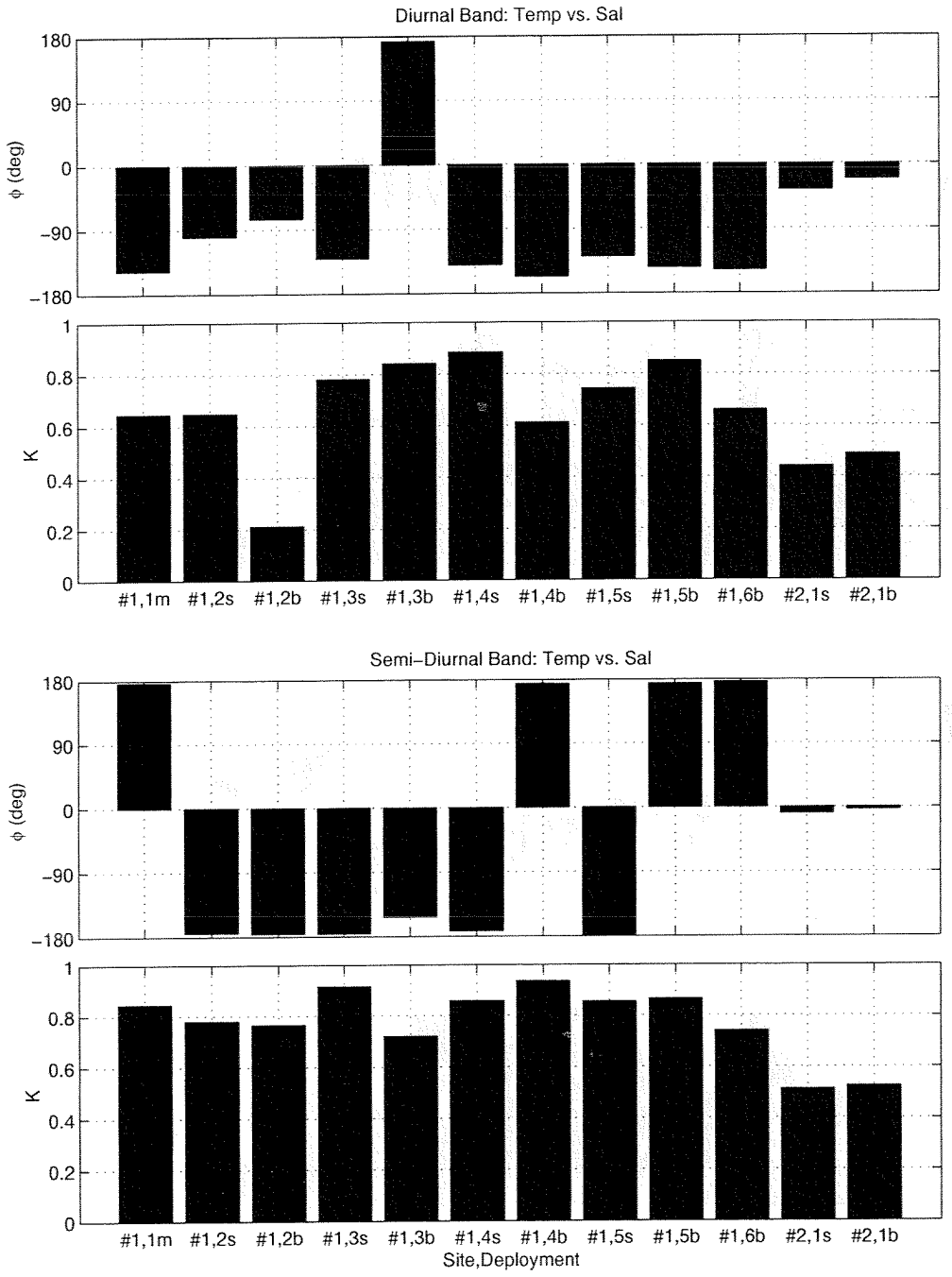

Fig. 48. Coherency and phase at the diurnal (upper two panels) and semi-diurnal (lower two panels) frequencies for the temperature versus salinity series. The x-axis identifies the SEACAT site, deployment number and location in the vertical (see Table 3). Here, K denotes coherency and ϕ is the phase (°).

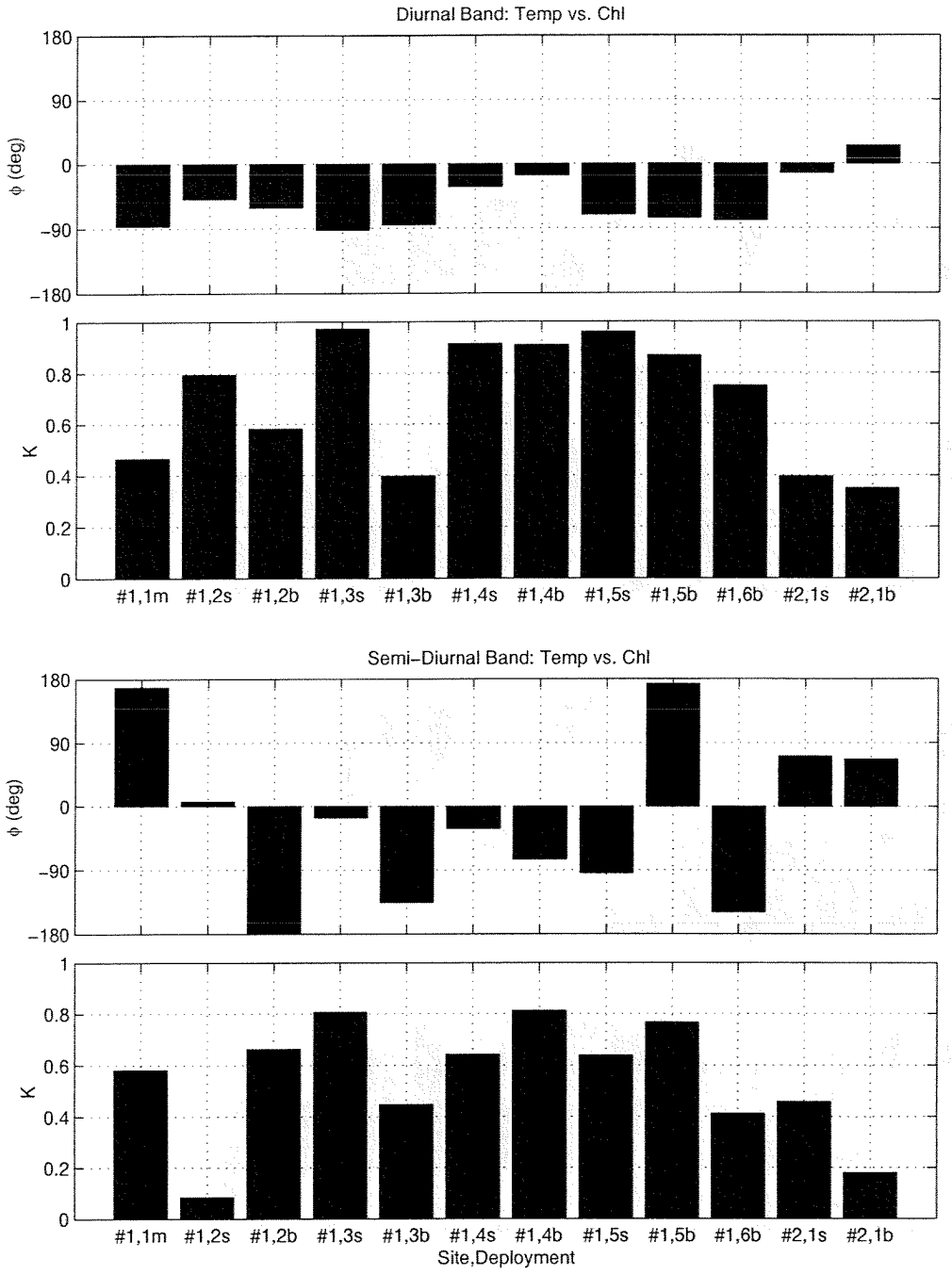

Fig. 49. Coherency and phase at the diurnal (upper two panels) and semi-diurnal (lower two panels) frequencies for the temperature versus chlorophyll series. The x-axis identifies the SEACAT site, deployment number and location in the vertical (see Table 3). Here, K denotes coherency and ϕ is the phase (°).

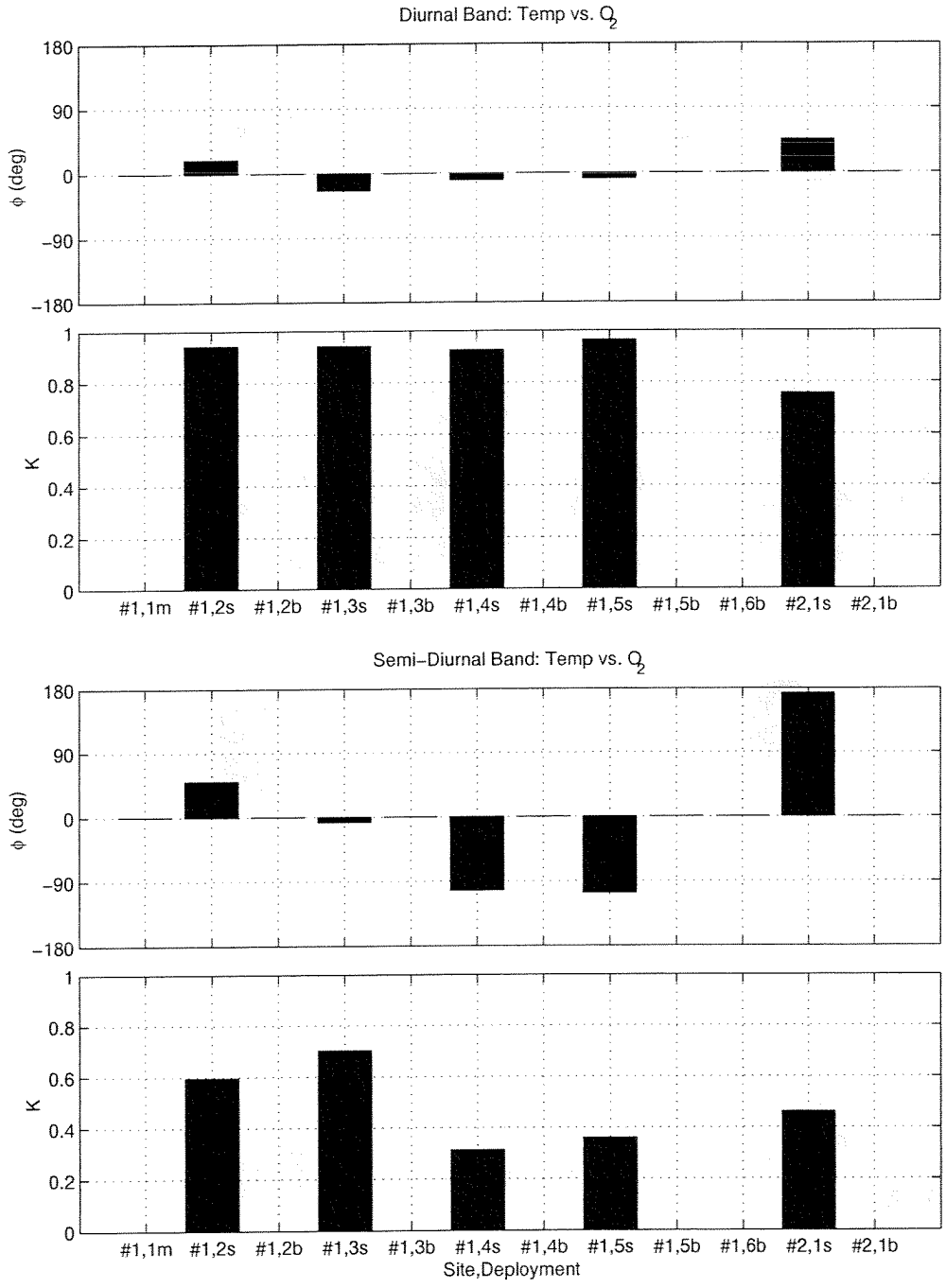

Fig. 50. Coherency and phase at the diurnal (upper two panels) and semi-diurnal (lower two panels) frequencies for the temperature versus oxygen series. The x-axis identifies the SEACAT site, deployment number and location in the vertical (see Table 3). Here, K denotes coherency and ϕ is the phase (°). Oxygen data is absent for some cases.

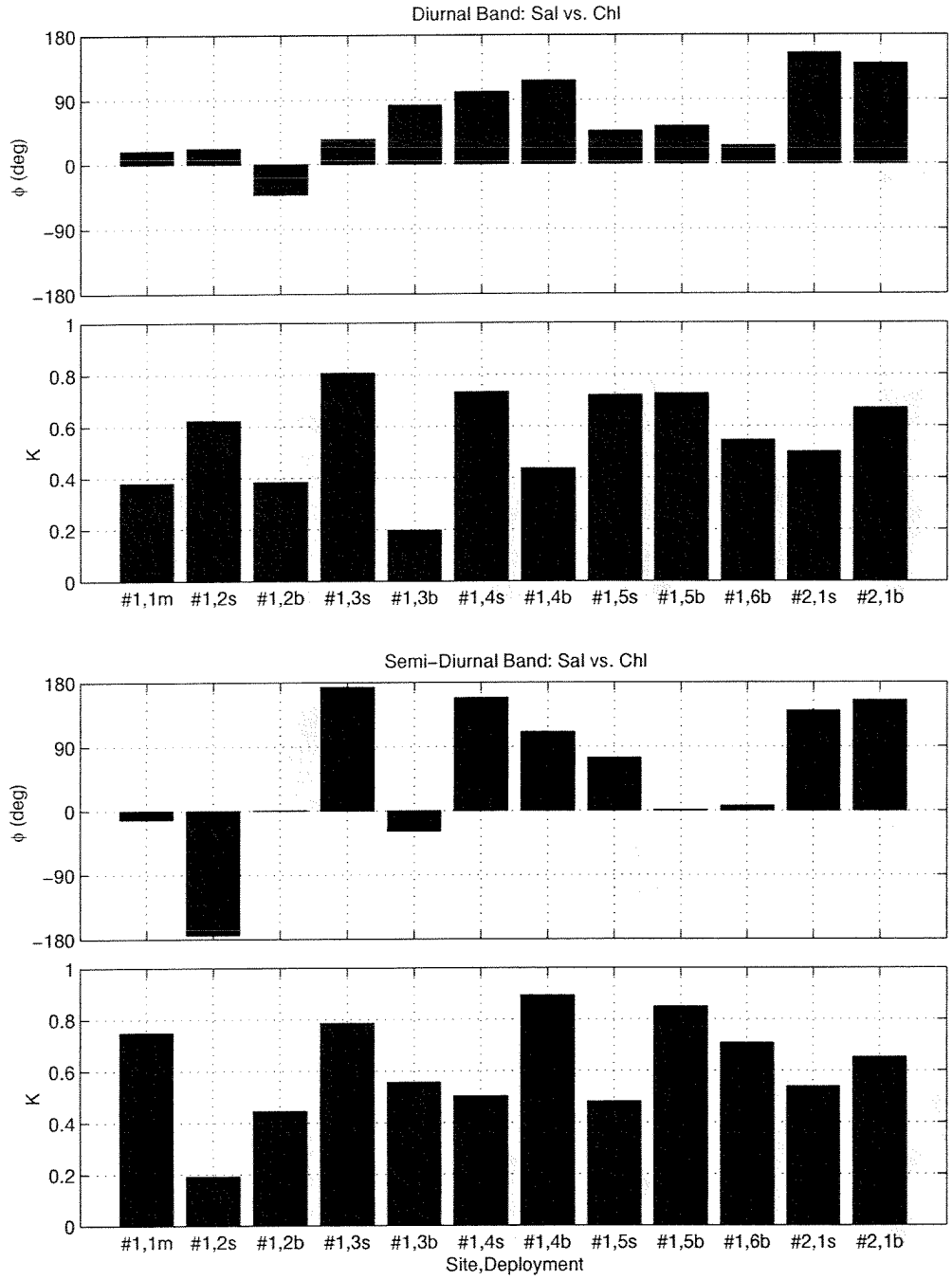

Fig. 51. Coherency and phase at the diurnal (upper two panels) and semi-diurnal (lower two panels) frequencies for the salinity versus chlorophyll series. The x-axis identifies the SEACAT site, deployment number and location in the vertical (see Table 3). Here, K denotes coherency and ϕ is the phase (°).

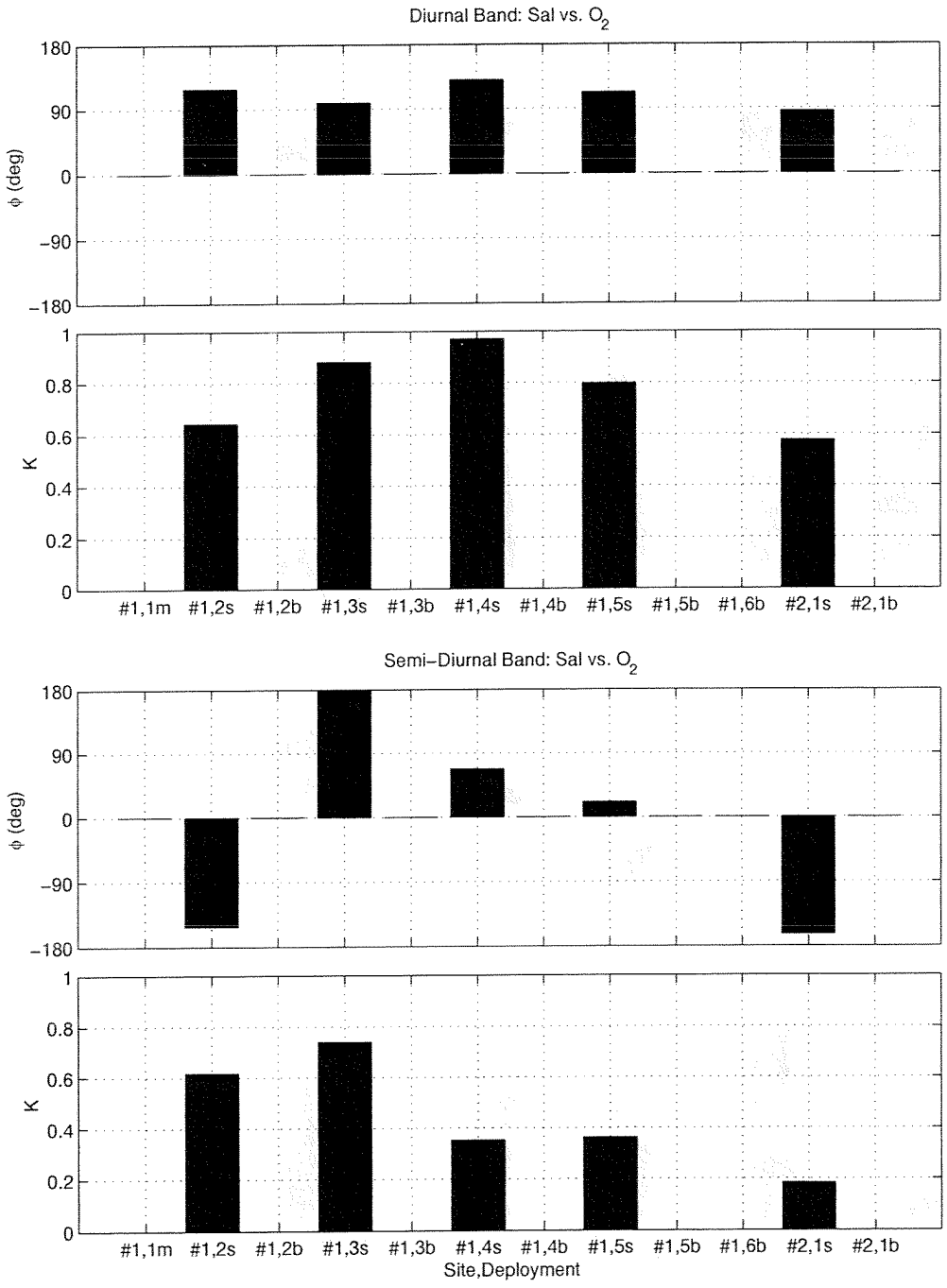

Fig. 52. Coherency and phase at the diurnal (upper two panels) and semi-diurnal (lower two panels) frequencies for the salinity versus oxygen series. The x-axis identifies the SEACAT site, deployment number and location in the vertical (see Table 3). Here, K denotes coherency and ϕ is the phase (°). Oxygen data is absent for some cases.

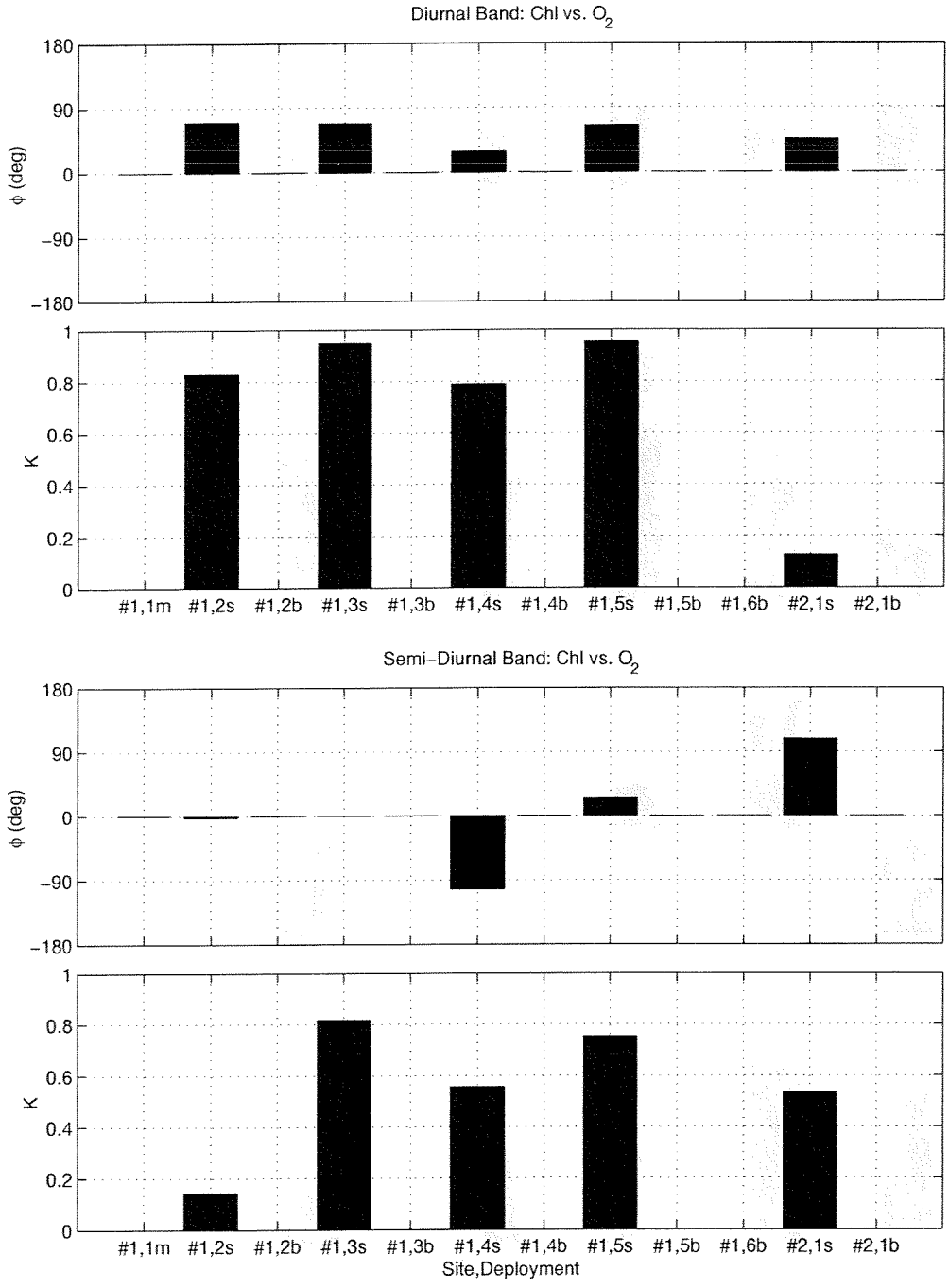

Fig. 53. Coherency and phase at the diurnal (upper two panels) and semi-diurnal (lower two panels) frequencies for the chlorophyll versus oxygen. The x-axis identifies the SEACAT site, deployment number and location in the vertical (see Table 3). Here, K denotes coherency and ϕ is the phase (°). Oxygen data is absent for some cases.

Appendix A: Temperature Records

This appendix contains temperature records obtained in Tracadie Bay during the summer of 1999. The locations for these temperature stations are given in Figure A.1. The time series records are found in Figure A.2.

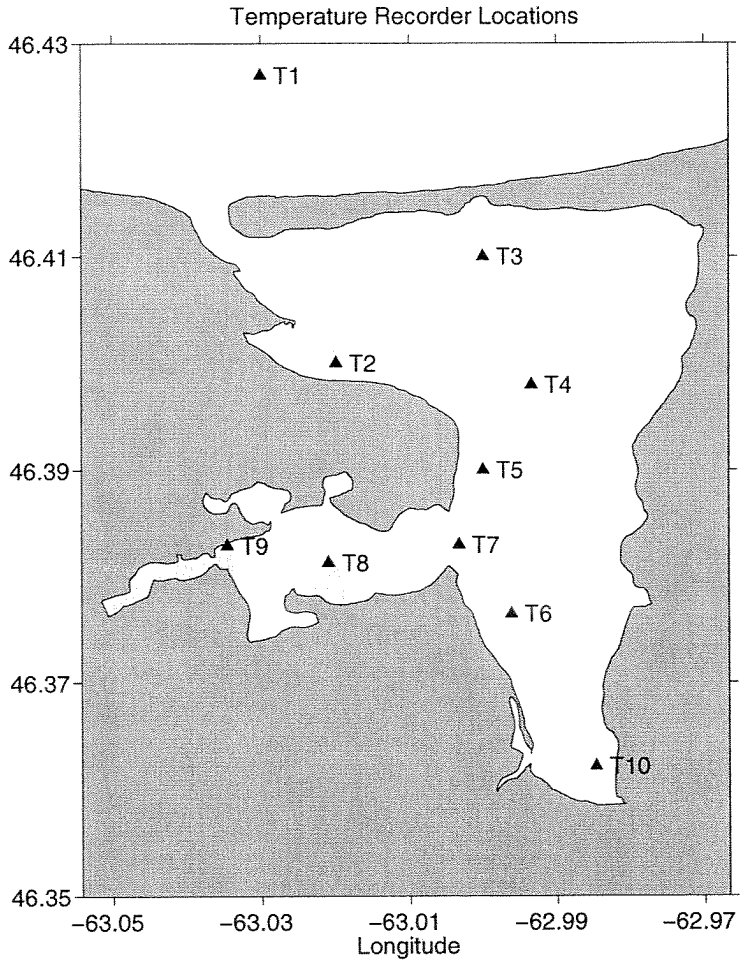

Fig. A.1: Location of the temperature recorders for the deployments in 1999.

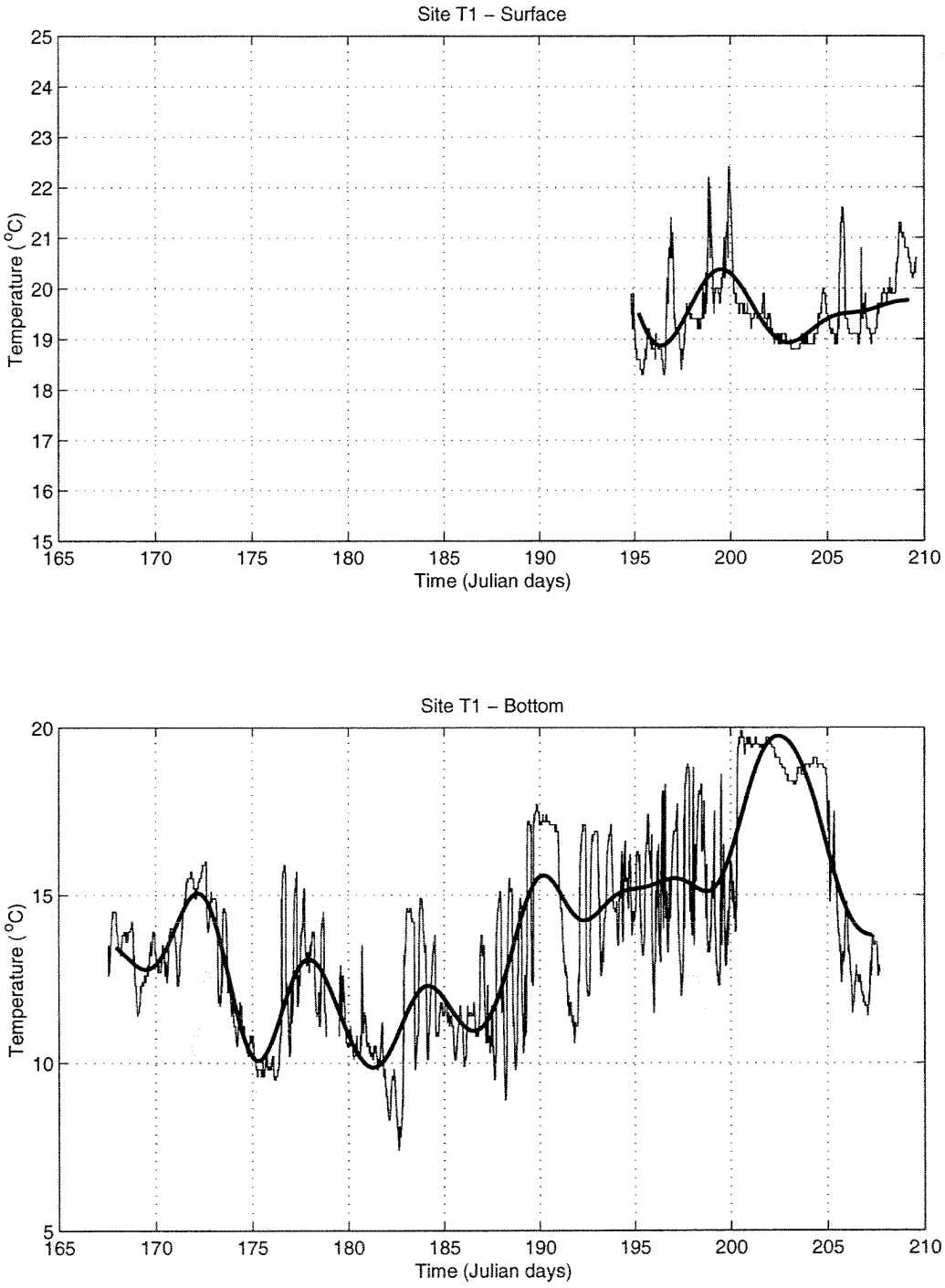

Fig. A.2: Temperature time series for Tracadie Bay. Time is in Julian Days for 1999. The locations are given by the station number in Fig. A.1. The thick solid line represents the low pass filtered series with cutoff period of 100 hours.

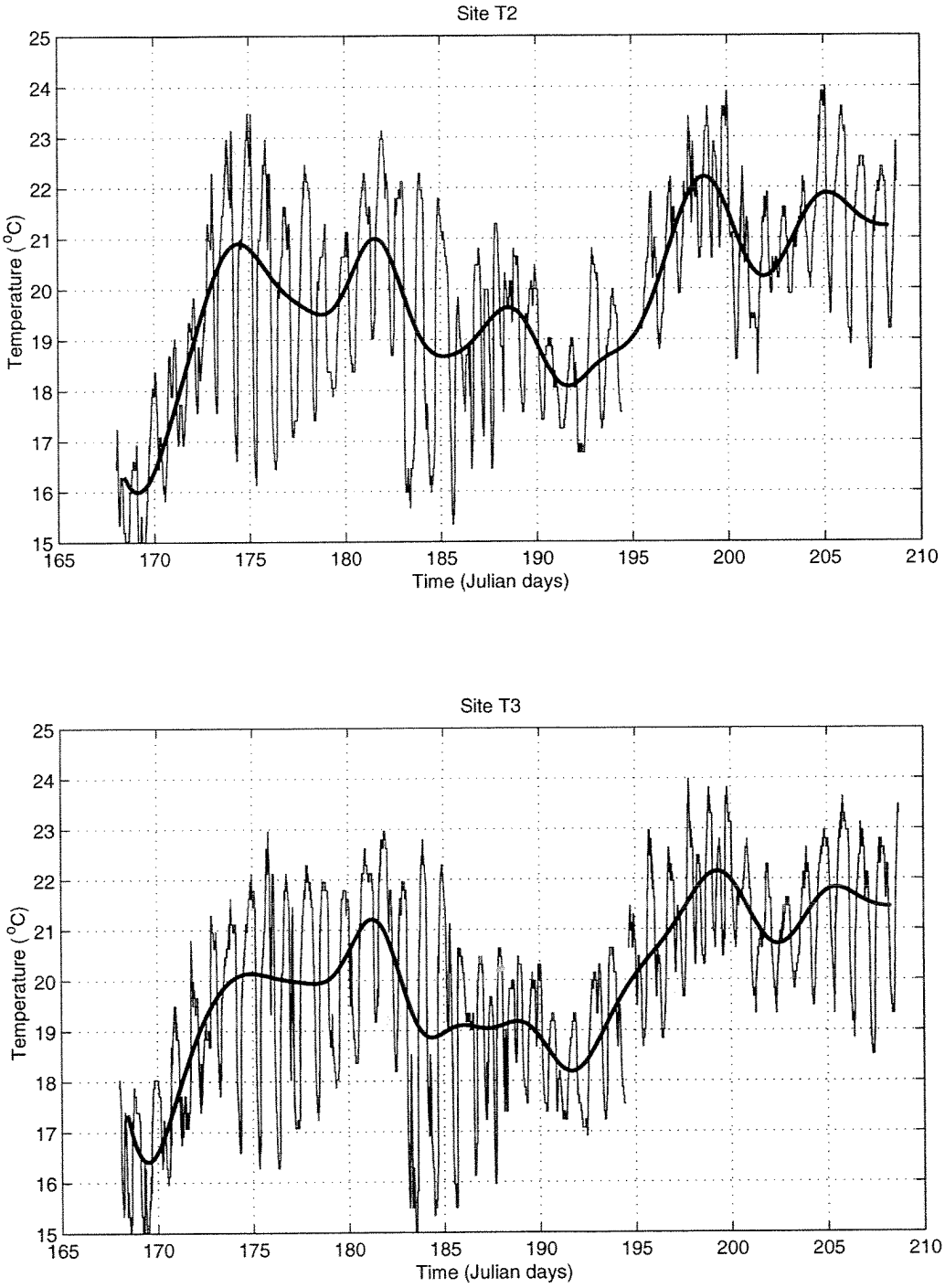

Fig. A.2: continued

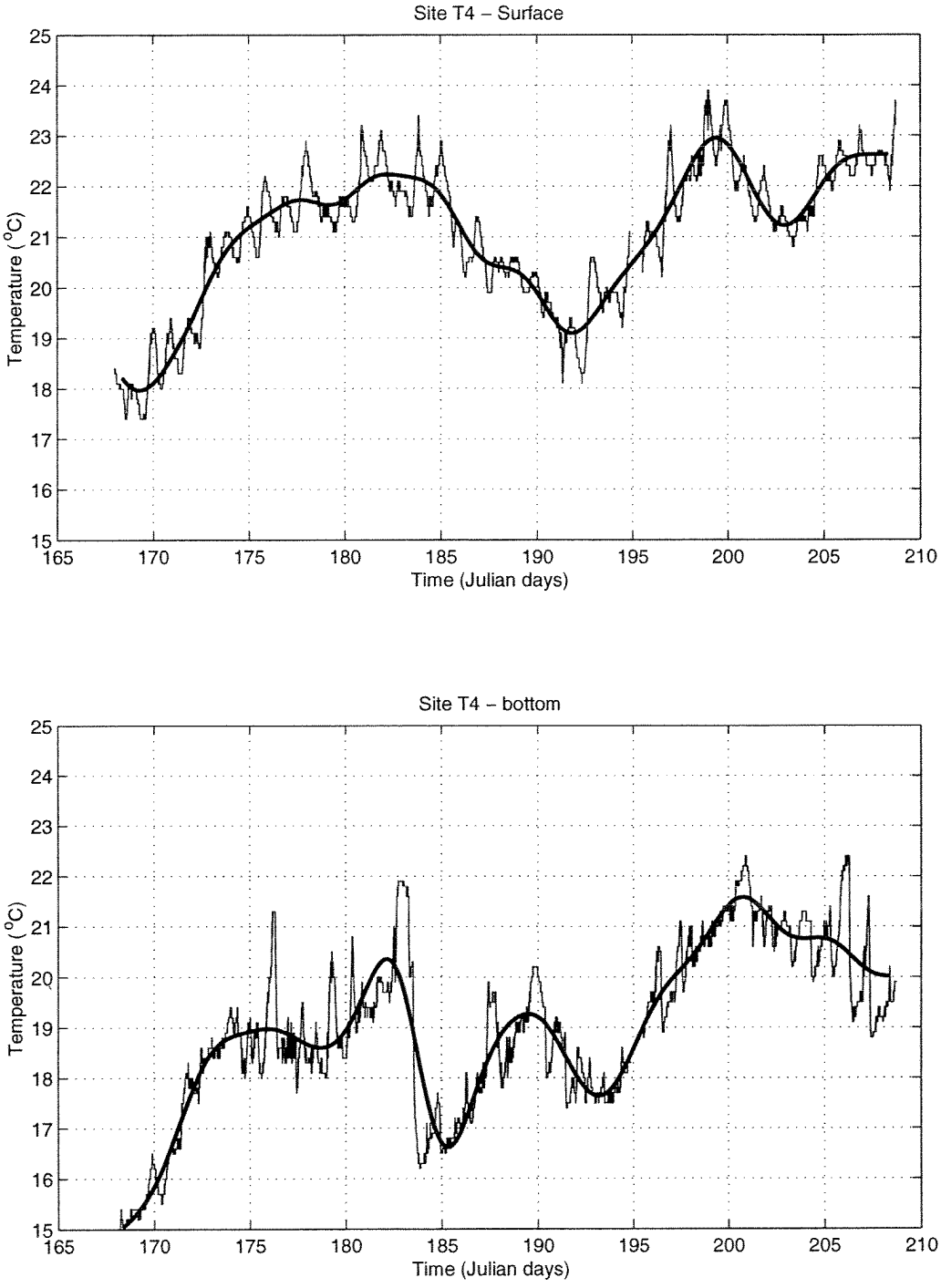

Fig. A.2: continued

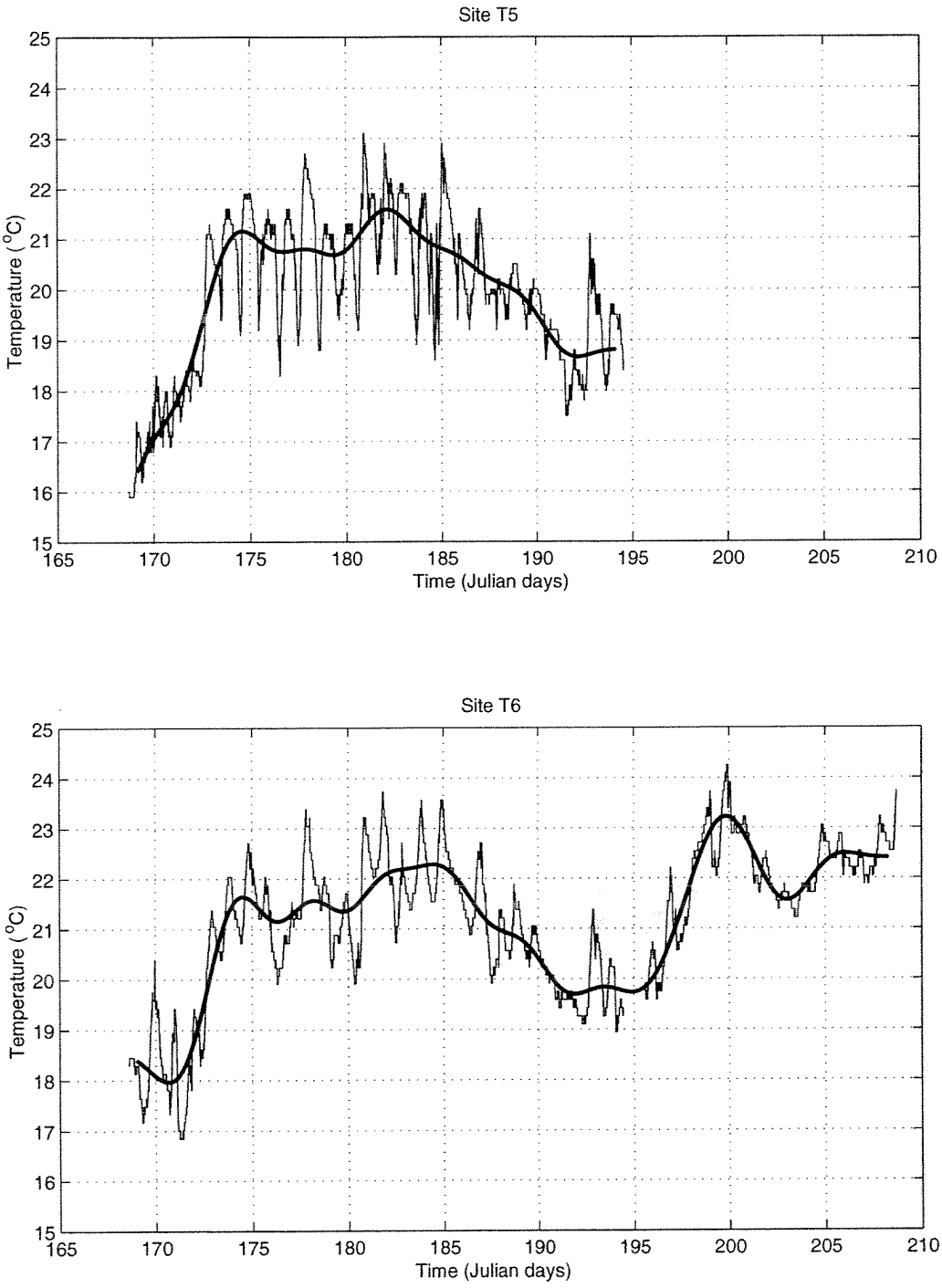

Fig. A.2: continued

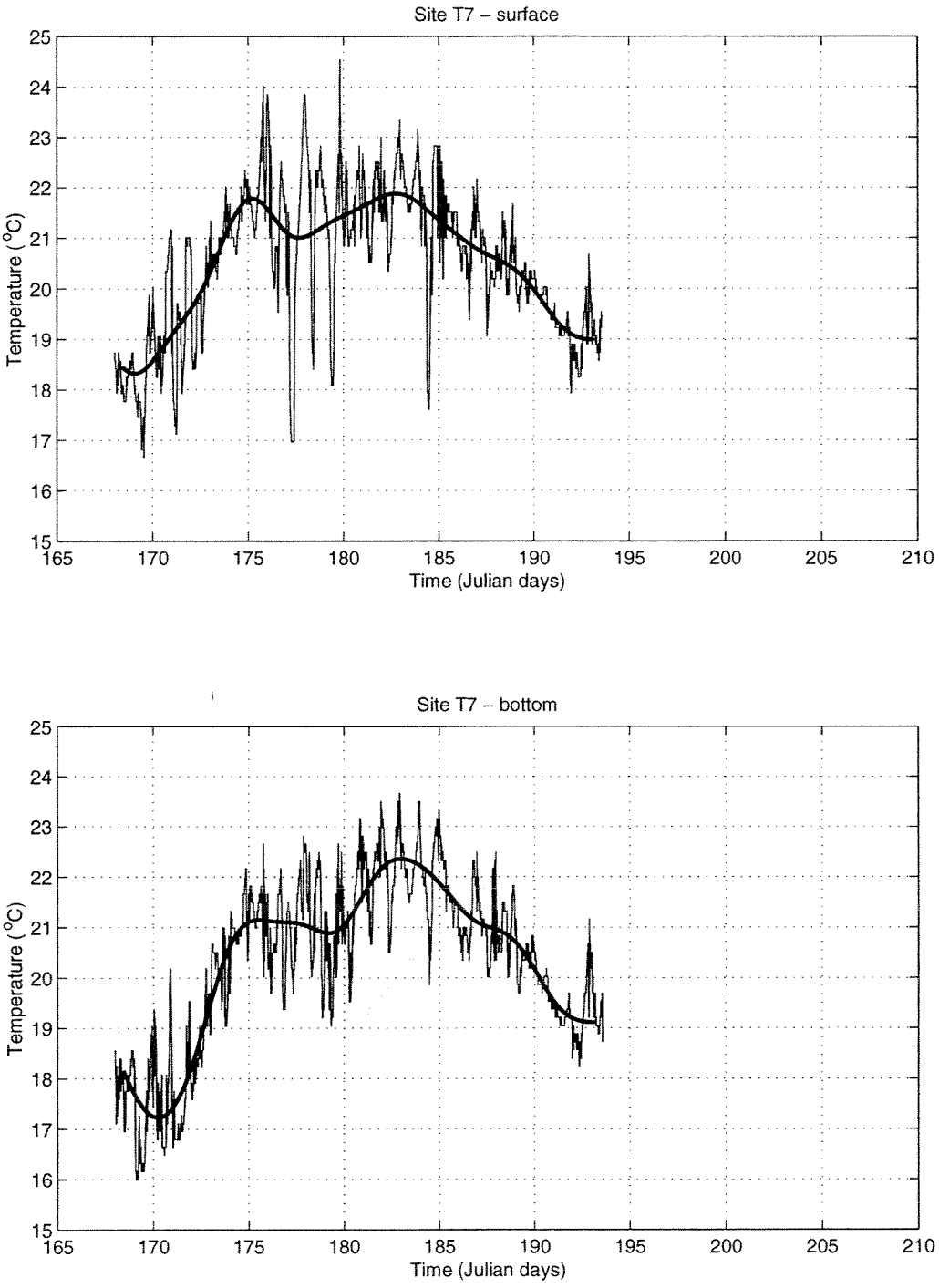

Fig. A.2: continued

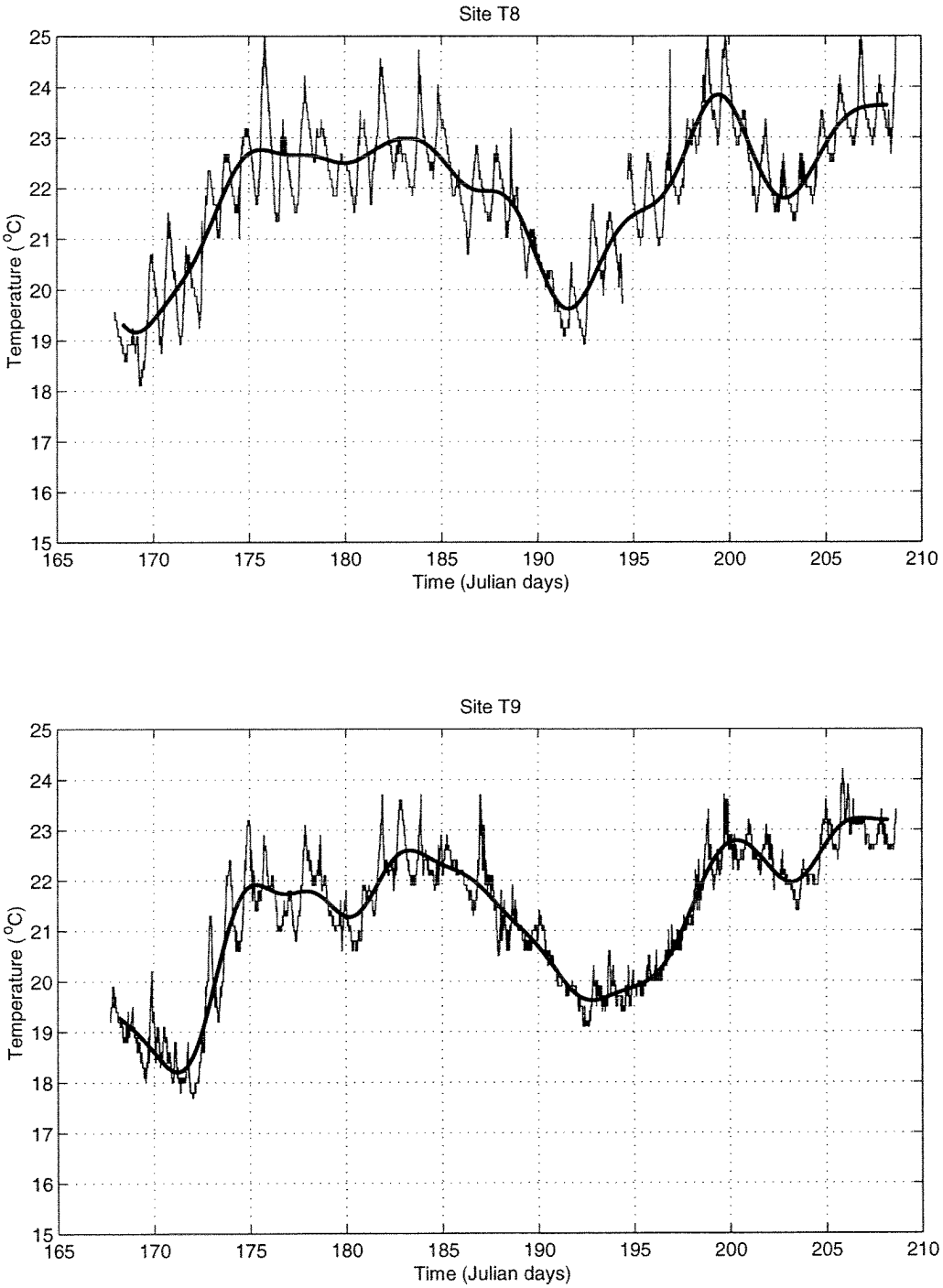

Fig. A.2: continued

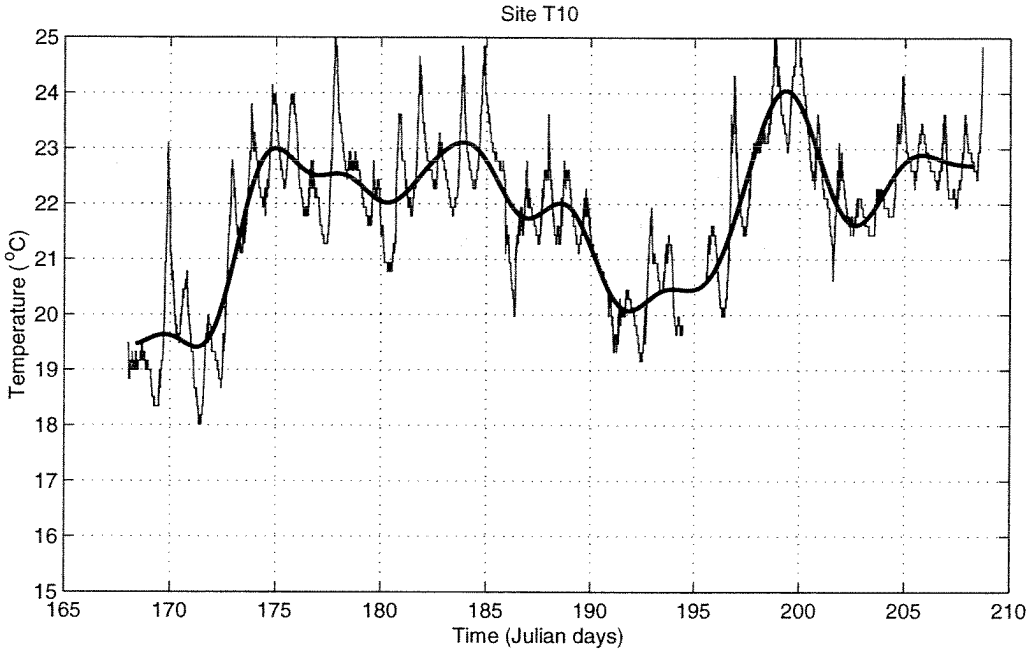

Fig. A.2: continued

Appendix B: Moored SEACAT Data

This appendix contains time series observations from moored SEACATs in Tracadie Bay during 1998 and 1999. Fig. B.1 shows the two mooring locations. Each of the remaining Figs B.2 - B.13 contains observations recorded at these two sites. These data include time series of temperature, salinity, fluoresence (chlorophyll), and oxygen. Temperature is reported in ^oC and salinity in psu (practical salinity units). A low frequency series is given for these variables based on application of a zero-phase, low pass Butterworth filter with cutoff frequency $1/100\text{hr}^{-1}$. Fluoresence (chlorophyll) and oxygen are reported in terms of detrended and standardized variables (which are designated as the nondimensional quantities Δchl and $\Delta 0_2$, respectively). Note that oxygen is not available for all deployments. See the report text for further details.

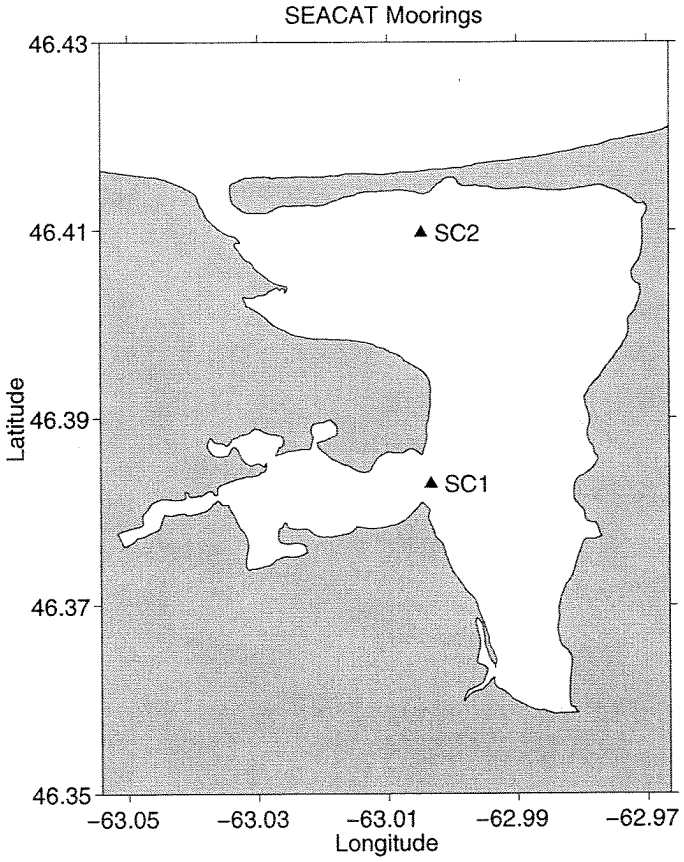

Fig. B.1: Map showing locations of the two sites for the moored SEACATs. These are designated SC1 (mouth of Winter Bay) and SC2 (the main entrance channel), respectively.

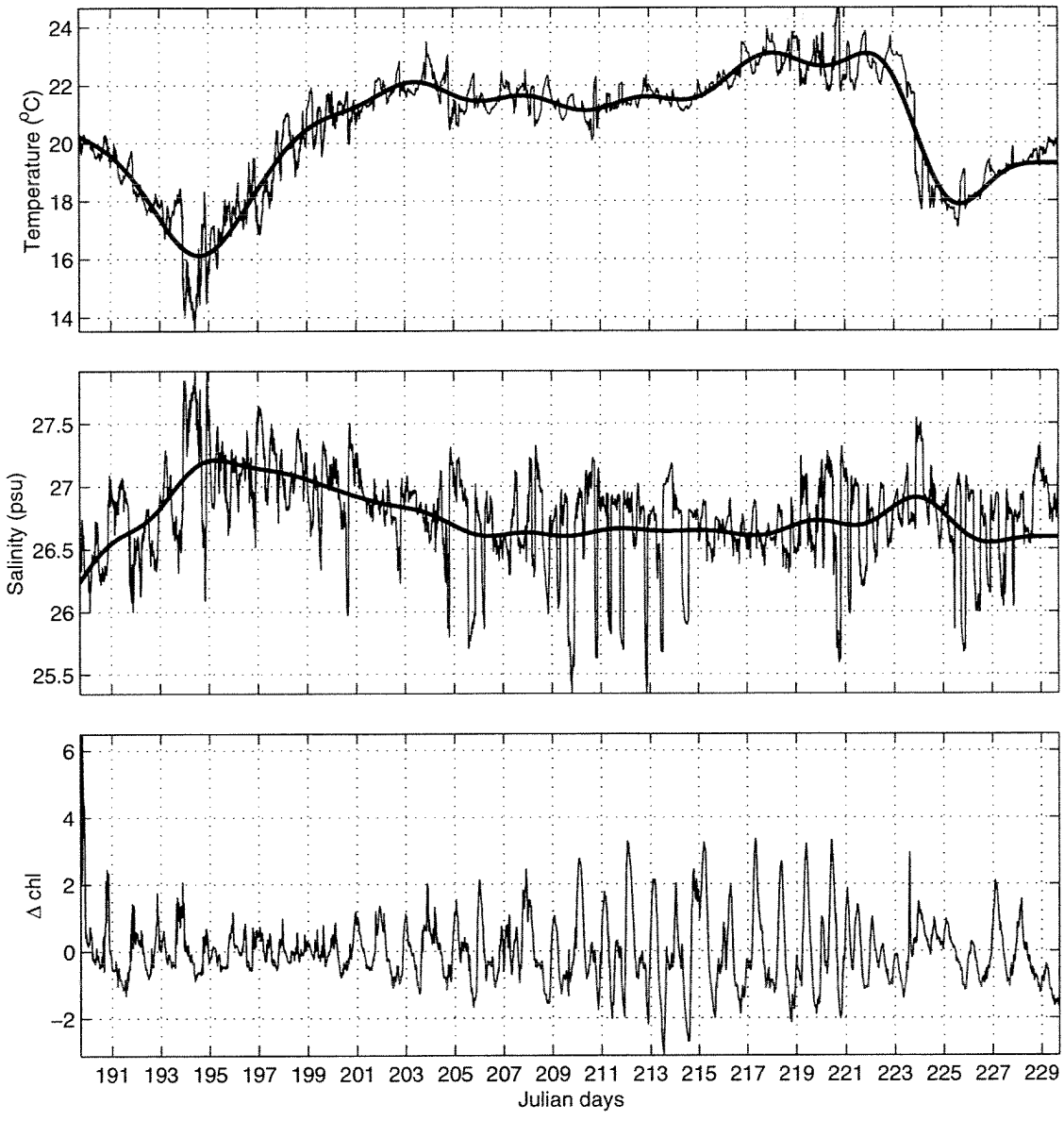

Fig. B.2: Moored SEACAT data from mid-depth at site SC1 (the mouth of Winter Bay) during the period Julian days 189-230, 1998.

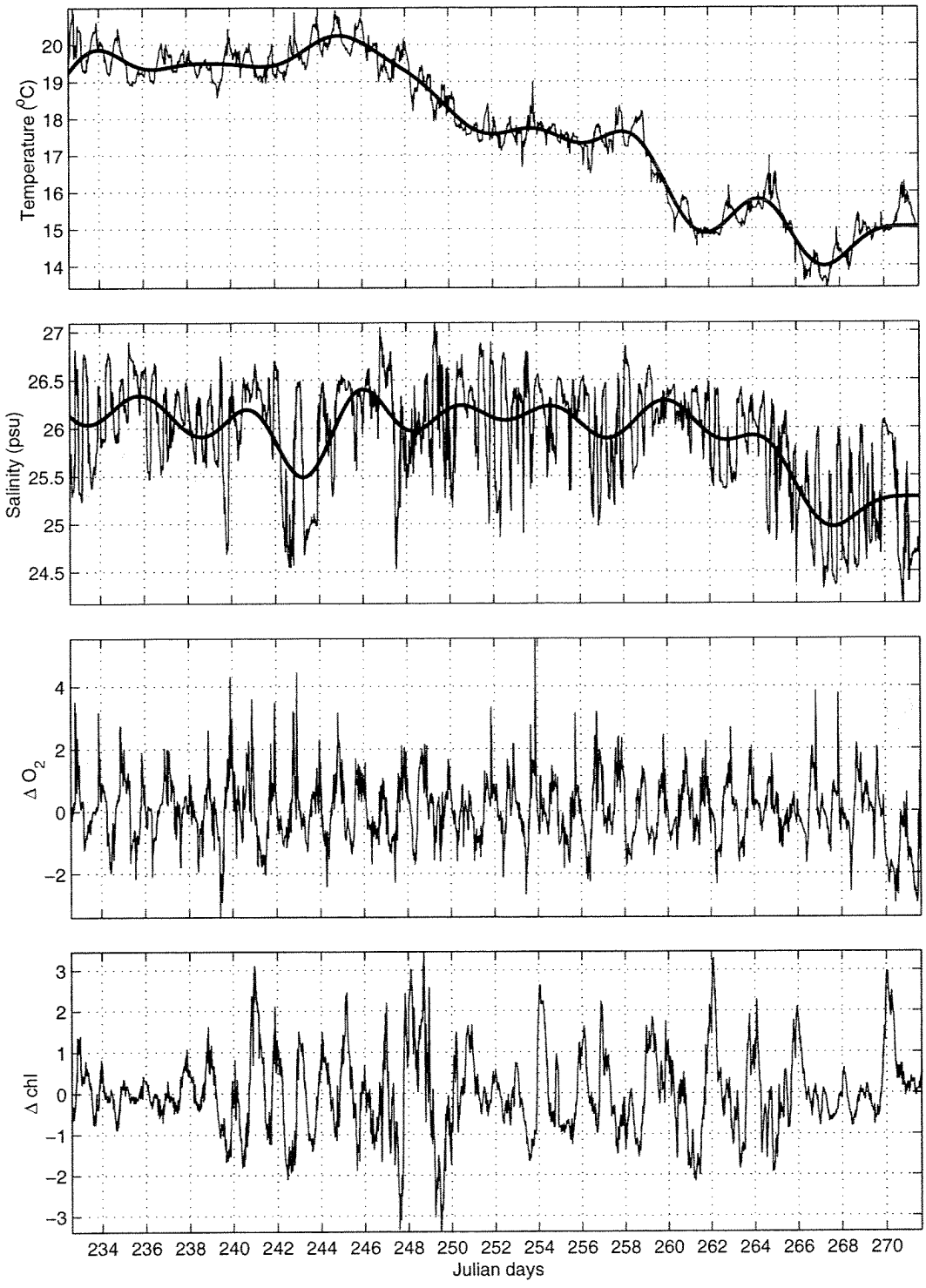

Fig. B.3: Moored SEACAT data from the surface at site SC1 (the mouth of Winter Bay) during the period Julian days 232-272, 1998.

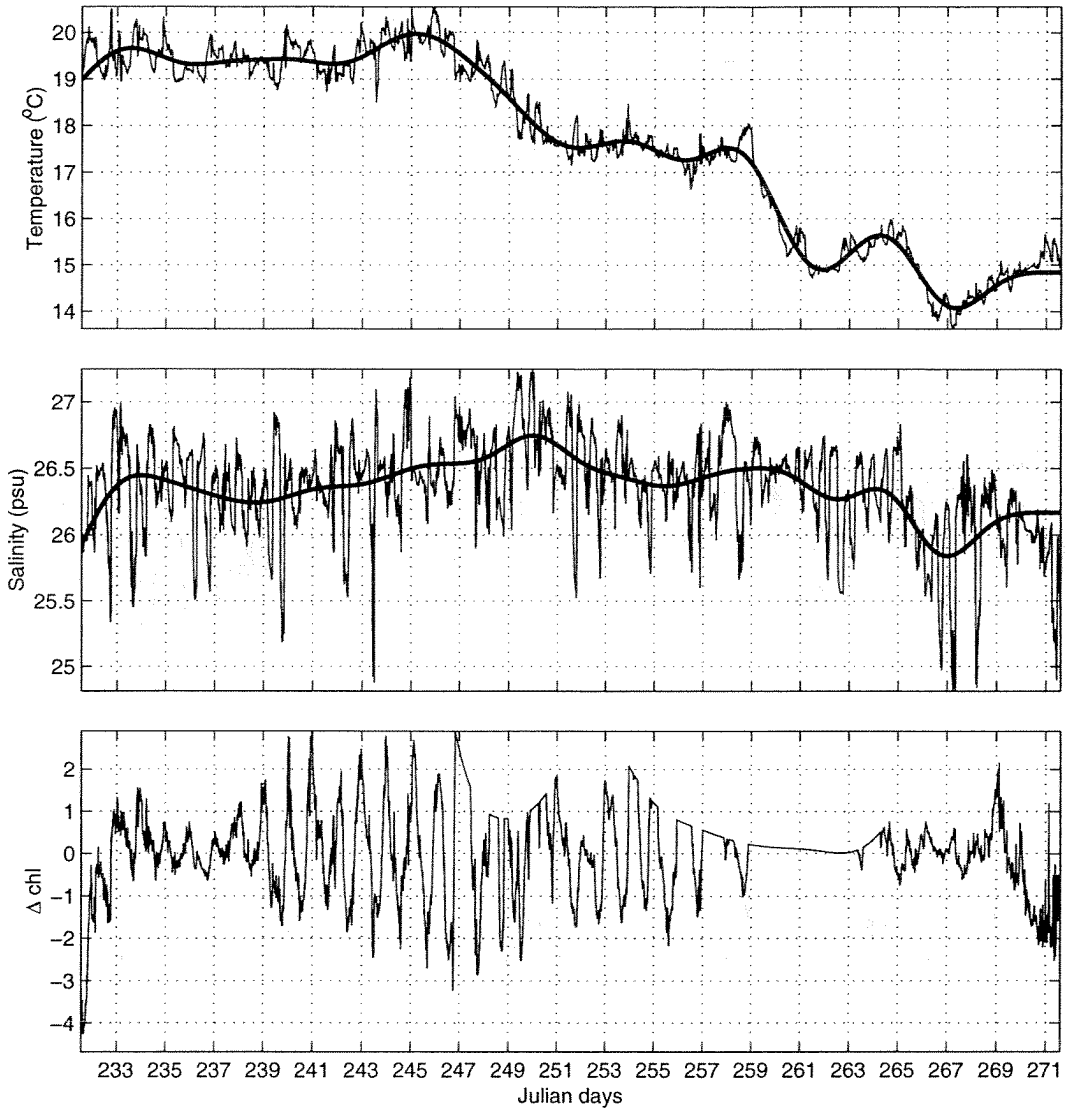

Fig. B.4: Moored SEACAT data from the bottom at site SC1 (the mouth of Winter Bay) during the period Julian days 231-272, 1998.

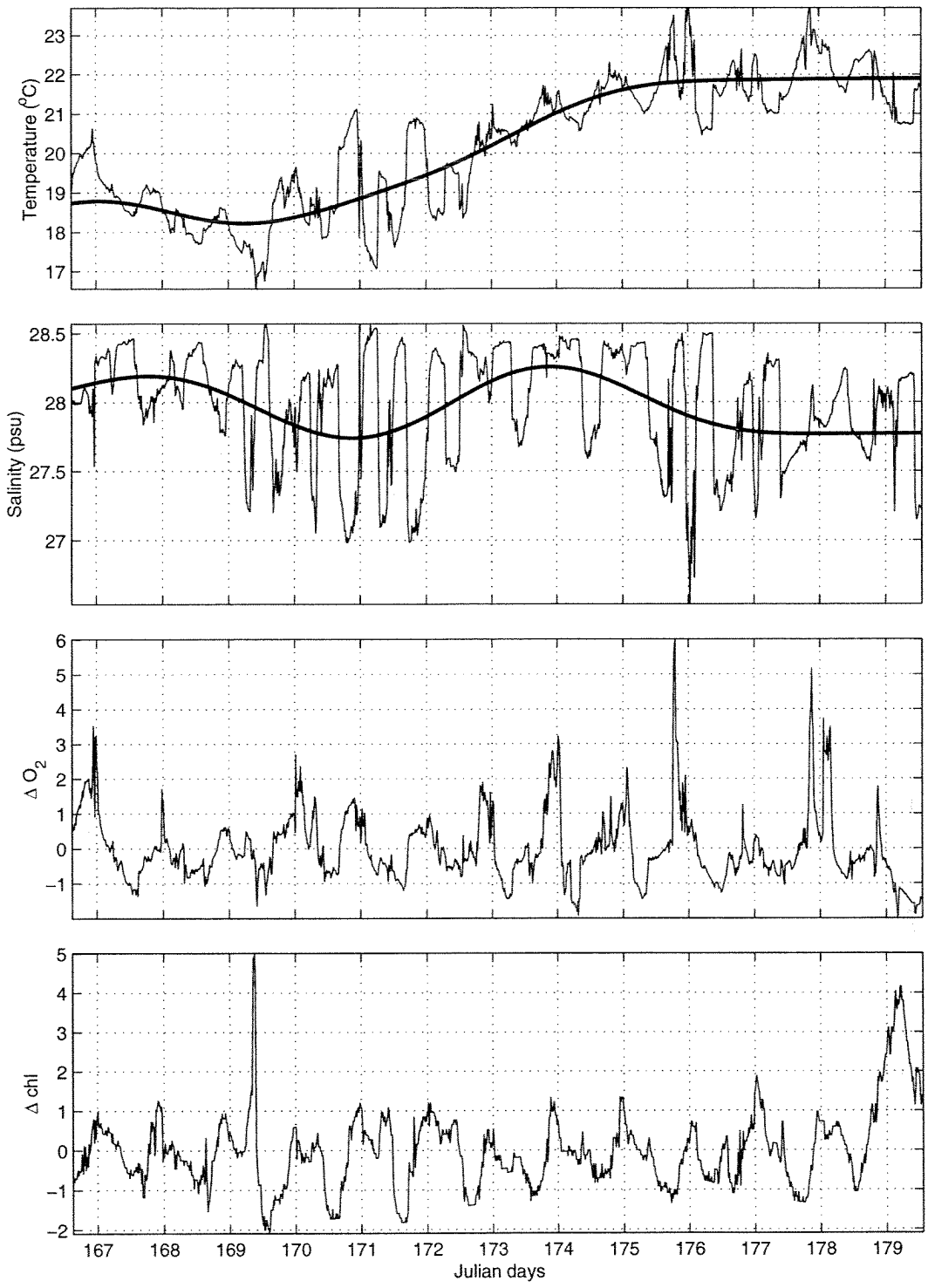

Fig. B.5: Moored SEACAT data from surface at site SC1 (the mouth of Winter Bay) during the period Julian days 166-180, 1999.

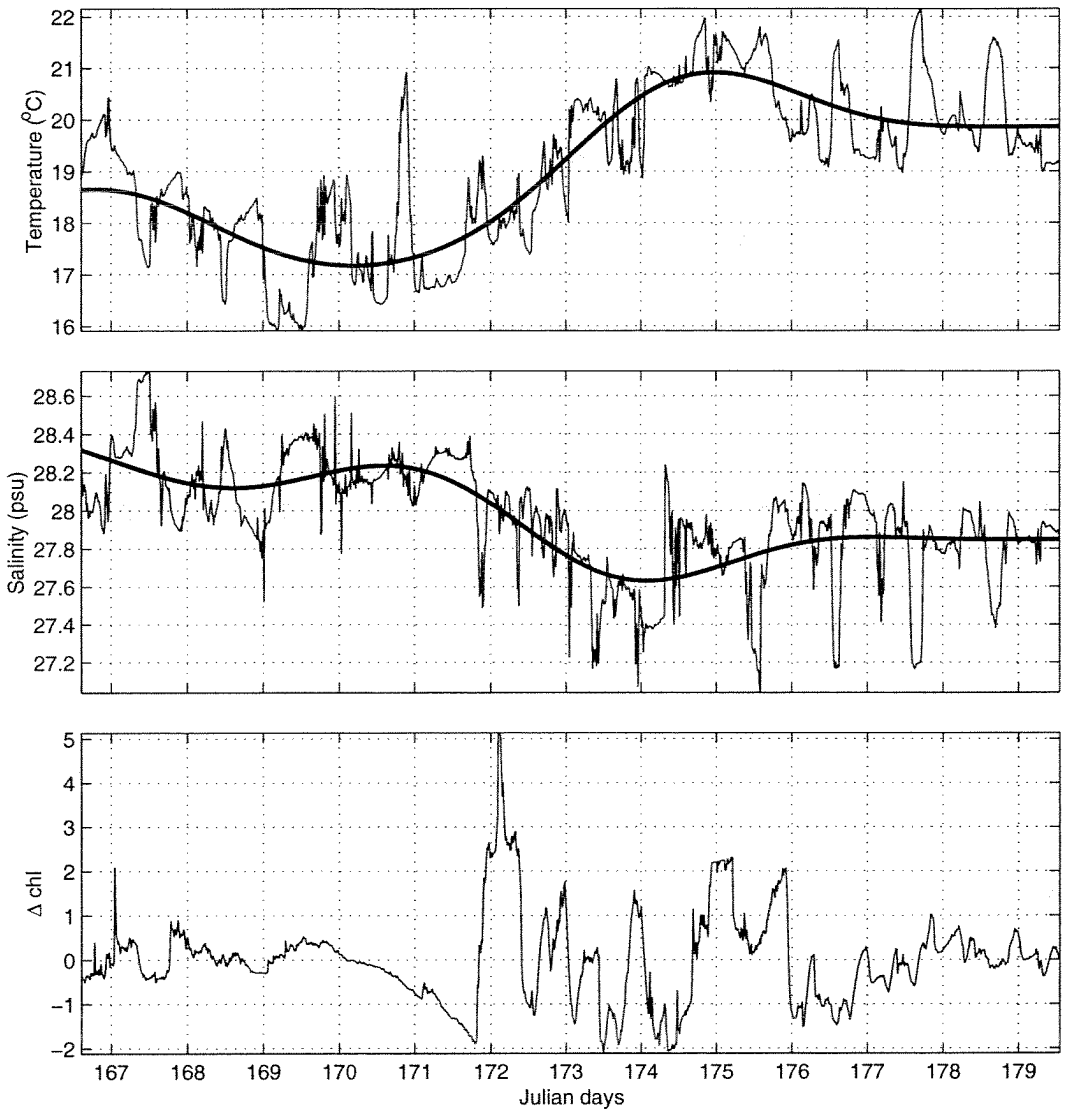

Fig. B.6: Moored SEACAT data from the bottom at site SC1 (the mouth of Winter Bay) during the period Julian days 166-180, 1999.

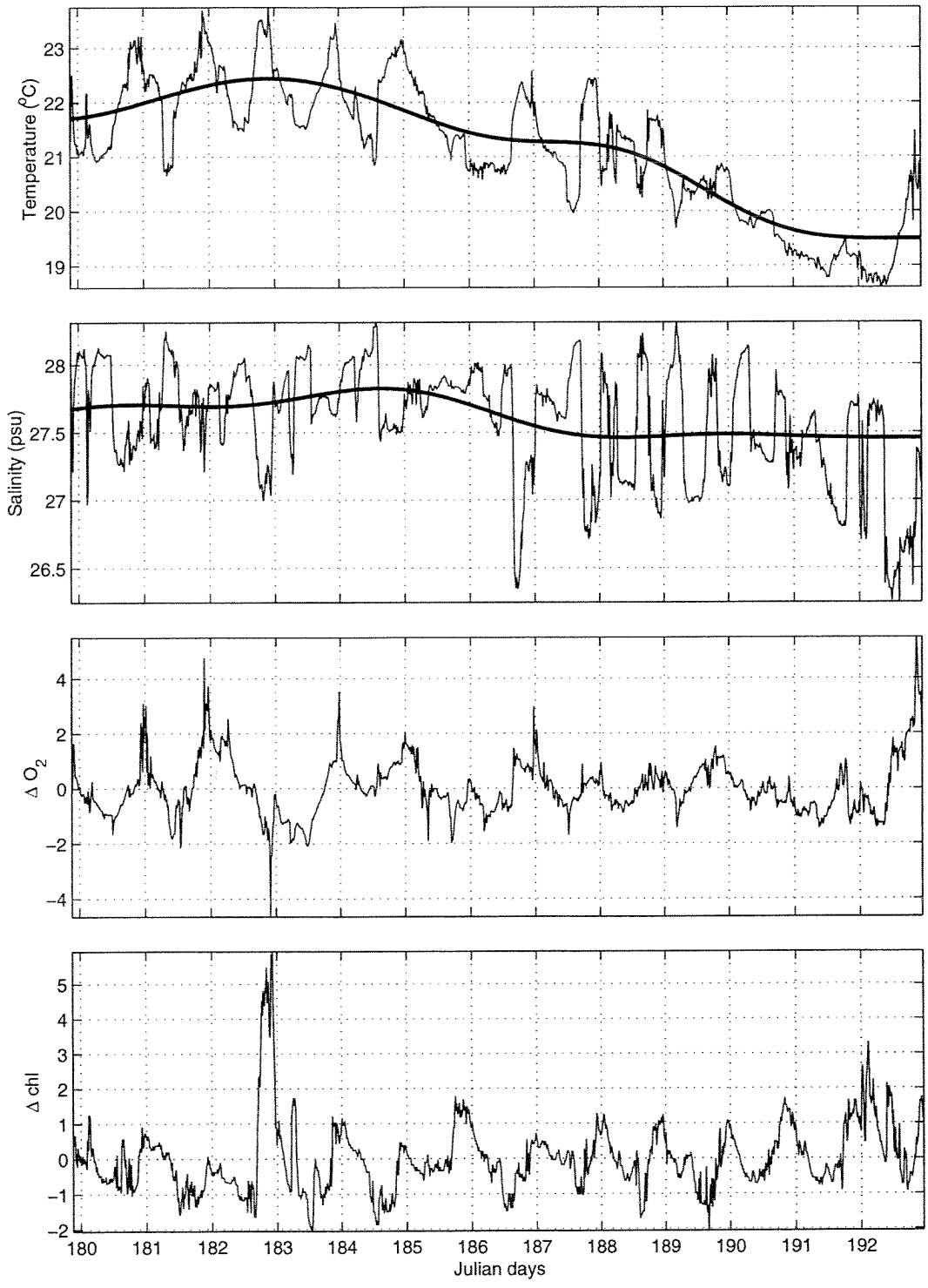

Fig. B.7: Moored SEACAT data from the surface at site SC1 (the mouth of Winter Bay) during the period Julian days 179-193, 1999.

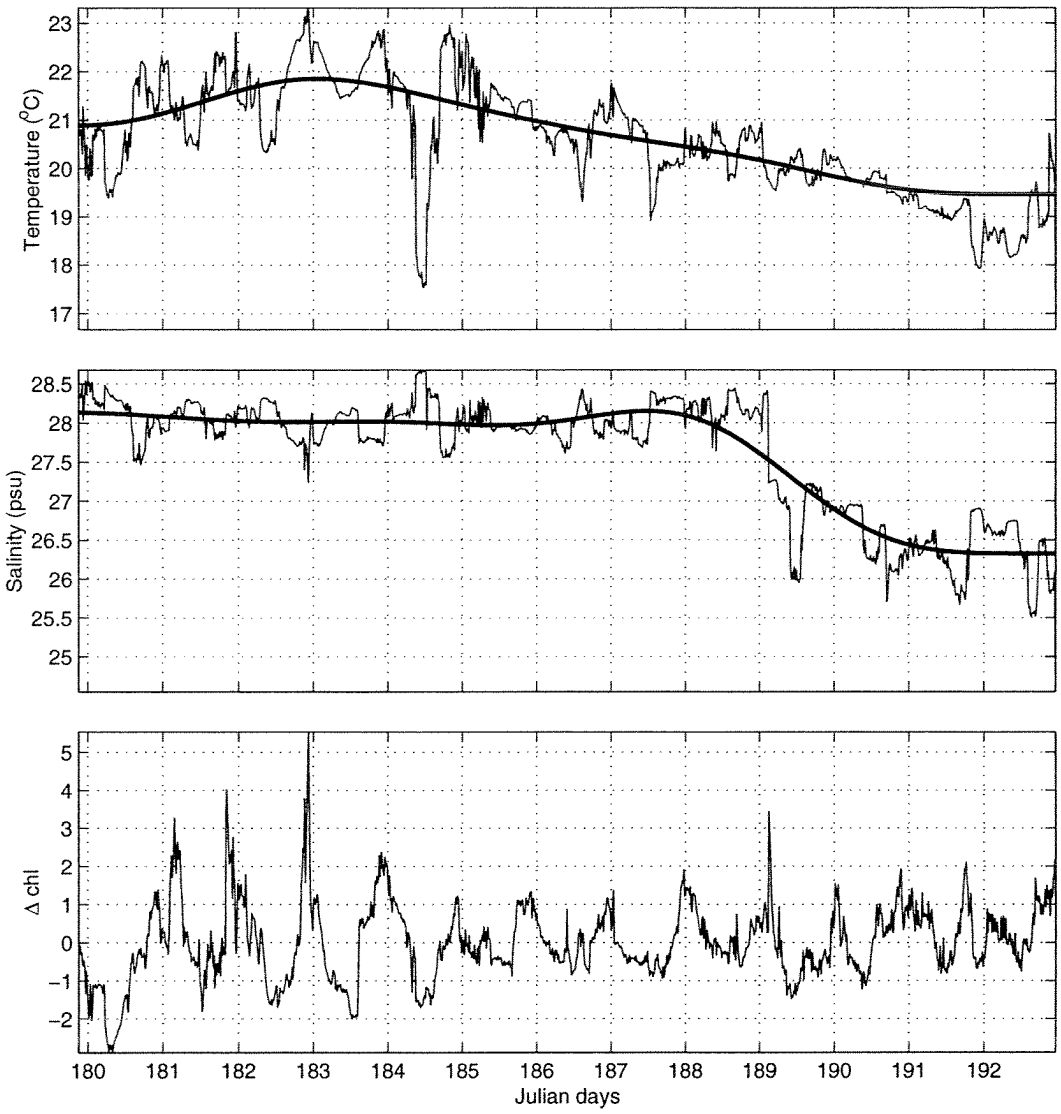

Fig. B.8: Moored SEACAT data from the bottom at site SC1 (the mouth of Winter Bay) during the period Julian days 179-193, 1999.

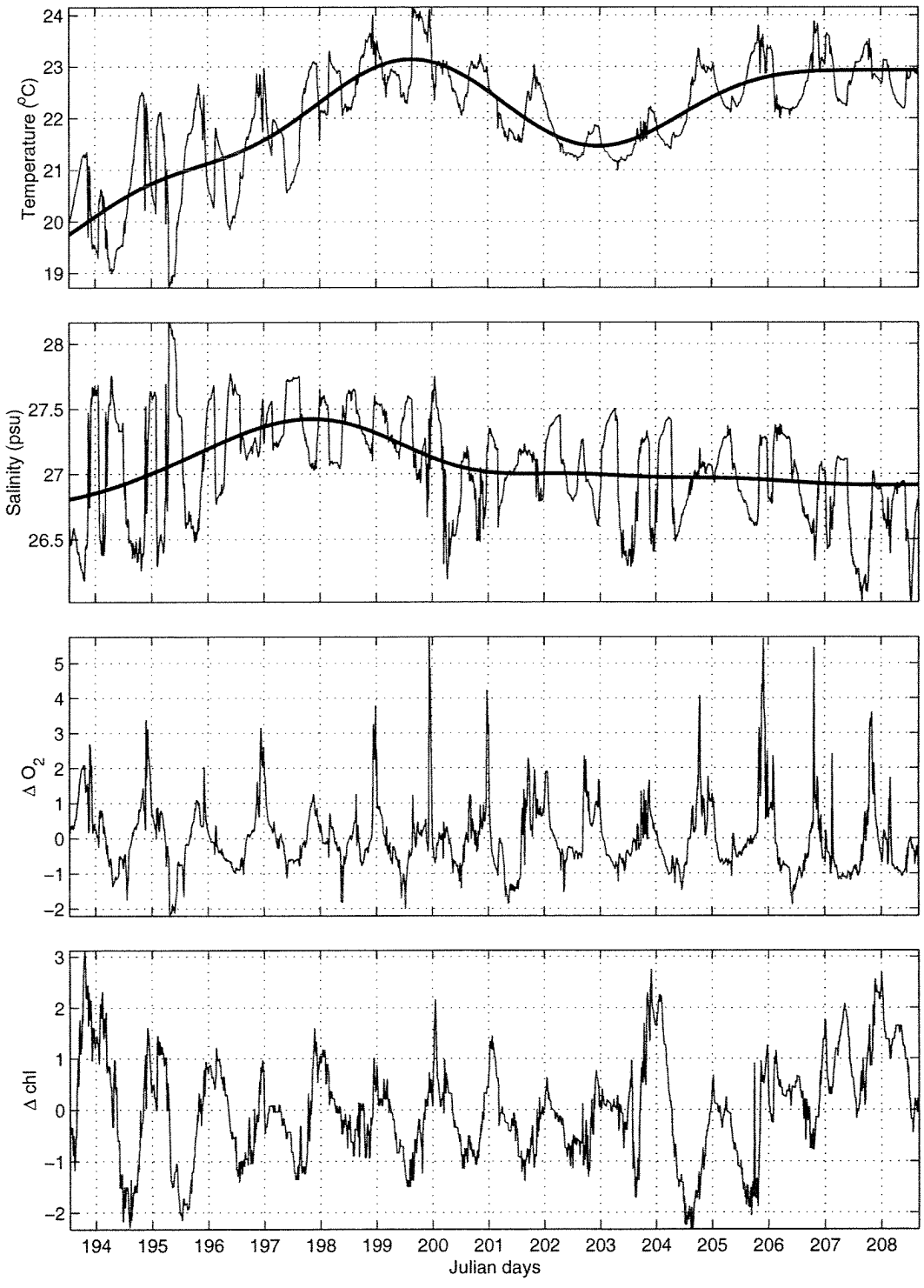

Fig. B.9: Moored SEACAT data from the surface at site SC1 (the mouth of Winter Bay) during the period Julian days 193-209, 1999.

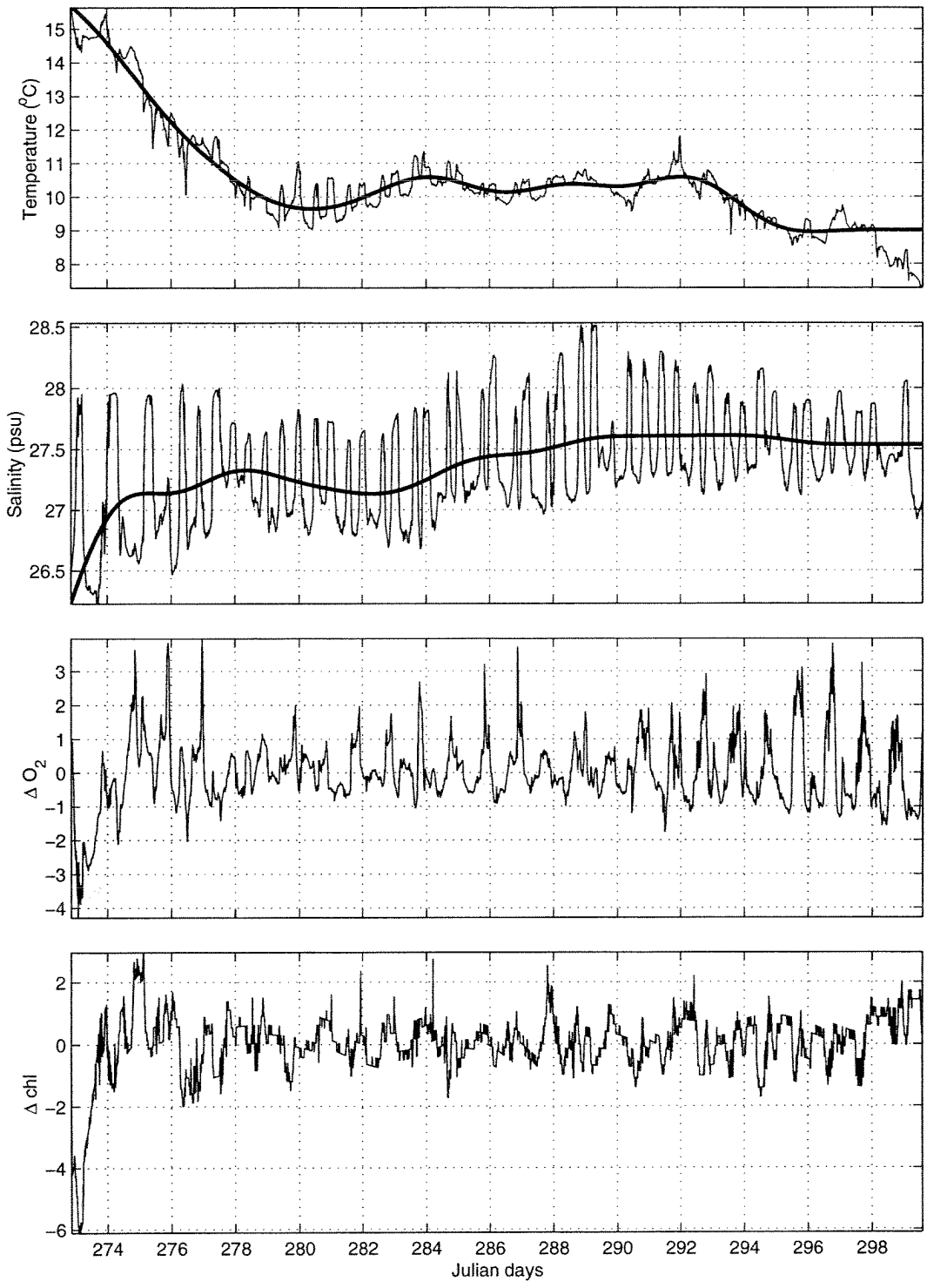

Fig. B.12: Moored SEACAT data from the surface at site SC2 (entrance channel) during the period Julian days 272-300, 1998.

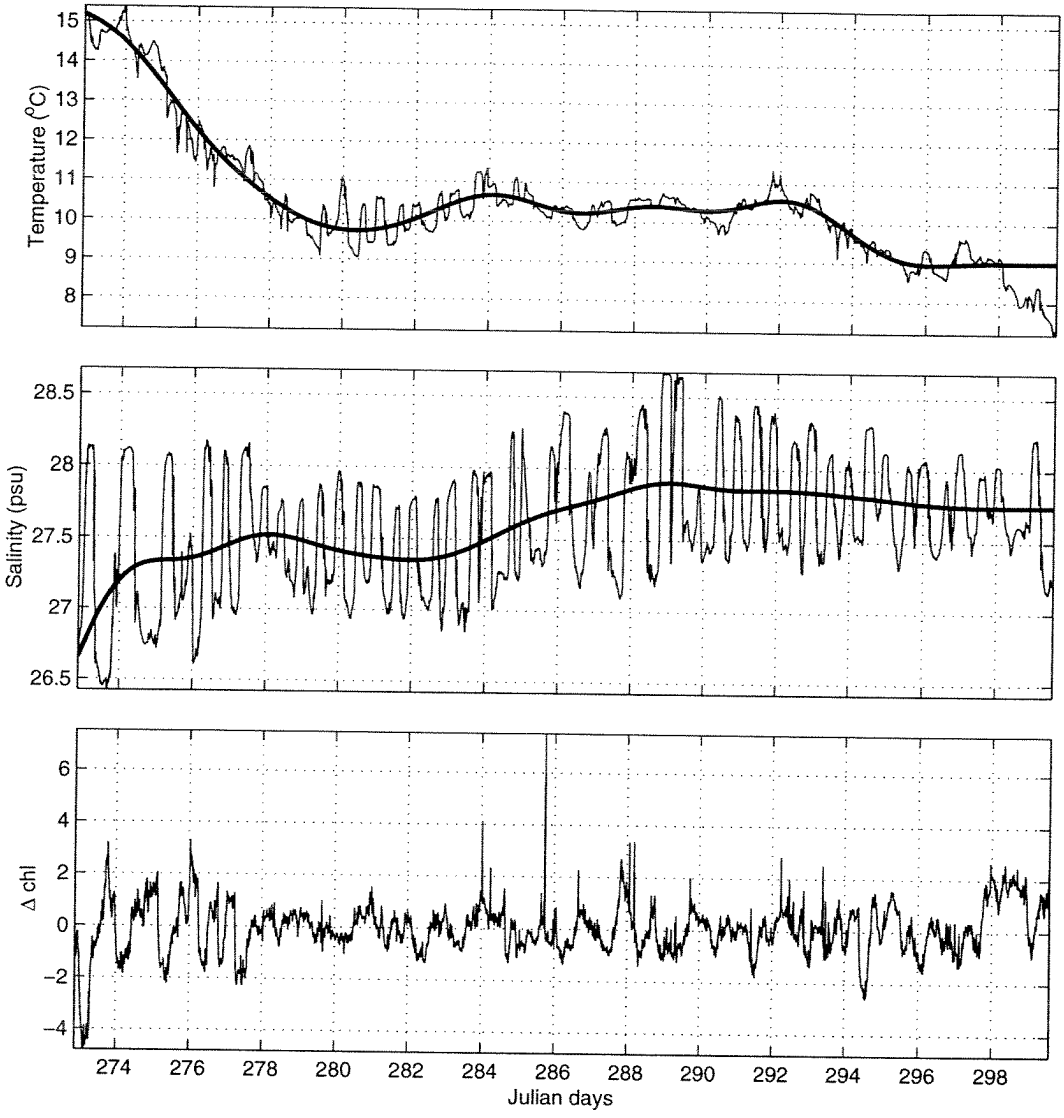

Fig. B.13: Moored SEACAT data from the bottom at site SC2 (entrance channel) during the period Julian days 272-300, 1998.